RESEARCH THESIS FOR:

Packed-bed rock thermal energy storage for concentrated solar power: Enhancement of storage time and system efficiency

SUBMITTED TO:

FACULTY OF ENGINEERING, THE BUILT ENVIRONMENT AND INFORMATION TECHNOLOGY

OF THE

NELSON MANDELA METROPOLITAN UNIVERSITY

FOR THE PROPOSED RESEARCH PROGRAMME:

Magister Technologiae: Engineering: Mechanical

BY:

Mohaman Bello Maidadi

Student Number: 209005654

Submitted: December 2013

Supervisor	:	Dr Russell Phillips
Co-Supervisor	:	Prof. Hannalie Lombard

ABSTRACT

Author: Mohaman Bello Maidadi

Title: PACKED-BED ROCK THERMAL ENERGY STORAGE FOR CONCENTRATED SOLAR POWER: ENHANCEMENT OF STORAGE TIME AND SYSTEM EFFICIENCY

Solar thermal energy harvesting is a promising solution to offset the electricity demands of a growing population. The use of the technology is however still limited and this can most likely be attributed to the capital cost and also the intermittent nature of solar energy which requires incorporation of a storage system. To make the technology more attractive and effective, cheap means of harvesting solar energy and the development of efficient and inexpensive thermal energy storage devices will improve the performance of solar energy systems and the widespread use of solar energy.

Heat storage in a packed-bed rock with air as the working fluid presents an attractive and simple solution for storing solar thermal energy and it is recommended for solar air heaters. A packed-bed rock storage system consists of rocks of good heat capacity packed in a storage tank. The working fluid (air) flows through the bed to transfer its energy. The major concern of the design for a packed-bed rock thermal storage system is to maximize the heat transfer and minimise the pressure drop across the storage tank and hence the pumping power. The time duration the stored energy can be preserved and the air flow wall effect through the bed are the common complications encountered in this system.

This study presents an experimental and analytical analysis of a vacuum storage tank with the use of expanded perlite for high temperature thermal energy storage in a packed-bed of rocks. Dolerite rocks are used as the storage medium due to their high heat capacity and as they are locally available. To minimise the pressure drop across the tank, moderate rock sizes are used. The tank contains baffles, allowing an even spread of air to rock contact through the entire tank, therefore improving heat transfer.

There is a good correlation between the predicted and the actual results (4 %) which implies that the baffles incorporated inside the vacuum tank forces the air through the entire tank, thereby resulting in an even lateral temperature distribution across the tank.

The investigation of heat loss showed that a vacuum with expanded perlite is a viable solution to high temperature heat storage for an extended period.

The research also focuses on the investigation of a proposed low cost parabolic trough solar collector for an air heating system as shown in Figure (1.3). The use of a standard solar geyser evacuated tube (@R130 each) has cost benefits over the industry standard solar tubes normally used in concentrating solar power systems.

A mathematical was developed to predict the thermal performance of proposed PTC and it was found that the measured results compared well with the predictions. The solar energy conversion efficiency of this collector is up to 70 %.

This research could impact positively on remote rural communities by providing a source of clean energy, especially for off-grid applications for schools, clinics and communication equipment. It could lead to a significant improvement in the cost performance, ease of installation and technical performance of storage systems for solar heating applications.

TABLE OF CONTENTS

LIST OF FIGURES

LIST OF TABLES

NOMENCLATURE

A	*Cross sectional area of the tank* (m^2)
$A_{Projected}$	*Projected area of the collectors* (m^2)
A_S	*Cross sectional area of the stainless steel heat barrier* (m^2)
A_T	*Cross section area of the Teflon fitting* (m^2)
A_1; A_2	*Surface area of Inside and outside tank respectively*
A_r	*Copper receiver tube surface area* (m^2)
A_c	*Glass tube covers surface area* (m^2)
B	*Number of collectors*
C_{pf}	*Specific heat capacity of air* ($J/kg.K$)
C_s	*Specific heat capacity of dolerite* ($J/kg.K$)
d	*Thickness of expanded perlite insulation / diameter of copper receiver tube (m)*
D	*Inside diameter of tank (m)*
D_e	*Equivalent diameter of rock (m)*
F_R	*Collector heat removal factor*
F'	*Collector efficiency factor*
Δp	*Pressure drop though the bed (Pa)*
Δx	*Thickness of rocks layer, space between baffles (m)*
Δt	*Time interval for finite difference numerical solution (s)*
G	*Sun irradiation* (W/m^2)
$G_\circ$	*Mass velocity of air* ($kg/m^2.s$)
h_{rad}	*Radiation heat transfer coefficient* (W/m^2K)
h_{fi}	*Convective heat transfer coefficient inside the receiver tube* (W/m^2K).
h_W	*Wind convection heat loss coefficient.*(W/m^2K)
$h_{r,c\text{-}a}$	*Linearized radiation coefficient from cover to ambient* (W/m^2K)
$h_{r,r\text{-}c}$	*Linearized radiation coefficient from receiver to cover* (W/m^2K)
h_V	*Volumetric heat transfer coefficient* ($W/m^3.K$)
K_T	*Thermal conductivity of Teflon (W/m.K)*
K_S	*Thermal conductivity of stainless steel (W/m.K)*

L	*Length of packed bed (m) / Collector length (m)*
L_S	*Length of stainless heat barrier (m)*
L_T	*Length of Teflon fitting (m)*
l	*Length of copper receiver tube (m)*
m	*Mass of dolerites (kg)*
$\dot{m}$	*Mass flow rate of air* (kg/s)
N	*Number of bed elements / Number of Al foils*
Nu	*Nusselt number*
NTU	*Number of transfer unit*
P	*Power (W)*
P_r	*Prandtl number*
Q_{Net}	*The collector net energy transferred to the working fluid (W)*
Q_{Loss}	*Heat loss across the collectors (W)*
Q_{Useful}	*Useful energy available to the collector working fluid*
Q_{st}	*Energy stored by the rocks (MJ)*
Q_U	*Sun energy* (W/m^2)
$Q_{U\circ}$	*Peak sun irradiation* (W/m^2)
Re	*Generalised Reynolds number*
t	*Time (s)*
T (1-6)	*Temperature stratification through the bed where T1 represents top layer and T6 bottom layer. (°C)*
T_a	*Ambient temperature (°C)*
T_c	*Surface temperature of the receiver glass tube (°C)*
T_r	*Surface temperature of the copper receiver tube (°C)*
T_{in}	*Temperature entering the tank (°C)*
U_L	*Overall thermal loss coefficient for a packed bed,* W/m^2K
T	*The storage temperature of the system (initial temperature* T_o*)*
V	*Storage volume* (m^3)
$\dot{V}$	*Flow rate of air* (l/s)

Greek symbols

σ	*Boltzmann constant (W/m^2.K^4)*
ρ	*Collector Reflectivity percentage, density*
η	*Collector solar energy efficiency conversion*
α	*Copper absorptivity / Shape factor of rocks*
μ	*Dynamic viscosity of a fluid (kg/m.s)*
ρ_f	*Density of atmospheric air (kg/m^3)*
ρ_s	*Density of rocks (kg/m^3)*
τ	*Glass tube transmittance / length of a day (s)*
ε	*Emissivity of glass tube / Void fraction of rock / Emissivity of the tank*
ε_c	*Emissivity of glass tube receiver*
λ	*Mirror reflectivity*
λ	*Thermal conductivity of expanded perlite (W/m.K)*

GLOSSARY OF TERMS

A

Absorber: Component of a solar energy collector that collects and retains as much of the radiation from the sun as possible.

Aperture: the opening trough which radiation passes prior to absorption in a solar collector.

B

Biot number: A dimensionless number used in heat transfer calculations. It is named after the French physicist Jean-Baptiste Biot (1774–1862), and gives a simple index of the ratio of the heat transfer resistances inside of and at the surface of a body. This ratio determines whether or not the temperatures inside a body will vary significantly in space, while the body heats or cools over time, from a thermal gradient applied to its surface.

Boltzmann constant: The Boltzmann constant, named after Ludwig Boltzmann, is a physical constant relating energy at the individual particle level with temperature.

C

CAD (Computer Aided Design) - The use of computer technology for the process of design and design-documentation.

Collector efficiency: The ratio of the energy collected by a solar collector to the radiant energy incident on the collector

Collector: Any device that can be used to gather the sun's radiation and converts it to useful energy

Concentrating collector: A solar collector that uses reflectors or lenses to redirect and concentrate the solar radiation passing through an aperture onto an absorber.

Concentration ratio: Ratio of aperture area of a solar collector to its receiver area.

CSP: Concentrating solar collector.

E

eDAQ: Electronic Data Acquisition systems

Emissivity: is the relative ability of its surface to emit energy by radiation. It is the ratio of energy radiated by a particular material to energy radiated by a black body at the same temperature

H

Heat exchanger: Device used to transfer heat between two fluids streams without mixing them.

I

Irradiation: The radiant energy falling per unit area on a plane surface per unit time.

N

NERSA: National energy regulator of South Africa

NMMU: Nelson Mandela Metropolitan University, a comprehensive university based in Port Elizabeth, South Africa.

NTU: Number of transfer units

Nu: Nusselt number

P

Phase change: Change of state from solid to liquid, solid to vapour, etc.

Power: The rate of which work is done.

PTSC: Parabolic tough solar collector

R

Re: Reynolds Number; a dimensionless number that gives a measure of the ratio of inertial forces to viscous forces in a flowing fluid.

Renewable Energy: is a renewable energy source which comes from natural sources such as the sun, wind, water, tides and geothermal heat.

Rotameter: is a type of flow meter based on the variable area principle and is used to indicate flow rates in fluid systems. The rotameter is placed vertically in the fluid system with the diameter end of the tapered flow tube at the bottom. When the fluid is poured into the tube, the float is raised from its position at the inlet allowing the fluid to pass between it and the wall. As it raises more fluid flows by until a point is reached where the flow area is big enough to allow the entire volume of fluid to pass the float.

S

Shape factor: Shape factor refers to a value that is affected by an object's shape but is independent of its dimensions.

Solar energy: Energy, in the form of electromagnetic energy, emitted from the sun and generated by means of a fusion reaction within the sun.

Sphericity of rocks: Sphericity describes how closely a rock particle resembles a sphere

Storage efficiency: The ratio of the energy delivered by the storage system to the energy supplied to the storage system.

Suntime: Time measured on a basis of the sun's virtual motion; see local solar time.

T

Thermal buoyancy forces: Forces acting on a liquid element due to its density difference that is caused by its temperature difference from its environment.

Thermal conductivity: The amount of heat that can be transferred by conduction through a material of unit area and thickness per unit temperature difference.

Thermal energy storage systems: A system in which the thermal of a body to do work is stocked.

Thermal stratification: Formation of layers or strata, of decreasing density by height that is caused by the effect of temperature on density.

Thermocouple: A thermo electrical device consisting of two dissimilar wires with their ends connected together. A small voltage is generated when two junctions are at different temperatures; if one junction is kept at reference temperature, the voltage generated in the other is a measure of the temperature of the other junction above the reference.

Transmittance: The ratio of the radiant energy transmitted by a given material to the radiant energy incident on a surface of that material; depends on the angle of incidence.

V

Void fraction: is a measure of the void (i.e., "empty") spaces in a material, and is a fraction of the volume of voids over the total volume, between 0 and 1

ACKNOWLEDGEMENTS

I would like to express my deepest gratitude to the following people and institutions; without their never-ending support and continuous contributions, the completion of this thesis would not have been possible.

- My supervisor and mentor, Dr Russell Phillips, for always motivating, inspiring and guiding me. You have been a great support system. Your great values, humility, effective communication and encouraging personality are what make you a remarkable mentor.

- My co-supervisor, Prof Hannalie Lombard, for continuously pushing me to improve myself, to persevere and achieve better results. Your constructive inputs helped me enhance my performance.

- NMMU Staff Members, for their much needed advice, suggestions and assistance.

- Colleagues and friends, for taking their valuable time to help me and for always being there for me and ensuring my well-being. Their inputs towards this thesis are much appreciated.

- My family, my brothers and sisters for always encouraging and supporting me. My mother, for all her prayers and motivating messages. My father, although he is no longer with me, I thank Him for his advice; it has stayed with me throughout the years and has moulded me into the man I am today. His words will forever remain within my heart.

- My mentor, Abdou Iyagarou, for his advice and financial assistance.

- Nelson Mandela Metropolitan University, for being the foundation of my education.

- The advance mechatronic technology center (AMTC), for sponsoring the project.

DECLARATION BY CANDIDATE

NAME: **Mohaman Bello Maidadi**

STUDENT NUMBER: **s209005654**

QUALIFICATION: **Magister Technologiae: Engineering: Mechanical**

DECLARATION:

In accordance with Rule G4.6.3, I hereby declare that the above-mentioned treatise/ dissertation/ thesis is my own work and that it has not previously been submitted for assessment to another University or for another qualification.

SIGNATURE: ____

DATE: ____

CHAPTER 1: RESEARCH PROPOSAL AND CONCEPT OVERVIEW

1.1 INTRODUCTION

Solar thermal energy harvesting is a promising solution to offset the electricity demands of a growing population. The use of the technology is, however, still limited and this can most likely be attributed to the capital cost and also the intermittent nature of solar energy which requires incorporation of a storage system. To make the technology more attractive and effective, cheap means of harvesting solar energy and the development of efficient and inexpensive thermal energy storage devices will improve the performance of solar energy systems and the widespread use of solar energy.

Countries are realising the importance of getting power from sources other than conventional fossil fuels. This is a consequence of an increasing population, people becoming more aware of environmental constraints and the climbing costs of conventional fuels. Solar energy is superior to other renewable energy sources due to its quantitative abundance [1]. To face the problem of the energy crisis and global warming as a result of continuous use of fossil fuels, research has been carried out to develop technologies for effective use of solar energy. Solar energy can be applied to many fields (electricity generation, transport, industry, heating and cooling). But due to the intermittent nature of solar energy, integration of solar energy storage systems is required to make the solar energy source more reliable [12].

Developing efficient and inexpensive thermal energy storage devices is seen as vital to improve the performance of solar energy systems.

Heat storage in a packed-bed rock with air as the working fluid, presents an attractive and simple solution for storing solar thermal energy for the following reasons [1, 6]:

- Operating temperature constraints due to chemical instability of the working fluid and storage material being eliminated due to the use of air and rocks;
- Operating pressure being close to ambient pressure; therefore no need for complex sealing of storage tank;

- Thermal storage incorporated directly after receiver (parabolic trough collector); no need for heat exchanger;
- Rocks being inexpensive;
- Rocks acting both as heat transfer surface and storage medium;
- Heat transfer between the rock and air being good due to the large heat transfer area of the rocks;
- Low conductivity of heat between rocks in absence of air flow;
- High temperature stratification due to the heat transfer coefficient between the air and rocks being high.

The problems associated with solar energy storage in packed bedrock are [1, 12, 18]:

- Air pressure drop in the packed bed which leads to a high pumping power;
- Heat loss across storage tank which results in a short storage time;
- Air tending to take the path of least resistance through the rocks, resulting in a non-uniform and inefficient heat transfer to the rocks.

The main purpose of the research is to solve all the problems listed in section 1.2.

1.2 PROBLEM STATEMENT

This is to store thermal solar energy for a period of at least three days in an insulated vacuum tank using locally available rocks. At the end of the 3-day period, adequate energy should remain in the rock for the water heating requirements of a domestic household for one day.

1.3 SUB-PROBLEMS

1.3.1 Sub-problem 1:

Investigate the problem of air pressure drop across the bed rock to reduce pumping power.

1.3.2 Sub-problem 2:

Develop a system that will ensure even distribution of air flow through the rocks that will lead to reduction in charging time cycle because all the rocks will be in contact with hot air coming into the tank.

1.3.3 Sub-problem 3:

Investigate heat loss through the tank using a vacuum insulated tank to ensure at least three days of storage time is achieved.

1.3.4 Sub-problem 4:

Investigate the effect of constant and varying air flow to see how it affects heat transfer through the rocks.

1.3.5 Sub-problem 5:

Investigate the heat stratification over the rock bed.

1.3.6 Sub-problem 6:

Investigate the effect of rock size on heat transfer from the air to rocks.

1.3.7 Sub-problem 7:

Investigate the technical and economic feasibility of using rock to store solar energy for a typical domestic household with comparisons to other storage techniques currently in use.

1.3.8 Sub-problem 8:

Compare experimental test results to analytical computational simulations of heat transfer and flow through the rock bed.

1.3.9 Sub-problem 9:

Investigate the feasibility of using a parabolic trough collector to capture heat from the sun: Mathematical modelling and practical testing of heat transfer will be analysed.

1.4 HYPOTHESIS

High temperature thermal solar energy storage in a rock bed system heated using a parabolic trough collector will yield at least three days of heat storage at 300°C, resulting in improvement of cost performance and thermal performance of storage systems for solar heating applications.

1.5 DELIMITATIONS

The research limitations are as follows:

- Rocks (dolerite) are the only storage medium considered.
- Rock properties will be based on literature studies and no testing will be conducted to determine their properties.
- The working fluid considered in the research will be air. No investigation will be done on different types of working fluids.
- Heat extraction out of the tank is not covered by the research.

1.6 SIGNIFICANCE OF RESEARCH

The use of renewable energy as a replacement for conventional fossil fuels will reduce Greenhouse gas emissions [19]. When considering solar energy, both photovoltaic (PV) and solar thermal conversion devices are readily available. While PV systems present a promising source of electrical energy, solar thermal systems are ideally suited to offset heating loads. Also with the recent concerns over global warming and the environment, there has been a substantial increase in the use of solar energy systems [19].

On a socio-economic level, this research could impact positively on remote rural communities by providing a source of clean energy, especially for off-grid applications for schools, clinics and communication equipment.

This research could lead to a significant improvement in the cost performance, ease of installation and technical performance of storage systems for solar heating applications.

Due to the potential low cost of pumping power and long storage time, this would result in an increased technical and economic feasibility of using solar energy for multi-family residential and small commercial applications and it will also further the widespread use of renewable energy.

South African electricity generation depends mainly on conventional fossil fuels where coal represents the major source. As the country is currently struggling to keep up with the electricity demands of a growing population, solar thermal energy storage could assist in partially alleviating the problem.

1.7 RESEARCH METHODOLOGY:

Step 1: literature survey

This stage focuses on information gathering within the focus areas:

- In-depth understanding of solar energy and the need for storage
- Concentrated solar collectors
- Thermal energy storage systems
- Packed-bed rock storage systems and the problems encountered
- Rocks typically used in rock bed systems.

Step 2: Analytical and computational analysis of the system

- Calculations of heat that will be captured by the solar collectors
- Estimations of heat that will be stored in the packed-bed rock system
- Storage time and heat stratification in the packed-bed rock will be simulated
- Air pressure drop across the bed will be estimated and pumping power required
- Heat transfer between rocks and the air will be calculated.

Step 3: Design and manufacture of the system

- Parabolic trough collectors system (heat source)
- Storage tank
- Rock selection
- Heating element selection: This auxiliary heat source will be used to simulate exactly the amount of heat that is delivered by the parabolic trough collectors. That auxiliary heat source will be used to run continuous testing even during cloudy weather.

Step 4: Experimental testing of the system

- Collector testing
- Investigating the effect of air flow on heat transfer between air and rocks.
- Investigation of air pressure drop across the bed rock system and storage time.

Step 4: System refinement if needed

1.8 RESEARCH EXPENDITURE:

The table below indicates all the equipment and materials that have been purchased for the research and experimental testing.

Table 1.1: List of research expenditure.

Items	**Quantity**	**Cost**
Galvanized sheet Z-275: 2450x1225x0.8(mm)	4 items	R1134
Seamless tube ASTM A-106 Grade B: ID:65mm of 1m long	1 item	R240
Round rube hot rolled: 21.40x1.6x2000(mm)	2 items	R39.60
Equal angle beam: 25x25x2 of length 1850mm	4 items	R100
Equal angle beam: 30x3x2 of length 2100mm	4 items	R150
Angle beam forming an angle of 130 degree : 30x30x2 of length 1800mm	4 items	R160
A pack of rivets (3mm)	1 item	R100
Parabolic side plates material and laser cutting price estimation	4 items	R800
Gear material and laser cutting price estimation	1 item	R900
Evacuated solar receiver glass tubes	10 items	R2000
Deep groove ball bearing	4 items	R660
Material for bearing casing and laser cutting	4 items	R200
Equal angle beam: 25x25x5 of length 3000mm	1 item	R90
Rectangular tube hot rolled: 60mmx40mmx3mm of 1m long	2 items	R150
Rectangular tube hot rolled: 60mmx40mmx3mm of 3m	2 items	R450
Insulation material	2 item	R700
Electric motor	1 item	R3600
Reflective sheet	1 item	R10000
Storage tank	1 item	R25000
Blower	1 item	R800
Electronic and electrical equipment		R15000
Heating element	1 item	R6000
Rocks		R1000
Blower	1 item	R5500
Total		**R75000**

1.9 OVERVIEW OF THE CONCEPT

Figure (1.1) represents the overview of packed-bed rock storage for air heating systems. Ambient air is pumped through the collector unit using a fan. The collector unit absorbs the solar radiation and converts it to heat. This air temperature rises as it absorbs the heat accumulated though the collector unit. The hot air enters the storage tank through the inlet pipe from the top, flows through the packed bed and exits at the bottom of the tank. Thermal charging from the top allows the exploitation of the buoyancy effect of the heat on the rocks to create and maintain thermal stratification inside the packed bed, the hottest region being at the top [12].

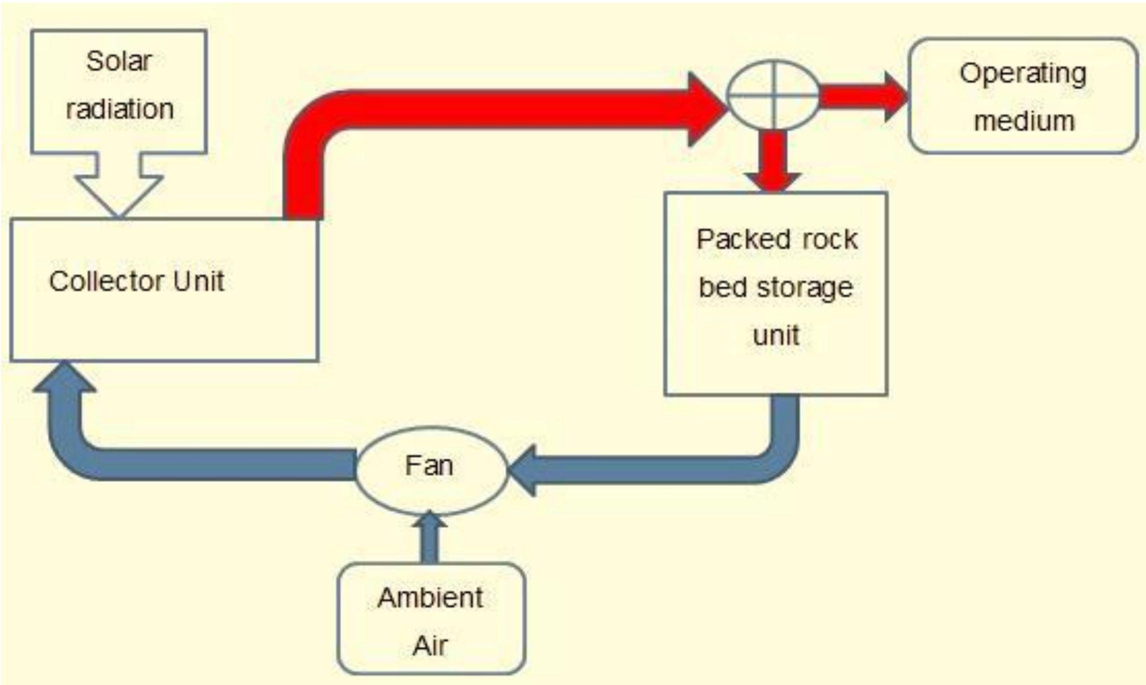

Figure 1.1: Flow Chart of packed rock thermal energy storage for solar air heating system

1.9.1 STORAGE TANK

This Research aims at solving the problems encountered in thermal storage in a packed bed of rocks and providing a cheap and efficient storage method for high temperature storage in a packed-bed rock storage system.

The objectives of the storage tank for a bed rock thermal system in this project are to:

- Enhance heat transfer while minimizing pressure drop. As explained in Chapter 2, the pressure drop increases as the rock sizes decrease. On the other hand, the smaller the rocks the better the heat transfer between the air and the rocks. Therefore to select a rock size that reduces pressure drop and that allows an effective heat transfer from the air to the rocks, an optimization parameter is defined in Chapter 2. This optimization parameter is the ratio of the energy stored by the rocks over the power consumed by the blower.
- Minimize heat losses through the tank using vacuum superinsulation techniques. This would be achieved by evacuating the cavity space between the inside tank and the outside tank as shown in Figure (1.2). Expanded perlite powder insulation is also introduced in that cavity space to slow down the radiation heat losses because radiation heat losses is the only heat transfer mechanism in a vacuum. This technique will ensure a long storage time, therefore reducing the cost of insulation material.
- One the complications related to storage of energy in a bed rock system is the wall effect [18]. The air usually takes the path of least resistance around the rocks. This results in ineffective heat transfer from the air to the rocks. The baffles will force the air over the rocks and this will result in effective heat transfer from the air the rocks.
- Dolerite rocks will be used because of the good thermal properties and also because they are locally available.

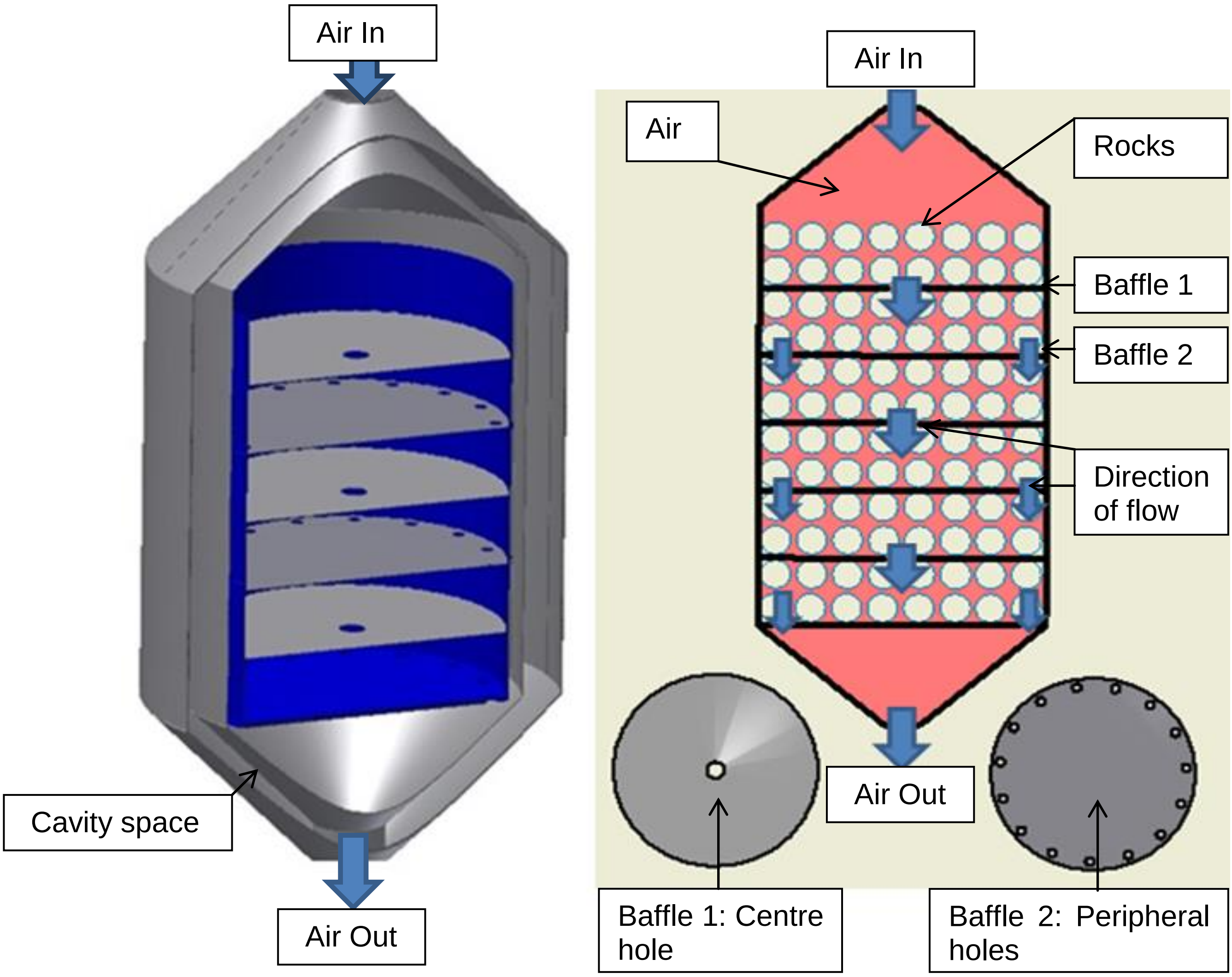

Figure 1.2: Baffles allowing air channelling

1.9.2 PARABOLIC TROUGH SOLAR COLLECTORS

The solar collector system is based on the design of a parabolic trough collector (Figure 1.3) focusing sunlight at a commercially available evacuated glass tube (which is usually used for low pressure solar geysers) with the air being heated while flowing through these evacuated tubes. The use of air as a working fluid eliminates the problem of chemical instability encountered for liquid heating, resulting in increased pressure due to the liquid reaching boiling point. That means the receiver tube does not experience high pressure; therefore the system is less complex and the design is cheaper. Since the heat transfer medium is air, any small leaks in the system are not critical as the extra air required to replace these losses is drawn in from the atmosphere [40]. This again creates a very robust and cheap solution.

The proposed low cost parabolic trough solar collector for an air heating system is shown in Figure (1.3). The use of a standard solar geyser evacuated tube (@R130 each) has cost benefits over the industry standard solar tubes normally used in concentrating solar power systems [40].

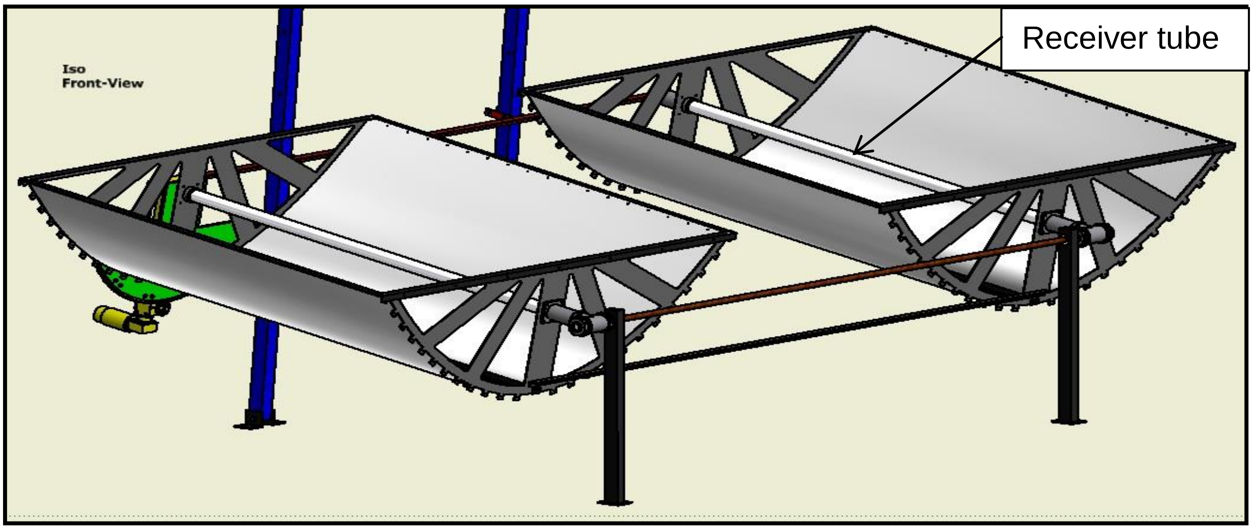

Figure 1.3: CAD Model of Parabolic Trough Collectors

1.10 SUMMARY

The objective of this chapter was to explain the research topic and provide an overview of the concept. The operation of a packed-bed rock storage system for air heating application is explained and the significance of this research is presented.

1.11 RESEARCHER QUALIFICATIONS

- Baccalareus Technologiae Mechanical Engineering [B Tech Mech Eng], Nelson Mandela Metropolitan University, 2012 – Cum Laude
- National Diploma Mechanical Engineering [N Dip Mech Eng], Nelson Mandela Metropolitan University, 2011

CHAPTER 2: LITERATURE REVIEW

2.1 OVERVIEW AND BACKGROUND

Energy is the most important factor in the economical and social development of a country and also an important parameter for sustainable development worldwide [10]. The climbing cost of fossil fuels such as oil, natural gases and coal, caused by the fast depletion rate of these resources and the environmental concerns caused by the conventional energy sources, made people realise the need for new alternative energy sources to fulfil their energy demand [4, 14]. In 2007 Goswani presented an alarming study, in order to better understand the effect of the depletion of conventional fossil fuels [8]. The production rate of oil was 80 million barrels per day and 7.36 billion m^3 of natural gases per day in 2007 and based on the world oil reserves in 2005 which were equal to 1200 billion barrels and the world natural gases reserves that were 180 million m^3 in 2004, his study estimated at that consumption rate, the oil and natural gas would meet the world demand for another 41 and 67 years respectively [4, 8]. Coal was in a better situation as the estimation showed that it could provide energy for another 230 years [4].

Renewable energy presents solutions to the problem of the actual energy crisis and is a more promising energy source for sustainable development because it is always available, being renewed by nature [14].

Teske *et al*. (2012) has illustrated in Figure (2.1) the growth which is due to renewable energy technologies over the last decade in the overall capacity of the global power market. Countries like Germany understood the need of shifting to renewable energy for a sustainable development with approximately 10% of the overall energy supplied from renewable energy [20]. At the moment a third of South Africa's population does not have access to energy due to the fact that many cannot afford it. South African electricity generation depends mainly on conventional fossil fuels where coal represents the major source. As the country is currently struggling to keep up with the electricity demands of a growing population and the rapidly climbing cost of coal which affects the electricity price, renewable energy sources could present a solution to this problem. The South African government (NERSA) has implemented policies allowing for generation of power using renewable energy sources. This initiative has the added benefit of job creation. The projection of job creation by the renewable energy industry in South Africa is presented in Figure (2.2) [27].

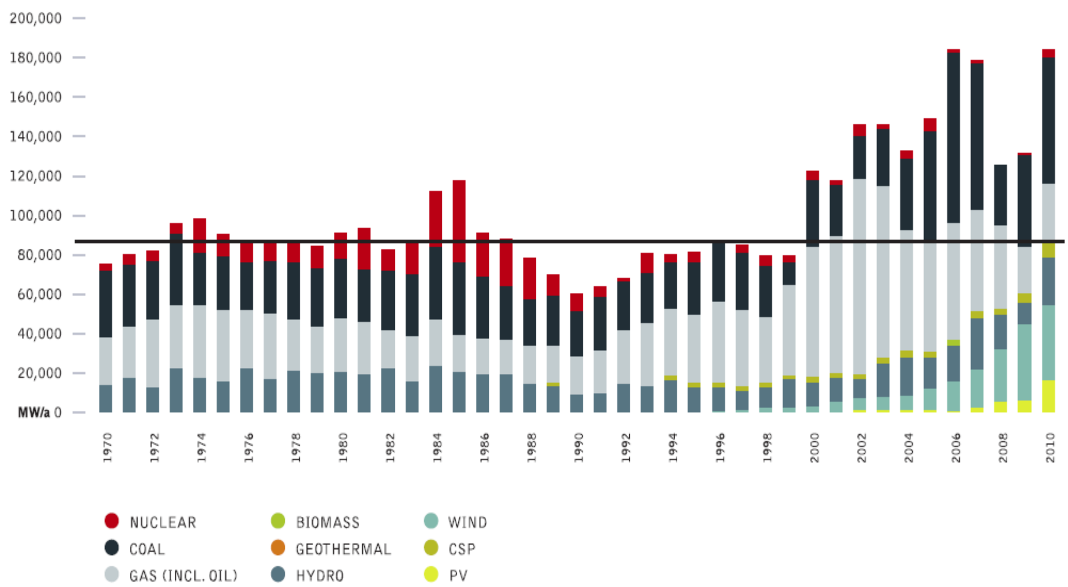

Figure 2.1: Global Power Plant Market 1970-2010 (Teske et al, 2012). [20]

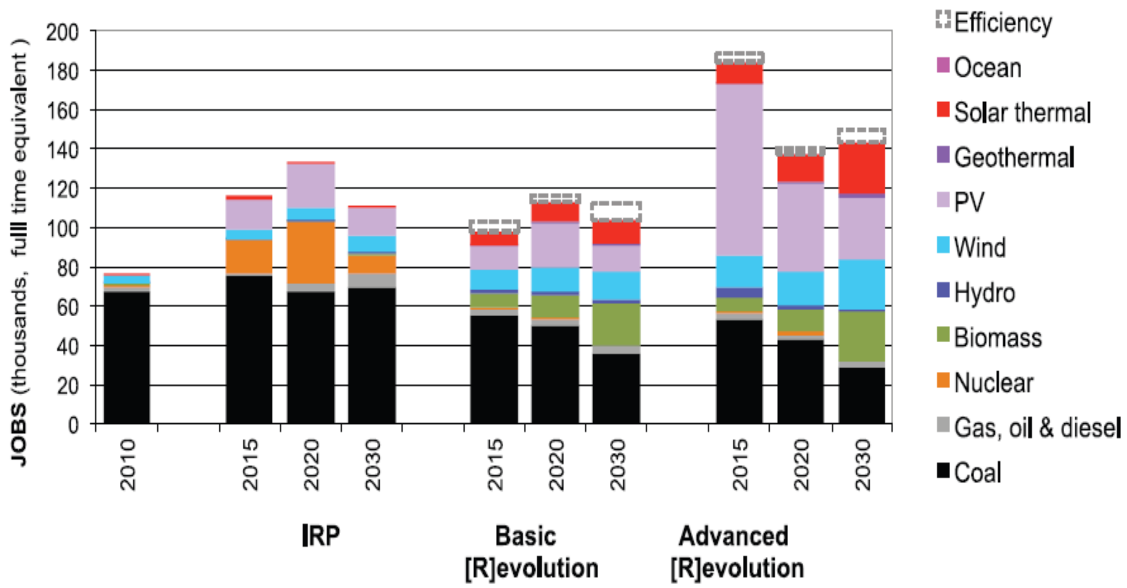

Figure 2.2: South African electricity sector jobs to 2030 (Rutovitz, 2011). [27]

Among the renewable energy sources solar energy is superior due to its quantitative abundance [1]. The benefits brought by the installation and operation of solar energy systems according to Abu-Zour and Riffet, 2006, are classified in two categories: [9]

i. From an environmental point of view the positive aspects of the solar energy technologies are:

- Reduction of the emission of greenhouse gases
- Reclamation of degraded land
- Reduced requirement of transmission lines within the electricity grid
- Improvement in the quality of water resources.

ii. The socio-economic benefits of solar energy technologies are:

- Increased regional and national energy independence
- Creation of employment opportunities
- Restructuring of energy markets and the growth of new production activities
- Acceleration of electrification of rural communities in isolated areas.

Solar energy constitutes the largest supply of renewable energy. The fraction of solar energy reaching the earth is equal to 1.7x10^14 kW and it is estimated that 84 min of solar radiation falling on earth is equal to the world energy demand for a year [4]. Solar energy has been used for centuries by both nature and humankind to dry and preserve their food, to dry their clothes and many more tasks. The possibility to harness solar energy has broadened its applications. It is used to heat and cool buildings, to heat water for domestic and industrial uses, to generate electricity, to operate engines and many more applications [1, 4]. The most important aspect of solar energy as compared to other forms of energy is that is clean and does not produce environmental pollution. Solar energy is harnessed and captured, using two techniques: The first one is the use of photovoltaic cells to convert the sun’s light into electricity and the second one is to use solar collectors to capture sun light as heat [4, 15].

A basic solar thermal system consists of a collector with or without a storage device. Solar energy collectors are specific types of heat exchangers that convert the radiation energy of the sun to heat. It is the major component of solar thermal energy systems [1, 4]. The incoming solar radiation is absorbed and converted to heat by the collector and transfers the heat to the working fluid (air, water, oil, molten salt) [4]. The solar energy harvested is either directly used or stored in thermal energy storage tanks to be used at times when the sun is not available. There are two types of solar collectors: non-concentrating solar collector (stationary) and concentrating solar collector. A stationary solar collector does not track the sun's position and the area of solar radiation interception and absorption is the same; whereas a sun-tracking concentrating solar collector has concave reflecting surfaces to intercept and focus the sun's radiation to a smaller receiving area, hence the increase in the radiation flux [4]. Concentrating solar collectors are used for high temperature applications. The heat transfer fluids commonly used in solar collectors are: water, non-freezing liquid, air or oil. The different types of collectors and applications are summarised in Figure (2.3).

Motion	Collector type	Absorber type	Concentration ratio	Indicative temperature range (°C)
Stationary	Flat-plate collector (FPC)	Flat	1	30–80
	Evacuated tube collector (ETC)	Flat	1	50–200
	Compound parabolic collector (CPC)	Tubular	1–5	60–240
Single-axis tracking			5–15	60–300
	Linear Fresnel reflector (LFR)	Tubular	10–40	60–250
	Cylindrical trough collector (CTC)	Tubular	15–50	60–300
	Parabolic trough collector (PTC)	Tubular	10–85	60–400
Two-axis tracking	Parabolic dish reflector (PDR)	Point	600–2000	100–1500
	Heliostat field collector (HFC)	Point	300–1500	150–2000

Figure 2.3: Solar Energy Collectors. [4]

Solar energy as compared to fossil fuels is intermittent in nature and time dependant and also during rainy and winter seasons; solar radiation is reduced, hence the need for energy storage systems is required for a continuous operation of solar energy systems [14, 15]. Solar energy is usually stored as electrical energy in batteries and capacitors with the use of photovoltaic cells [15]. This storage technique is efficient but is still very challenging and expensive, particularly when large quantities of electrical power is stored (Spiers, 1995) [15]. Solar energy is also directly stored as thermal energy using solar collectors that convert the radiation of the sun to heat. Thermal solar energy storage is relatively simple to achieve; it is cost effective and the efficiency of those systems is high and the energy storage capacity is larger than that of an electrical storage system (Price et al., 2002; Montes et al, 2009) [15]. The stored energy can be retrieved at times when the sun is not available to power thermal power plants in the electricity generation field or for sundry applications like domestic water heating, household heating and industrial heating processes.

The overview of techniques of thermal energy storage used in solar energy systems is presented in Figure (2.4).

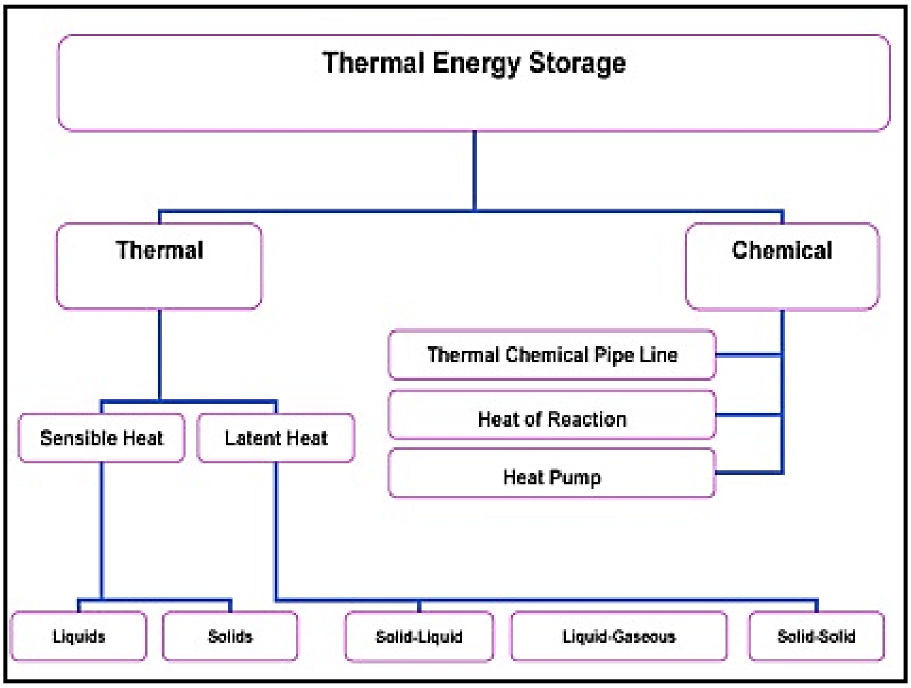

Figure 2.4: Means of storing solar thermal energy [14].

As seen in Figure (2.4), thermal energy can be stored as latent, sensible and chemical energy. Latent thermal energy storage refers to systems that store energy in materials while undergoing a phase change. This storage system is a compact heat storage system but the design of the heat exchanger that transfers the heat from the working fluid to the storage material is complex and expensive [14]. In the case of sensible heat storage, the temperature of the storage material is increased without undergoing a phase change. It is the most simple and cheap way of storing thermal energy, hence the choice of that storage technique in the proposed research. The storage media in sensible heat storage are classified in two categories which are liquid storage media such as oils, molten salts, water and solid storage media for rocks, peddles, bricks and many more [14, 15].

Thermal energy storage offers the potential of increasing overall efficiency of energy systems [11]. Thermal energy storage, in combination with concentrating solar power (CSP), allows for electricity production when sunlight is not available. Parabolic trough collectors are commonly used in CSP plants as illustrated in Figure (2.5). The heat transfer fluid is either a synthetic oil or molten salt. Of the two fluids, growing interest is in nitrate molten salts due to the availability of higher operating temperatures to improve plant efficiency, as well as lower material cost relative to oil [11].

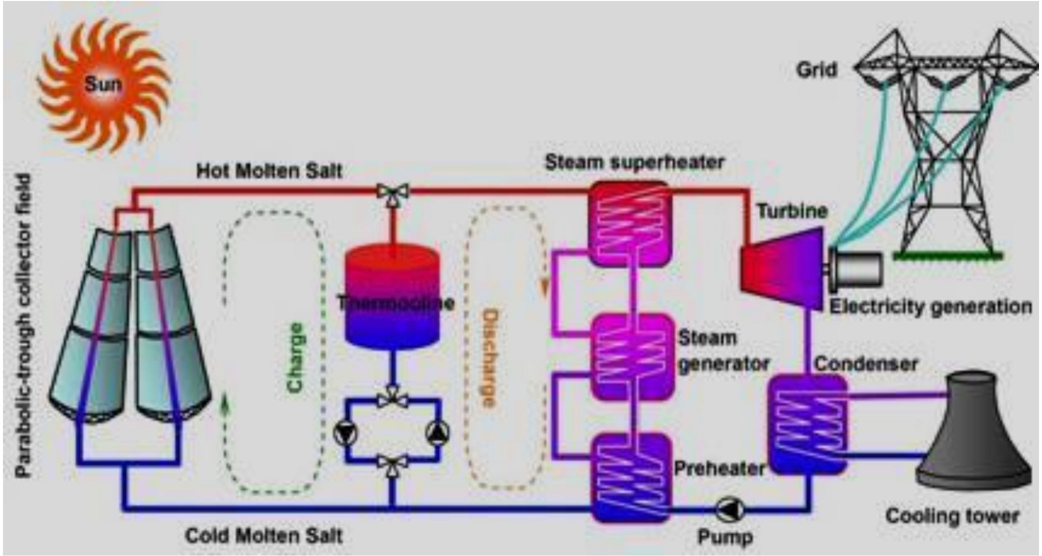

Figure 2.5: Solar power plant [11].

2.2 OVERVIEW OF SENSIBLE THERMAL ENERGY STORAGE TECHNIQUES

An important parameter in thermal energy storage systems is the time duration the stored energy can be preserved. An ideal storage will be a system that does not lose any energy over time; in other words, when the energy-carrying fluid is retrieved the temperature would be the same. According to this fundamental basis, thermal energy storage systems can be grouped into two categories: [11, 15]

- A system with direct heat storage of the heated working fluid. The performance of this system is close to an ideal storage system.
- A two-medium heat storage system which consists of a fluid that plays the role of a heat-carrying fluid and another medium where either solid materials or liquid are used as the primary thermal storage material. This storage system is simple and cost effective but less efficient than a direct storage system [15].

The first type of direct heat transfer fluid storage system consists of two storage tanks where the first one was for the hot fluid and the second one for the cold fluid as seen in figure (2.6) [11,15]. During the charging cycle the fluid in the cold tank is circulated through the solar collectors where it is heated; this energy is stored in the hot tank and during discharging of the energy, the fluid contained in the hot tank is extracted to provide heat for the power plant; afterwards that fluid is circulated to the cold tank and the cycle restarts. Even though this thermal energy storage system uses two tanks, it was later realised that even a single tank would achieve the same objective because the heat transfer fluid only occupies a volume that is equivalent to that of a single tank at any instance in time [11]. Therefore a new type of direct heat transfer fluid storage system was developed in which only one storage tank as illustrated in Figure (2.7) was used. In single tank thermal storage systems, the stratification of heat maintains the hot fluid on top of the tank and the cold fluid on the bottom [15]. The hot fluid enters the tank from the top during the charging cycle; whereas cold fluid is extracted from the bottom of the tank; during the discharging cycle the opposite occurs where the hot fluid is pumped out from the top of the tank and the cold fluid enters through the bottom of the tank.

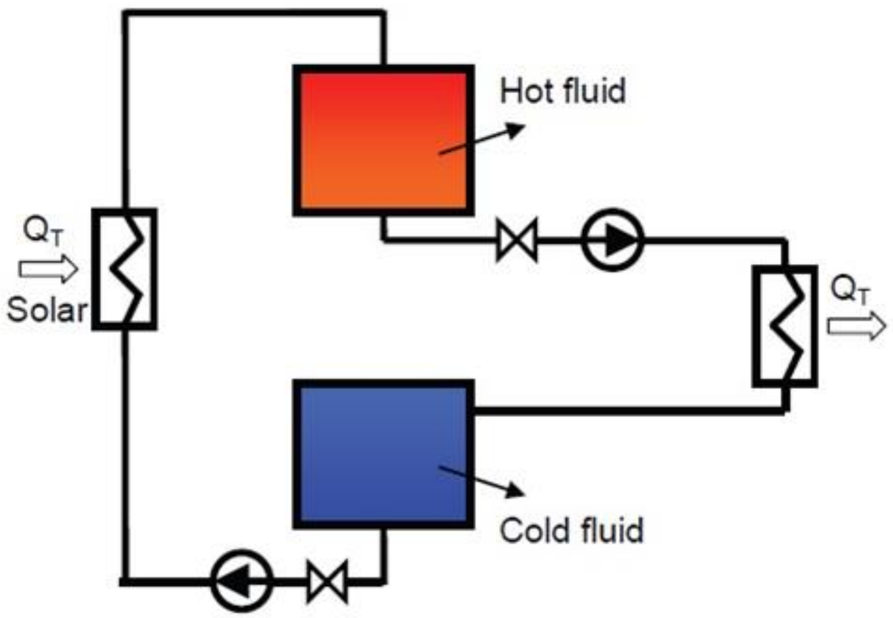

Figure 2.6: Two-tank thermal storage system using heat transport fluid only [11, 15].

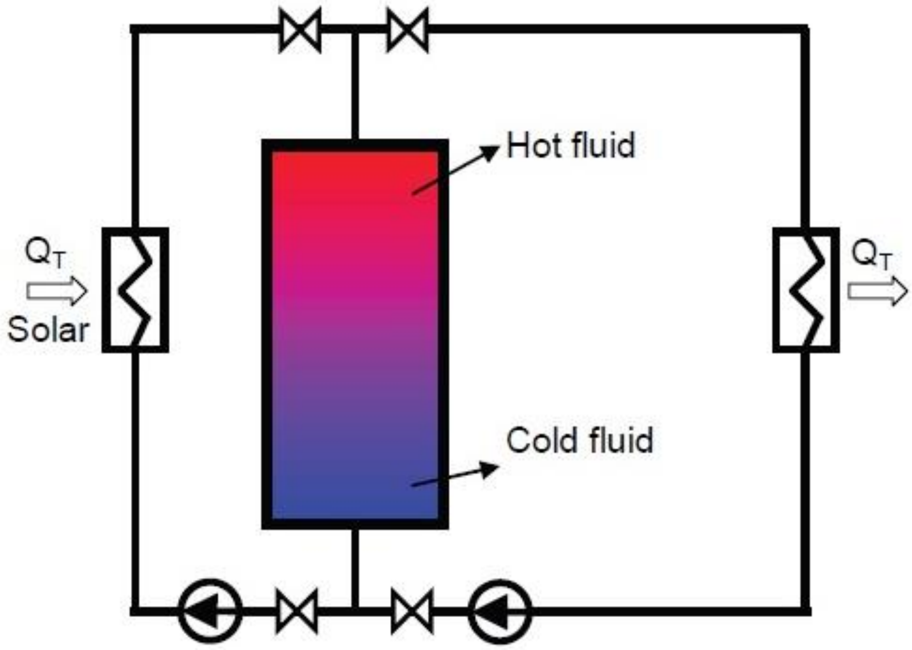

Figure 2.7: One-tank thermal storage system using heat transport fluid only [11, 15].

As explained earlier, a two-medium storage system has a heat transport fluid and a primary thermal storage material (solid or liquid) and only one storage tank is used in this system [15]. Based on the energy interaction and the contact between the working fluid and the energy storage material, there are two types of a two-medium storage system. The first type has loosely packed solid materials such as rocks inside a thermal storage tank and the heat transport fluid flows through the bed to transfer its energy to the solid materials as shown in Figure (2.8). The heat transport fluid is in direct contact with the storage materials therefore the heat transfer between the fluid and the solid materials is efficient. The second type of a two-medium storage system is illustrated in Figure (2.9). In this type, there is no contact between the working fluid and the storage materials as the working fluid flows inside tubes. The storage material can be solid or liquid in this set up [15]. This system is less efficient as compared to the first type because of the reduction of contact heat surface.

When selecting a thermal energy storage system for a specific application the primary factor in the choice is the cost of the system. The cost of a thermal energy storage system is influenced by many factors. As an illustration the cost of the heat transfer fluid is an important factor in the choice of whether a direct heat transfer storage system or a two-medium storage will be used. A tank that withstands high pressure will be used in case the vapour pressure of the working fluid is high or to eliminate the problem of corrosion, a stainless steel tank will be used [11, 15].

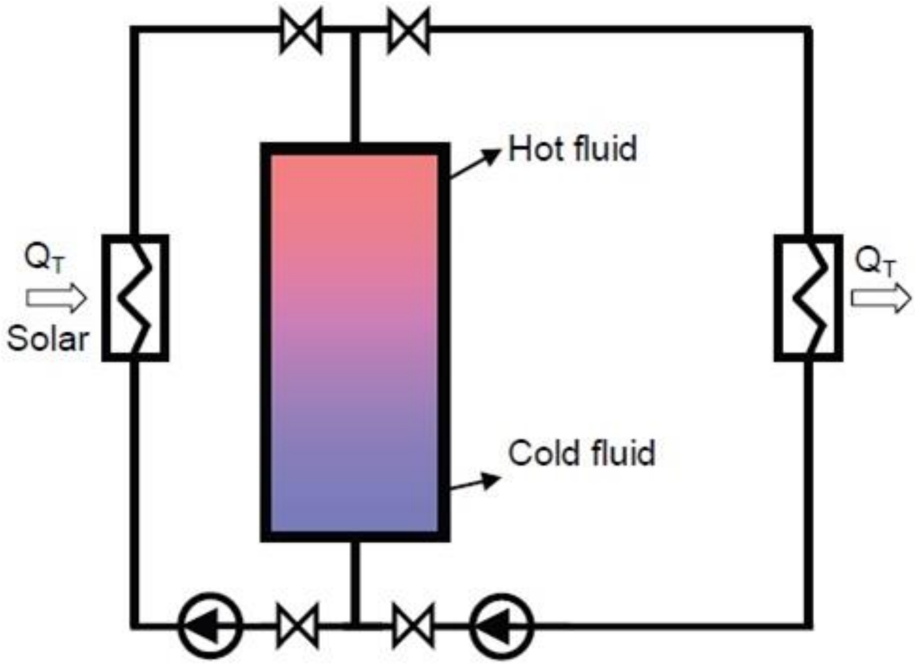

Figure 2.8: Two-medium heat storage with direct contact heat transfer [11, 15].

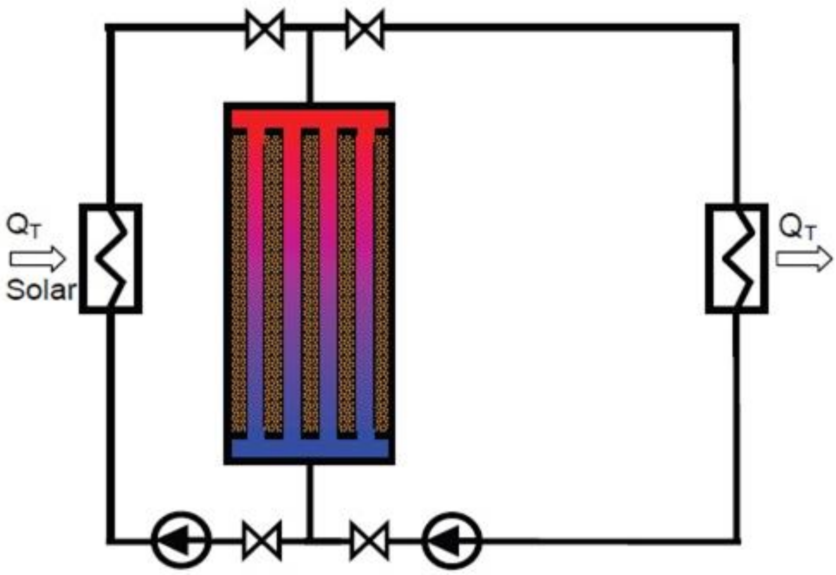

Figure 2.9: Two-medium heat storage with heat transfer through fluid pipes [11, 15].

The choice of the storage materials and the heat transport fluid to be used depends on many criteria. Solid materials used for thermal energy storage applications must have good thermal storage properties such as high specific heat, high thermal conductivity, low cost, low thermal expansion and a large density so that the required volume of the storage container is small. The common solid materials used for thermal energy storage are shown in Figure (2.10).

Medium	melting(°C) (or crumbles)	ρ (kg/m³)	C(kJ/kg·°C)	$\rho\cdot$C(kJ/m³·°C)	k(W/m·°C)
Aluminum	660	2700	0.92	2484.0	250
Brick (common)	1800	1920	1.0	1920.0	1.04
Fireclay	1800	2100-2600	1.0	2100-2600	1-1.5
Soil (dry)	1650	1200-1600	1.26	1512-2016	1.5
Granite	1215	2400	0.79	1896	1.7-4.0
Sand (dry)	1500	1555	0.8	1244	0.15-0.25
Sandstone	1300	2000-2600	0.92	1840-2392	2.4
Rocks	1800	2480	0.84	2086.6	2-7
Concrete	1000 (Crumbles)	2240-2400	0.75	1680-1800	1.7
Graphite	3500	2300-2700	0.71	1633-1917	85
Silicon carbide	2730	3210	0.75	2407.5	3.6
Taconite	1538	3200	0.8	2560	1.0-2.0
Cast iron	1150	7200	0.54	3888	42-55

Figure 2.10: Solid material suitable for thermal energy storage and their properties [15].

The heat transport fluids commonly used in thermal energy storage systems are molten salts and oil due to the fact that they are chemically stable at high temperatures. Molten salts can operate at higher temperatures than oil and they have low vapour pressure, hence there is no need for an expensive tank to withstand high pressures. However, the problem with molten salts is that their freezing temperature is high, near to 200 °C, which means that not all heat energy can be extracted from the salt [4 ,15, 18]. This high freezing point can lead to problems with salt freezing in pipes and stopping the flow. Oil does not experience the problem of freezing but is not environmentally friendly. Air is also used as a working fluid for high temperature storage because it is chemically stable at high temperatures and environmentally friendly.

The ideal storage system would be a system that maintains its energy for a considerable period of time. This would be achieved by keeping heat losses to a minimum [11]. Heat losses across the tank can occur through conduction heat losses from the storage material to the surroundings, through convection heat losses and through radiation heat losses. The reduction of heat flux is necessary to slow the temperature change of the system. In general, there are three major types of insulation techniques which differ regarding their applications and performance: [20]

- Conventional insulation material: This is the most common technique. Materials having very low thermal conductivity are wrapped around the storage tank to minimise the heat losses.
- Vacuum insulation: A vacuum insulation is realized by evacuating an empty space between two walls. The use of vacuum insulation eliminates the possibility of heat losses by conduction and convection as those heat transfer mechanisms require a material medium. Therefore only radiation heat losses occur. This insulation technique allows a compact design of the storage tank because the space between the walls to be evacuated does not have to be significant. Vacuum insulation can be unfavourable in the case of high temperatures, since the radiation heat transfer increases with the fourth power of temperature.
- Vacuum super insulation: This insulation technique is used for high temperature storage. It is a combination of vacuum insulation and materials that reduce radiation losses. As mentioned in the previous section, radiation is the only significant heat transport mechanism that occurs in vacuum so inserting materials having low emissivities and opaque materials can reduce the radiation heat losses. The two common material types with practical relevance used to reduce radiation heat losses are: foil insulation and powder insulation [20]. Filling a powder or a similar bulk material into this gap prior to evacuating is often easier than installing plates of conventional insulation materials or a multilayer insulation there. For this reason the vacuum super insulation technique using expanded perlite powder is used in this research for the storage of high temperatures in a packed-bed rock.

2.3 PACKED-BED ROCKS BED SOLAR THERMAL ENERGY STORAGE

Packed bed sensible heat energy storage consists of solid material of good heat capacity packed in a storage tank through which the heat transport fluid is circulated [14, 19]. It is the most suitable energy storage unit for air based solar energy storage systems. Hot air from the collector flows through the bed and the energy is transferred to the rocks. The hot air enters through the inlet pipe from the top, flows through the packed bed and exits at the bottom of the tank. Charging from the top allows the exploitation of the buoyancy effect to create and maintain thermal stratification inside the packed bed, the hottest region being at the top. The energy is discharged from the bed by pumping cold air through it. The heat transfer and pressure drop in the bed have been the subject of several theoretical and experimental investigations. Generally storage materials in the size range of 1 to 3 cm have been investigated as the storage medium [14, 19].

Small size material presents a large heat transfer area but pressure drop is usually large, which leads to high pumping power required to circulate the air. This reduces the overall benefit of the solar energy utilization system. To minimize pressure drop, a large material size is used instead. Reduction in the heat transfer rate to large size material elements due to smaller surface area per unit volume of storage, is compensated by substantial reduction in the amount of energy consumed by the blower due to the low pressure drop in the packed bed [14]. It can therefore be concluded that the large size material could be more beneficial for use as the storage material. The schematic of a packed-bed rock thermal energy storage system is presented in Figure (2.11).

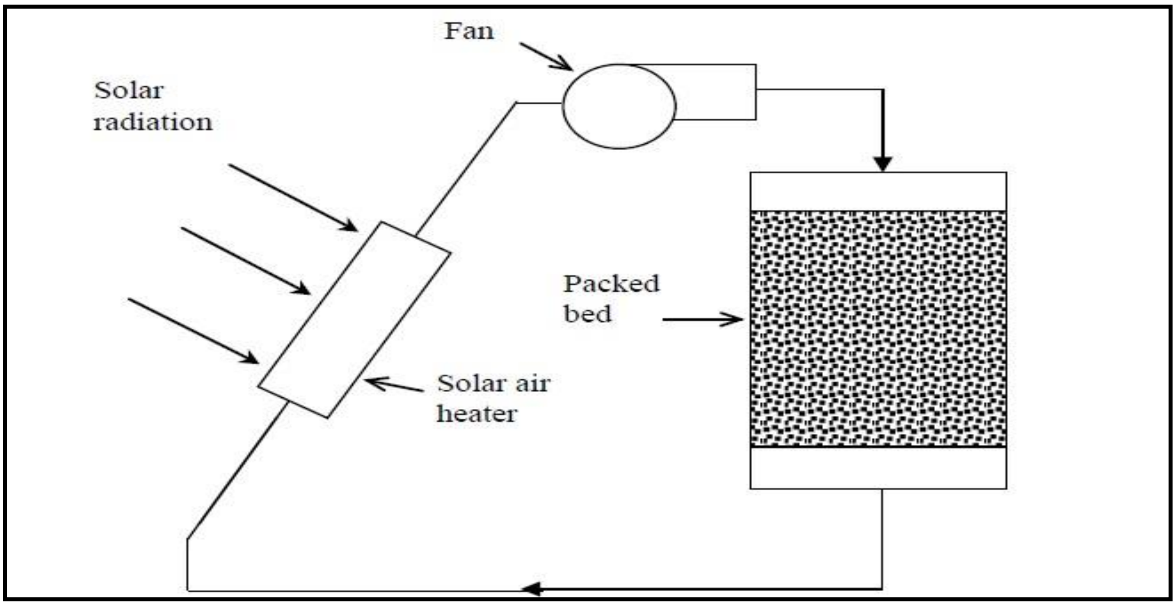

Figure 2.11: Schematic of packed bed solar energy storage system [13].

Research has been conducted on packed bed energy storage systems. The pressure drop and the coefficient of volumetric heat transfer between the air and the rock beds depend on the rock size and the air flow rate [14, 16]. The energy consumption by the blower to pump the air through the rocks is a significant expenditure in operating a rock bed energy storage system. The thermal heat stratification of the bed has a significant effect on the power consumed by the blower and the thermal performance of the collectors. The primary design objective of a packed-bed rock system is to have minimum energy consumption by the blower per unit of energy stored; therefore the design of the system should be based on thermo-hydraulic performance rather than the thermal performance alone [18, 22].

For this purpose, optimization of the system parameters has been carried out to make an optimal combination of the available energy stored in the bed and the energy consumption by fan to propel the air through the bed. Considering available energy stored in the rocks (Qat) and the energy consumption by the blower (Wt) for pumping air through the bed, thermo-hydraulic optimization of the packed bed solar energy storage system has been carried out on the basis of maximizing the optimization parameter ‘Qat/Wt’ [22].

Kenneth Guy Allen (2010) discussed in detail the theoretical and experimental correlations that were developed to predict the pressure drop and the thermal performance through packed-bed rocks systems [18]. The method pursued in the thesis for the prediction of the thermal energy is the Effectiveness NTU method of Hughes (1975) which was recommended by Duffie and Beckman (1991) [1]. In his thesis Kenneth Guy Allen found that the NTU- method correlates well with the measured results. The difference in the prediction and actual results was about 15 %. The percentage error can even be lower than the achieved results by Allen by preventing the edge effect. The edge effect is one of the complications encountered in the packed-bed rocks system where basically the air takes the path of least resistance through the rocks; therefore not all the rocks are in contact with the hot air, resulting in an ineffective heat transfer through the rocks. Allen suggested in his thesis, “The airflow distribution in large beds needs to be planned and analysed to determine a means of distributing the air evenly through the bed while minimising pressure drop” [18].

In this research baffles force the air though the rocks, therefore allowing even flow distribution over the rocks. The use of the baffles will give a better prediction than the 15% agreement achieved by Allen because the NTU-method assumes that all the rocks are in contact with the hot air; the use of baffles will ensure that. When it comes to pressure drop prediction, many authors use a method which they believe is relevant to their analysis. When dealing with pressure drop prediction, different types of models were achieved [18]. In this research the rocks that are investigated are crushed dolerite rocks, whose specific properties are not easily quantified such as the shape factor, void fraction and the sphericity. These factors are used in most correlations developed for pressure drop predictions. Shewen et al. (1978) recommended the equation of Dunkle and Ellul (1972) when measurements of the void fraction (ε) and the surface area shape factor (α) of the rock are not known. This is the method that was used in the pressure drop prediction in this research [1].

2.4 SUMMARY

This chapter investigated the potential of renewable energies and more precisely solar energy as a replacement of fossil fuels. The alarming facts related to conventional energy sources such as pollution and rapid climbing cost due to their fast depletion were presented and the benefits brought by the implementation of the solar energy system were discussed in detail. The chapter also presented an overview of the different thermal energy storage and collectors used in solar energy systems. The types of storage materials and heat transport fluids used for thermal storage application were also investigated. Ways of reducing heat losses from the storage tank to ensure long storage time were discussed. A detailed explanation of packed-bed rock thermal energy storage for solar air heating system was presented and parameters that affected their performance were evaluated. The previous works performed on the rock bed systems were analysed. Solving the problems encountered in the packed bed system and the recommendations constitute the primary objective of this research.

CHAPTER 3: DESIGN OF THE EXPERIMENTAL SET UP

3.1 INTRODUCTION

The design of the experimental setup and the experimental platform, used to run the tests on the packed-bed rock thermal energy storage tank and the parabolic trough solar collectors, are discussed in this chapter. The experimental data were logged at the Nelson Mandela Metropolitan University in South Africa and the experimental platform consists of equipment from the renewable energy research group in the department of mechanical engineering.

3.2 THE PACKED-BED ROCKS STORAGE TANK THERMODYNAMICS SYSTEM:

The proposed thermodynamic system for a vacuum insulated storage tank used for the high temperature thermal energy storage in the packed-bed rock is shown in Figure (3.1). Dolerite rocks are used as the storage medium due to their high heat absorption properties, as they are locally available. The tank contains baffles; allowing an evenly spread of air to rock contact through the entire tank. This enables improvement heat transfer as shown in Figure (3.1).

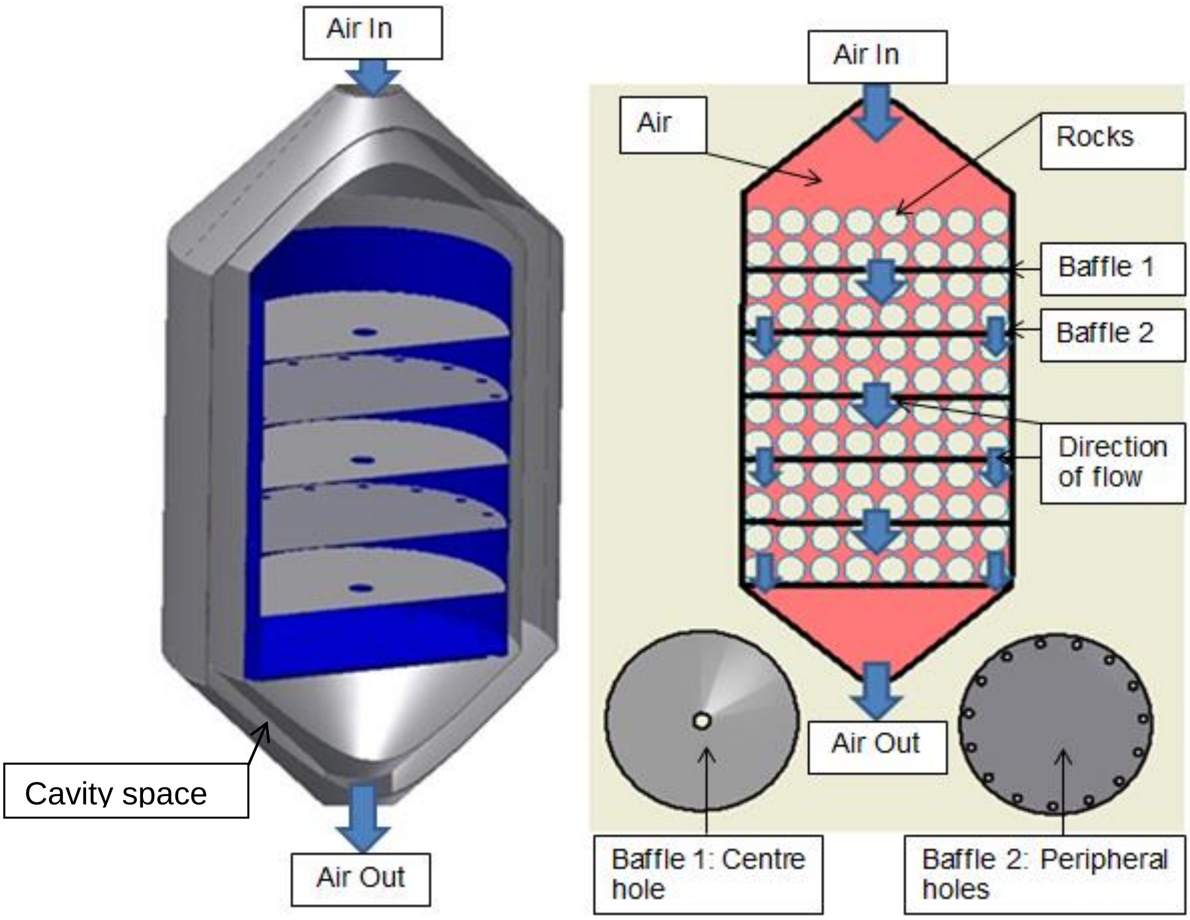

Figure 3.1: Packed-bed rock storage tank.

A 6kW electric heater was used to replace the parabolic trough solar collectors. It was placed above the entry to the storage tank to heat the air pumped through the system. The electric heater was well insulated with a 50mm ceramic blanket to reduce heat loss, and temperature output was controlled by a temperature controller. A blower, which was controlled by a frequency inverter, was used to pump the hot air delivered from the electric heater into the storage tank and a rotameter was used to measure the flow rate. The vacuum tank was made from mild steel, constituting an inside and outside tank. The inside tank where the dolerite rocks were packed was covered by a 30 mm calcium silicate blanket. The dimensions of the inside tank were a diameter of 0.9m and a height of 1.6m, whereas the outside tank had a 1m diameter and 1.8m height. The space between the outside and inside tank was filled with expanded perlite insulation and also evacuated to reduce heat losses. The storage volume of the tank is 0.25 m^3. The inside tank was filled with 320 kg of dolerite rocks having an equivalent sphere diameter of 4-6cm. The storage tank was divided into six equal layers by baffles which have the objective of allowing even distribution of air flow through the rocks. 53kg of rocks were packed in each layer. The hot air entered through the inlet pipe from the top, flowed through the packed bed and exited at the bottom of the tank. Charging from the top allowed the exploitation of the buoyancy effect to create and maintain thermal stratification inside the packed bed, the hottest region being at the top. Locally available Dolerite rocks were used as the storage medium due to their high heat absorption properties.

Temperatures were recorded using K-thermocouples which were connected to an eDAQ system, of which 12 were located inside the packed bed of rocks at different vertical positions and at a distance of 6cm from the lateral wall. Two additional thermocouples measured hot air coming into the system and ambient air. The pressure drop through the rocks was measured using a pitot tube that was connected to a pressure sensor.

A detailed description of testing and designed experimental platform shown in Figure (3.2) is discussed in section 3.1.1 and 3.1.2.

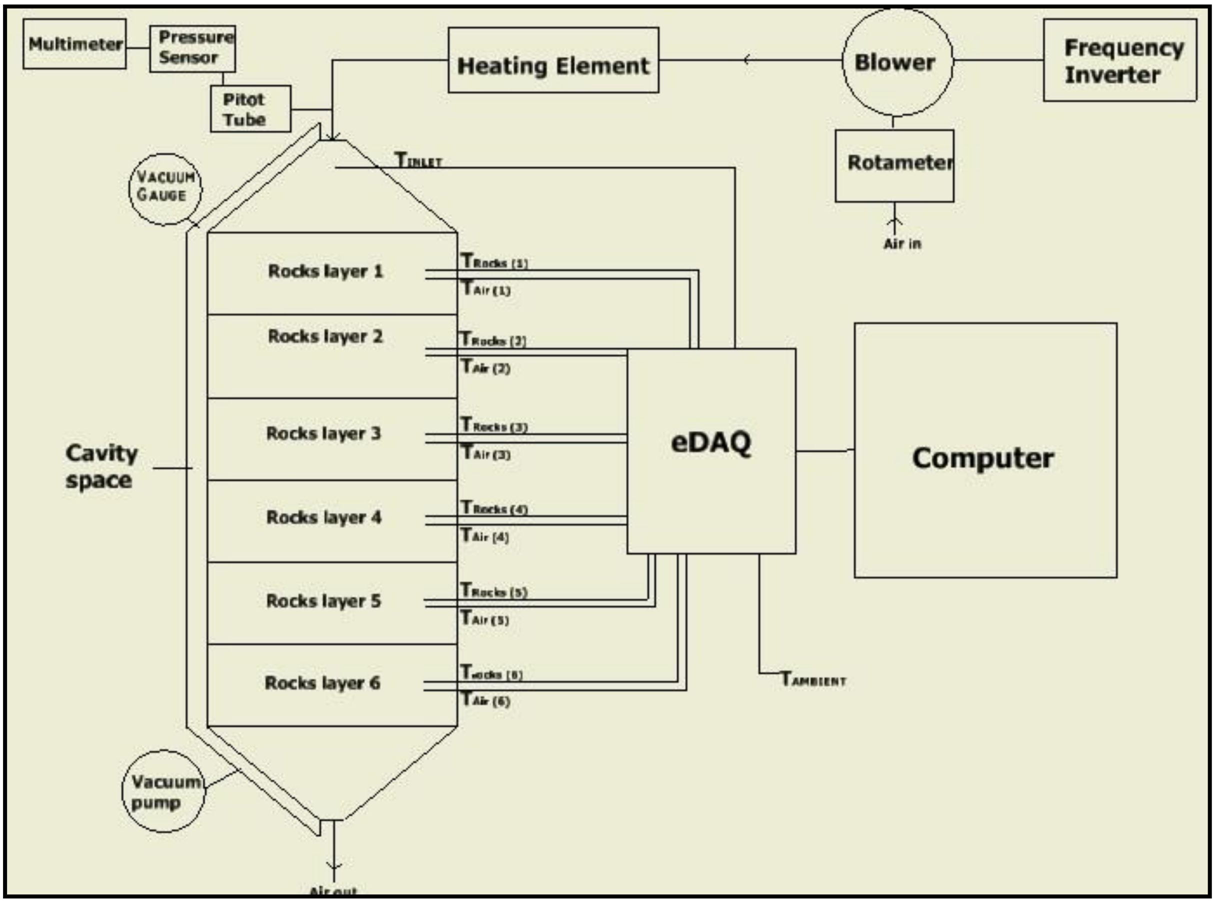

Figure 3.2: Flow diagram for the packed-bed rock storage tank.

3.2.1 THERMAL TEST

The two-step procedure, followed to test the rocks storage tank, will now be discussed in detail.

Step 1: Setting up the tank, packing of rocks and thermocouples mounting.

Expanded perlite grade M45 as seen in Figure (3.5) was filled in the cavity space between the inside and the outside tank. The layout of the tank is shown in Figure (3.3).
Dolerite rocks were packed in the inside tank as shown in Figure (3.1). The tank was divided into 6 equal layers by baffles that allow even air distribution on the rocks. 53 kg of rocks having equivalent diameter ranging from 4 cm to 6 cm were packed in

each layer. In the middle of each layer, 2 k-thermocouples were mounted at a distance of 6cm from the lateral wall so that one measures the air temperature and the second one, which was inserted into the rock by drilling a hole to the centre of the rock, measures the inside core temperature of the rocks. Figure (3.4) shows the thermocouples' mounting in the drum and Figure (3.6) shows the dolerite rocks and the baffles used. The rocks must be washed to remove all the dust before packing them because the dust can cause an increase in pressure drop.

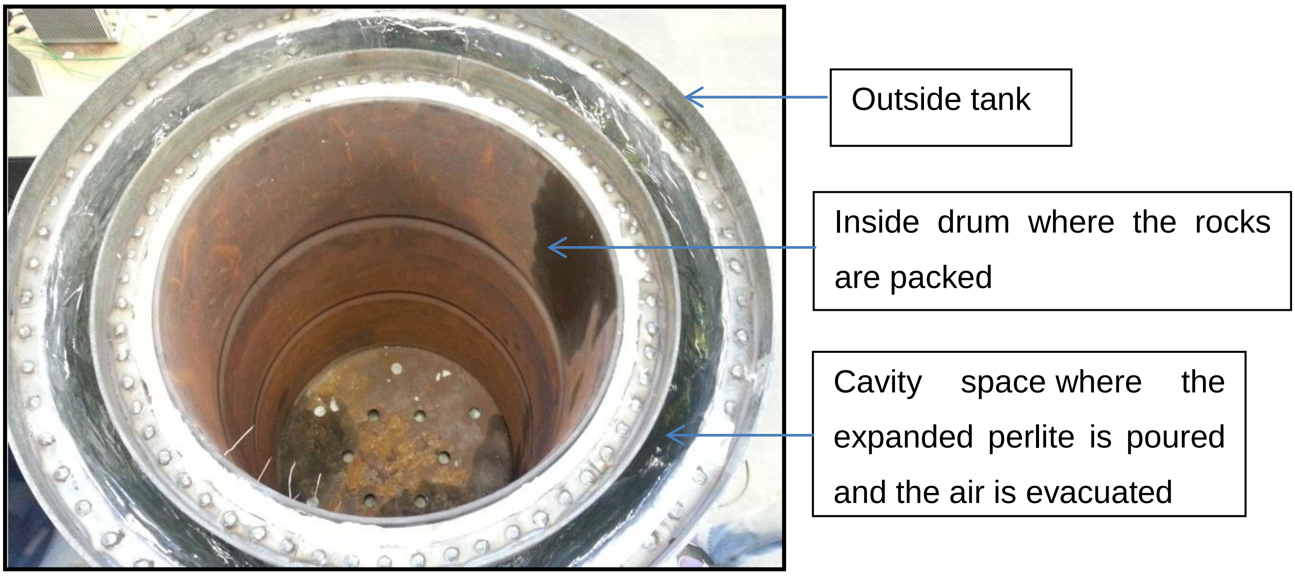

Figure 3.3: Storage tank layout

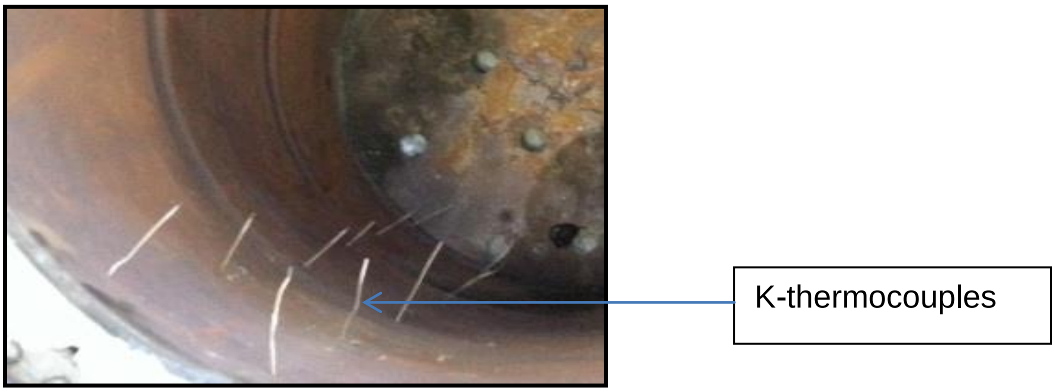

Figure 3.4: Thermocouples

Figure 3.5: Expanded perlite insulation powder

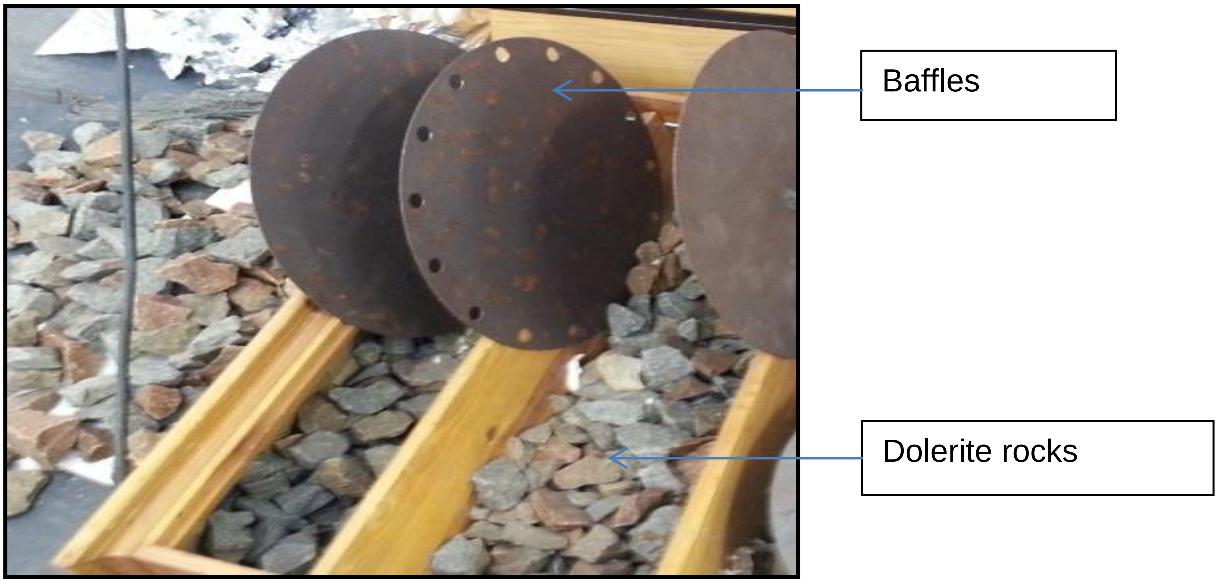

Figure 3.6: Dolerite rocks and baffles

Step 2: Test description and equipment used

A 6 kW electric heater was used to heat the air. A k-thermocouple was placed in the heating element shell and its temperature was controlled by an AC temperature controller. The choice of the electric heater was based on the amount of power that the parabolic trough collectors that was designed could produce. Figure (3.7) shows the electric heater.

Figure 3.7: Electric heater with temperature controller.

The hot air delivered by the heating element was pumped into the rocks using a centrifugal blower model K04-MS and type H80B/2 having a serial number of S8846 as seen in Figure (3.8). The selected blower has to overcome the pressure drop through the rocks and the collectors. This blower can handle a pressure drop of 12 kPa and its maximum power is 1.1 kW.

Figure 3.8: Model K04-MS Blower.

A micromaster 440 Siemens frequency inverter having a serial number of XAN419-000095 was used to control the blower and also the adjustment of air flow rate as seen in Figure (3.9).

A KI type rotameter was used to measure the air flow rate. The rotameter is screwed on the inlet pipe (cold side) of the blower because it does not withstand heat. Figure (3.10) shows the rota meter and where it was applied.

Figure 3.9: Micromaster 440 Siemens frequency controller.

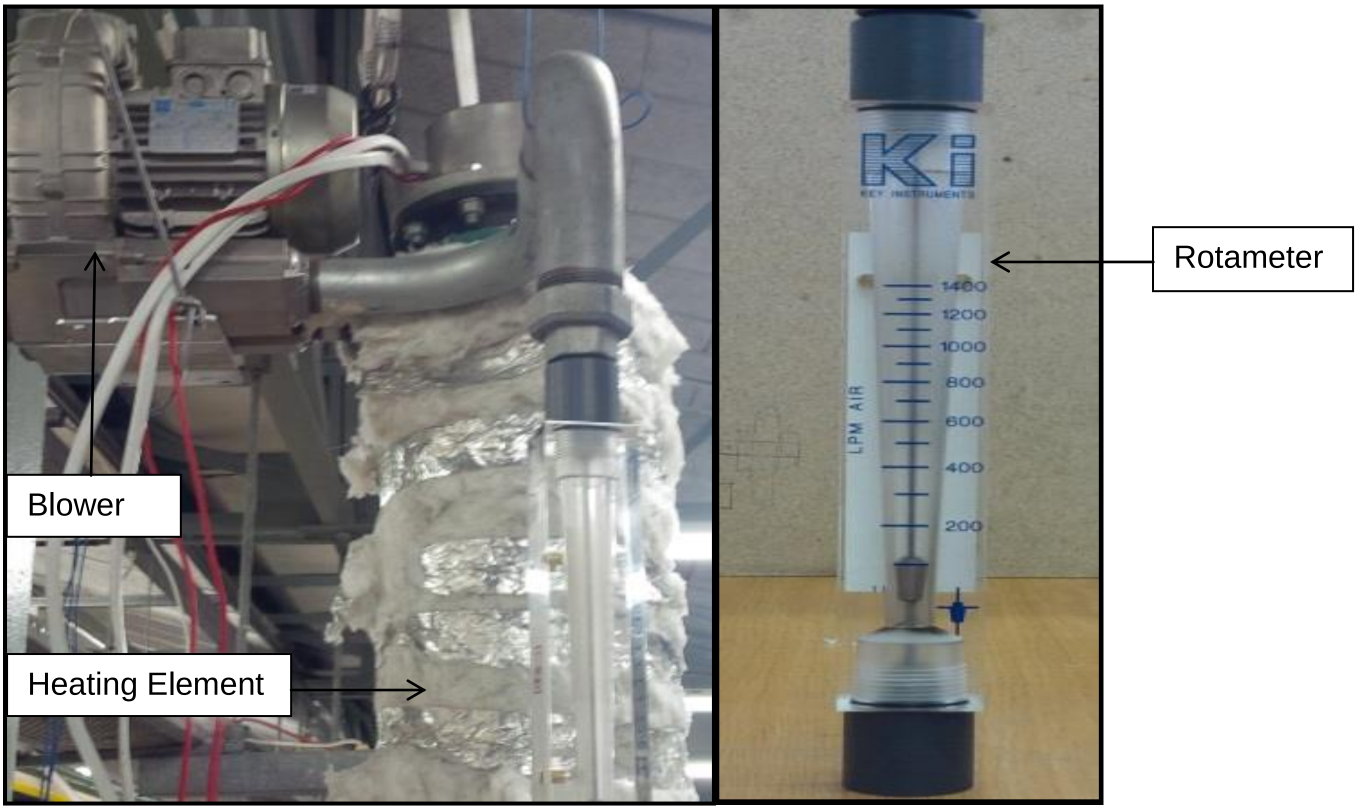

Figure 3.10: Rotameter and application.

A rotary vacuum pump, having a capacity of 1 kW, was used to draw the vacuum in the cavity space and vacuum gauge was used to monitor the vacuum level. The vacuum pump and the pressure gauge are shown in Figure (3.11).

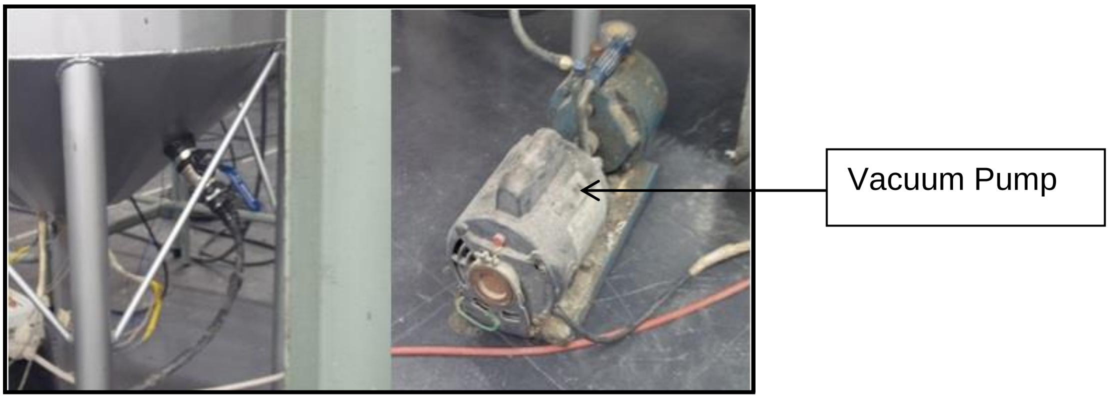

Figure 3.11: Vacuum pump and vacuum gauge.

The thermocouples were connected to an eDAQ logger. The eDAQ was connected to a computer and the temperatures recorded were displayed. Figure (3.12) shows the eDAQ logger and how it was connected.

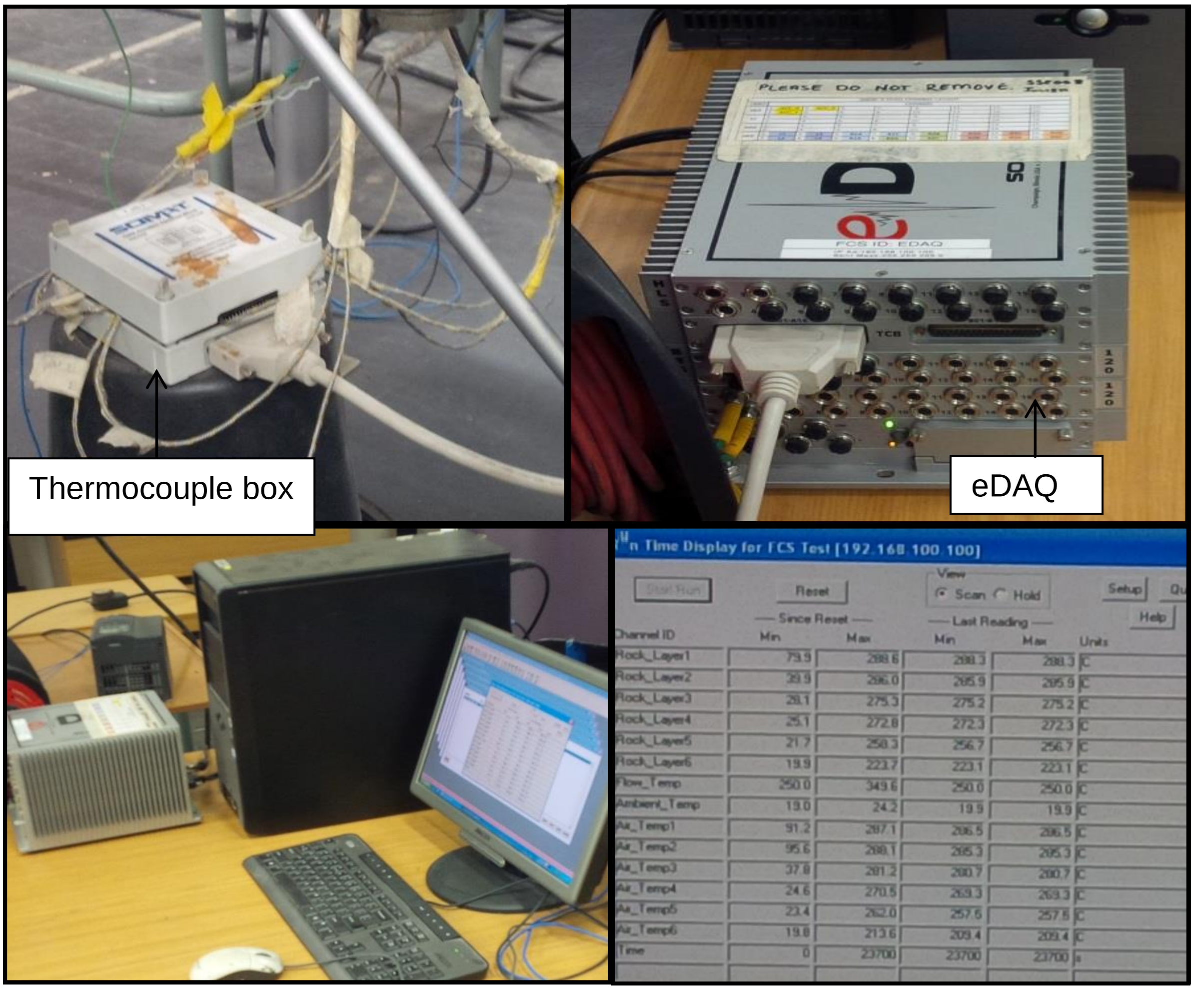

Figure 3.12: Temperature logging.

3.2.2 MEASURING PRESSURE DROP IN THE STORAGE TANK

The setup of the experimental platform to measure pressure drop in the tank is shown in Figure (3.15).

The pressure drop through the rocks was measured using a differential pressure transmitter PS-9101-8003 designed by Johnson controls as seen in Figure (3.13). The pressure sensor was connected to a power supply that was set to the operating voltage of the pressure sensor namely as indicated in Figure (3.14). The pressure sensor was also connected to a pitot tube inserted on the inlet pipe to the storage tank as shown in Figure (3.15). The pitot tube sensed the air pressure drop as air flow velocity was varied. The pressure sensor that was connected to a multimeter displayed a voltage reading converted to Pascal using the transmitter conversion.

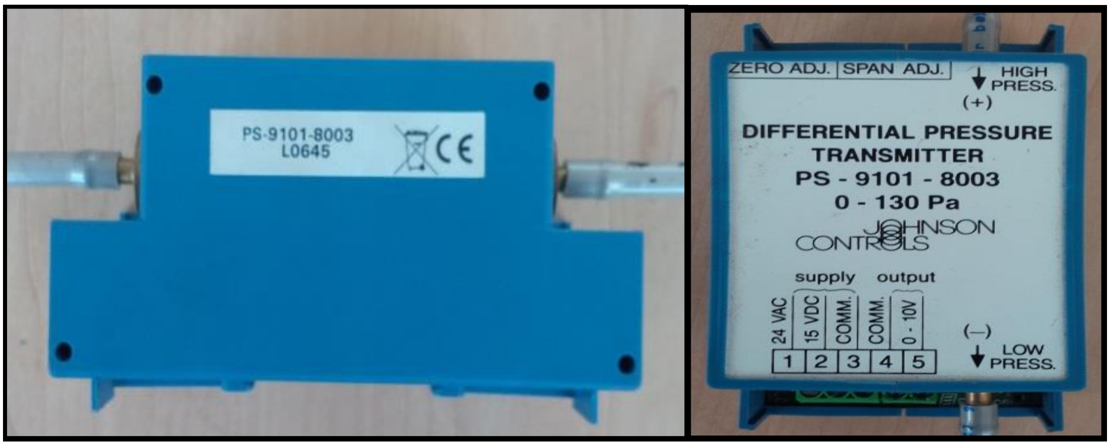

Figure 3.13: Pressure sensor.

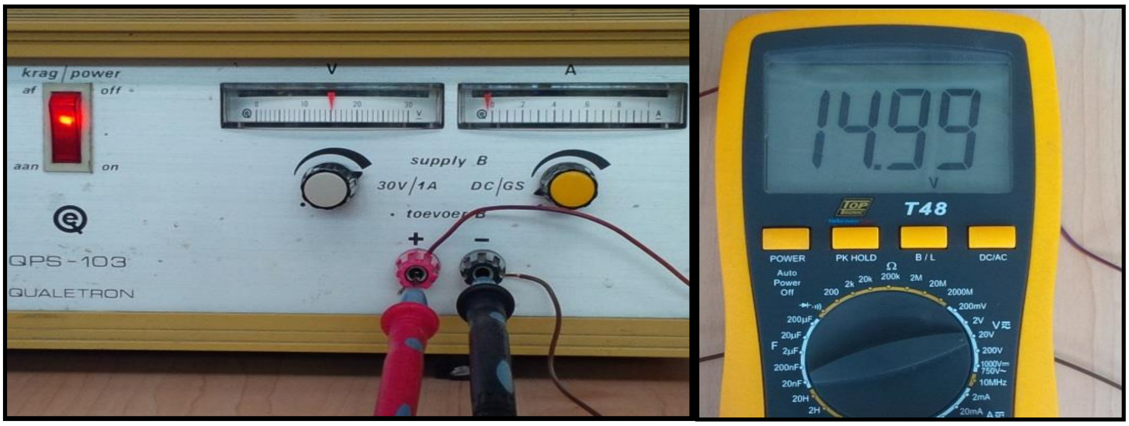

Figure 3.14: Power supply

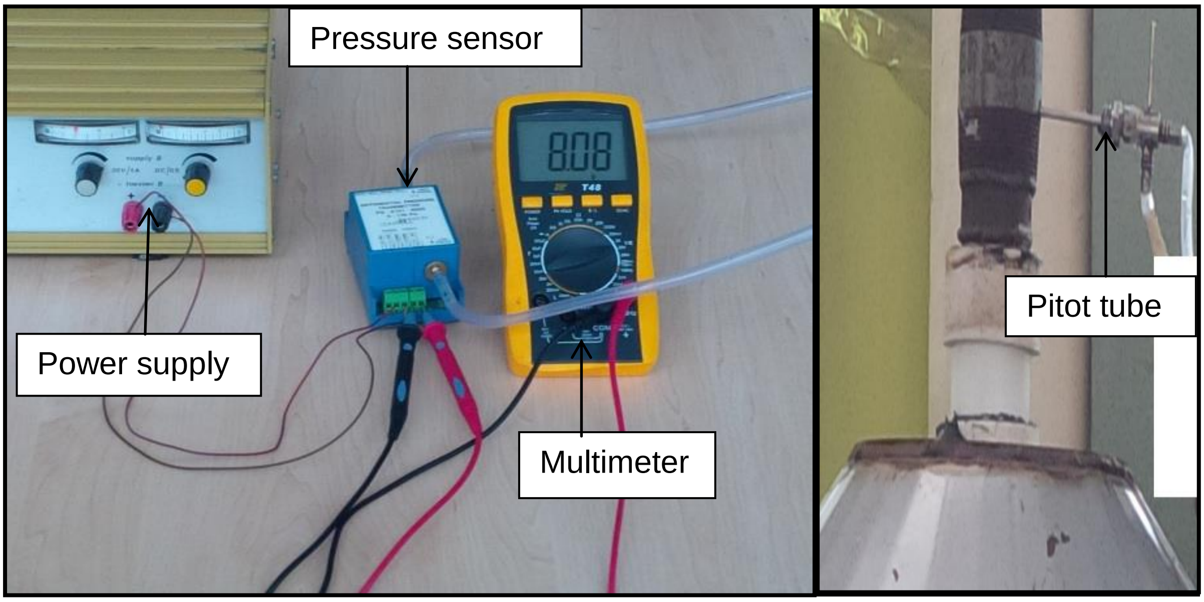

Figure 3.15: Pressure drop set up.

3.3 TESTING OF THE PARABOLIC TROUGH COLLECTOR:

Two parabolic trough collectors having a total aperture area of 7.2 m^2 were connected in series to heat the air. Ambient air was pumped through the system by a centrifugal pump that was controlled by a frequency inverter. Six type k-thermocouples were inserted at various locations across the collectors as depicted in Figure (3.16). The first thermocouple, which was placed before the rotameter, measured the ambient temperature; the second thermocouple measured the air entering the first collector; the third thermocouple measured the air exiting the first collector, the fourth thermocouple measured the air entering the second collector, the fifth thermocouple measured the air exiting the second collector and the sixth thermocouple measured the air exiting the system. The thermocouples were connected to an eDAQ logger which was connected to a computer that displayed the results. The collectors were faced perpendicular to the incoming solar radiation to focus the irradiation to a solar evacuated receiver tube which was placed at the focal line at the collectors. The Davis Pro 2 weather station shown in Figure (3.17) measured the radiation of the sun. The collectors tracked the position of the sun throughout a day.

The flow diagram of the parabolic trough collectors testing is shown in Figure (3.17).

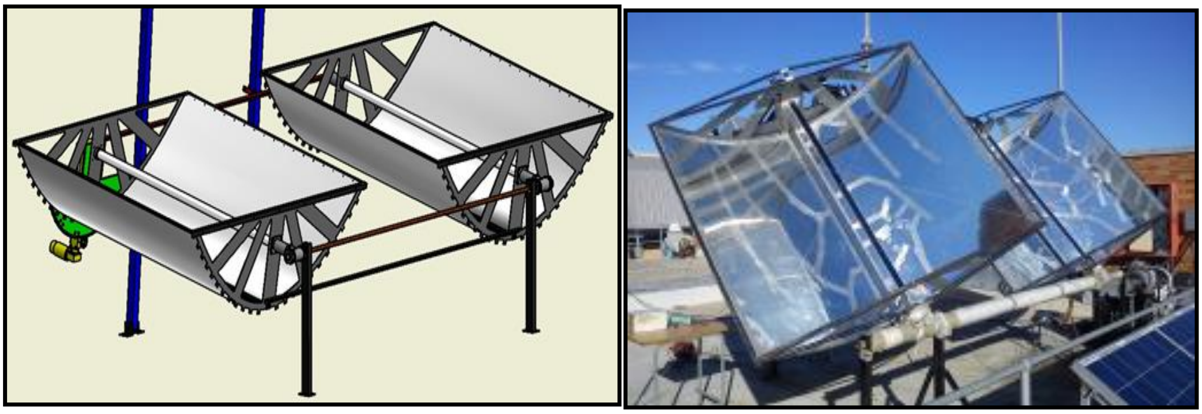

Figure 3.16: CAD and actual picture of the parabolic trough collectors.

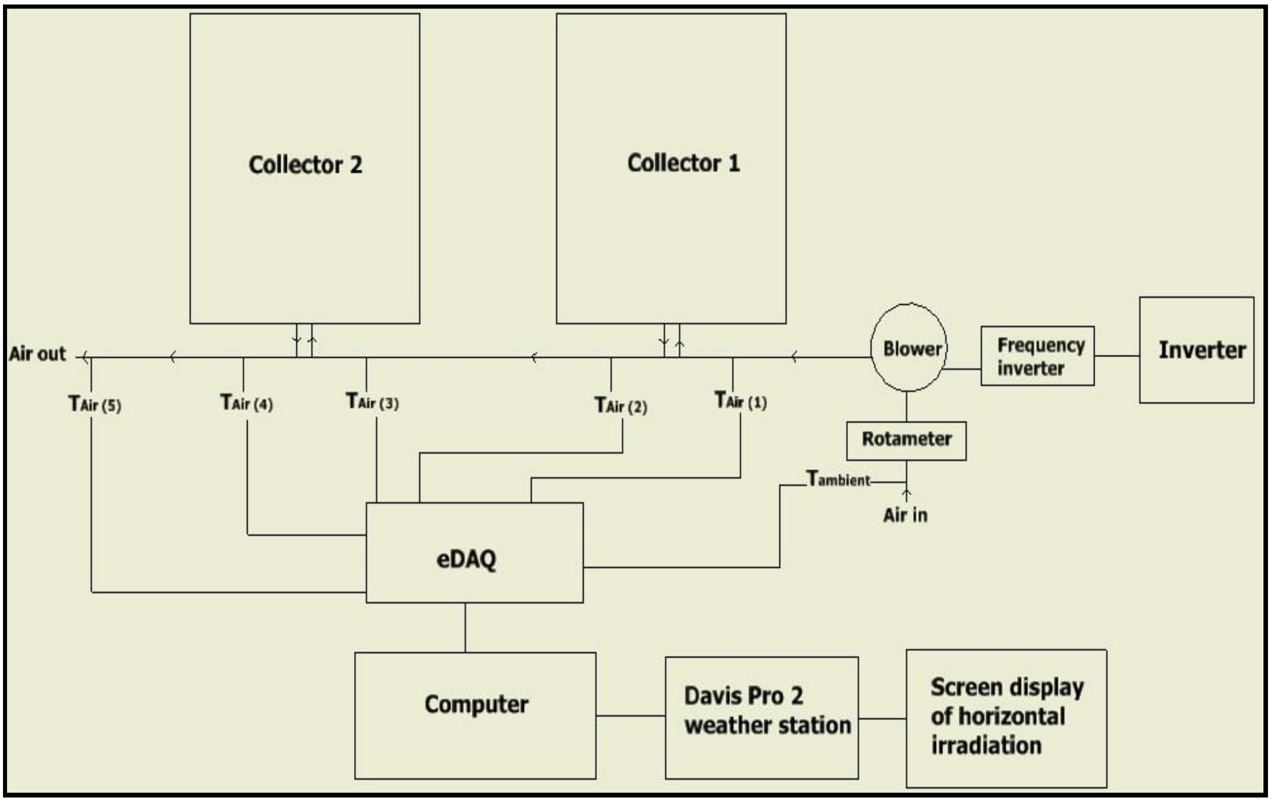

Figure 3.17: Flow diagram of Collectors test.

3.3.1 THERMAL TEST

The procedure followed to test the parabolic trough solar collector is discussed in this section:

Step1: Setting up the collectors

According to the month of the year in which testing took place, the collectors were tilted into the right position to obtain parallel rays of sunlight incident on the collectors. The collectors were cleaned before testing because the presence of dust would diffuse the reflectivity of the collector and alter the position of the focal point as required by the design for optimal use. Figure (3.16) shows the position of the collectors during the testing in the month of June

.

Step 2: Test description and equipment used

Ambient air is pumped through the collectors using the centrifugal pump Model K04-MS described in Figure (3.8). The micromaster 440 Siemens frequency inverter having a serial number of XAN419-000095 described in Figure (3.9) was used to control the blower and also the adjustment of air flow rate.

A KI type rotameter was used to measure the air flow rate. The rota meter was screwed on the inlet pipe (cold side) of the blower because it does not withstand heat as its operating temperature is 60 ^{0}C.

Six k-thermocouples were used to measure the temperature across the collectors.

The first k-thermocouples were mounted on the inlet of the blower to measure the ambient temperature. The second k-thermocouples measured the temperature of the exit air to the blower corresponding to the inlet temperature of the first collector. The third k-thermocouples measured the exit temperature of the first collector. The fourth k-thermocouples measured the inlet temperature to the second collector. The fifth k-thermocouples measured the exit temperature of the second collector and the last thermocouples measured the air exiting the system. The recorded results were logged using the eDAQ logger described in Figure (3.12). The eDAQ logger was connected to a computer that displayed and logged the recorded temperature. The horizontal solar irradiation was logged using Davis Pro 2 weather station as seen in Figure (3.18).

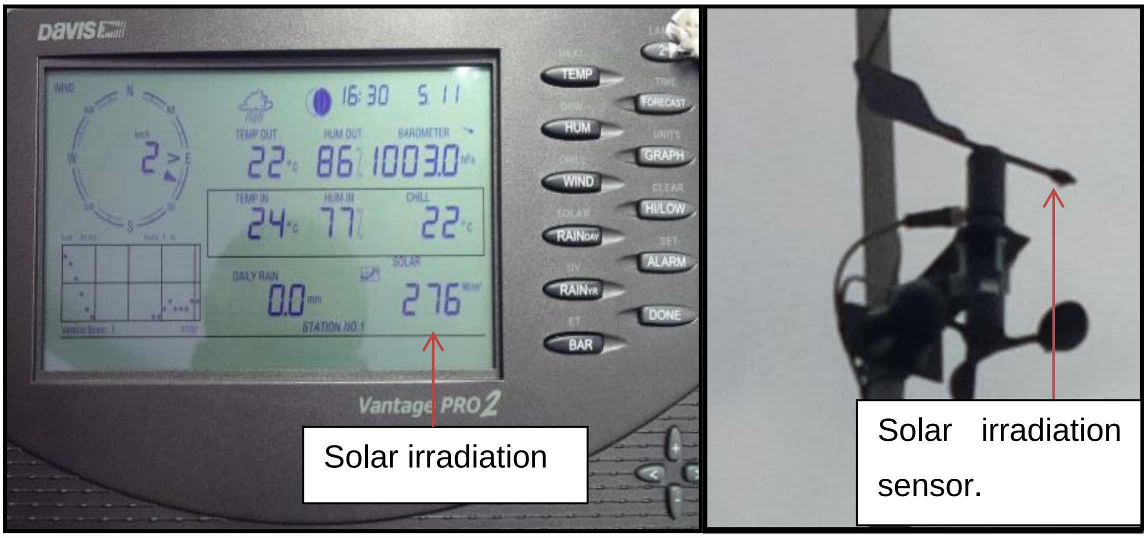

Figure 3.18: Davis Pro 2 weather station.

3.3.2 POWER DRAWN BY THE BLOWER TEST

The frequency inverter that controls the blower was connected to a 2 kW inverter. The inverter displayed the percentage of the power drawn when the blower was in use.

3.4 SUMMARY:

This chapter described the experimental set-up for experimental testing conducted on the packed rocks storage tank and the parabolic trough collectors. The experimental data obtained will be discussed in Chapter 7.

CHAPTER 4: NUMERICAL APPROACH PREDICTING THERMAL PERFORMANCE AND PRESSURE DROP OF THE PROPOSED VACUUM INSULATED ROCK BED STORAGE TANK

4.1 INTRODUCTION

The objective of this chapter is to discuss the details of the mathematical model used to predict the thermal performance and pressure drop during the charging cycle for packed-bed rock storage systems. Excel software was used to solve the numerical equations. The spreadsheet will be used as an operational manual to quantify any output requirement and also to optimise the performance of packed-bed rock storage systems by allowing the user to understand the behaviour of the system by varying the flow rate of air and rock size.

4.2 CONCEPT AND PARAMETERS USED IN THE SPREADSHEET DESIGN

Packed bed sensible heat storage consists of solid material of good heat capacity packed in a storage tank through which the heat transport fluid is circulated. Air was the heat transport fluid and dolerite rocks were used as the storage medium for this analysis. The hot air enters through the inlet pipe from the top, flows through the pack bed and exits at the bottom of the tank. Baffles are used to divide the bed into six equal horizontal layers in the air flow as shown in Figure (4.1). Each layer contains the same amount of rocks. The spreadsheet is designed to analyse each layer separately as a heat exchanger where the hot air entering that layer transfers energy to the rocks and the remaining hot air flows to the next layer to repeat the process till the air exits the tank. Thermal charging from the top allows the exploitation of the buoyancy effect to create and maintain thermal stratification inside the packed bed, the hottest region being at the top. The flow diagram of how the process works is shown in Figure (4.1). The hot air enters the first layer of rocks where it transfers part of its energy to the rocks and the remaining energy is tranferred to the adjacent layer and so on till the air exits the tank.

Assumptions made in the design of the spreadsheet :

- Heat loss to the surroundings is negligible due to effective insulation.
- All the rocks are in contact with the air due to the incorporation of the baffles therefore effective convection heat transfer.
- Temperature gradients within the rocks are not significant (Schumann assumption) [1]. This assumption is because the Biot number is less than 0.1. When the Biot number is greater than 0.1, The Jefferson (1972) factor must be used to take into consideration the temperature gradients across a layer [1].

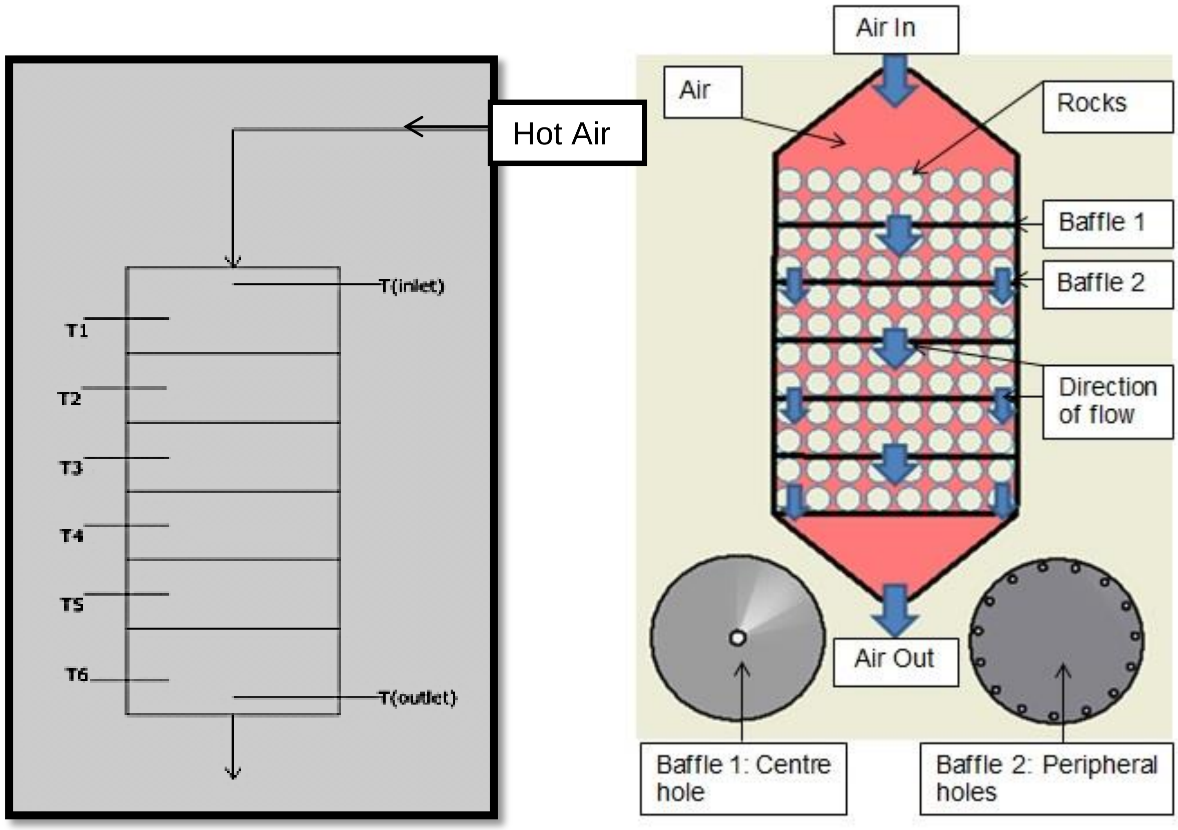

Figure 4.1: Flow diagram

The design of the rock bed system parameters used in the spreadsheet are listed in Table (4.1). The excel spreadsheet can be used for any other packed bed storage system by just replacing the design parameters.

Table 4.1: Operating parameters [1, 4, 18]:

Parameter	**Value**
Length of packed bed (L)	0.9m
Inside diameter of tank (D)	0.56m
Number of bed elements or layers (N)	6
Specific heat of dolerites (C_s)	1050 $J/kg.K$
Time interval (Δt)	60 s
Density of dolerites (ρ_s)	2800 kg/m^3
Specific heat of air (C_{pf})	1005 $J/kg.K$
Equivalent diameter of dolerites(D_e)	0.05 m (average)
Mass of dolerites (m)	320 kg

4.3 THEORY USED TO DEVELOP THE SPREASHEET

Research has been conducted on packed bed energy storage systems. The pressure drop and the coefficient of volumetric heat transfer between the air and the rock beds depend on the rock size and the air flow rate [14, 16]. The energy consumption by the blower to pump the air through the rocks is a significant expenditure in operating a rock bed energy storage system. The primary design objective of a packed-bed rock system is to have minimum energy consumption by the blower per unit of energy stored, therefore the design of the system should be based on thermo-hydraulic performance rather than the thermal performance alone [18]. An optimization factor which is defined as the ratio of the energy stored by the rocks divided by the power consumed by the fan to pump the air, is used to select an optimum rock size. The optimum rocks must reduce the pressure drop in the rock system while storing efficiently the energy. The rocks that were used in this dissertation are crushed dolerite rocks. The size of the rock will be varied using the developed mathematical to obtain the optimum rock size. The optimum rock size will be selected for the experimental test to verify the mathematical model. The heat transfer coefficient and friction factor correlations are commonly used to predict the performance of a packed bed storage system. Many correlations were found to get these properties as reported in the literature [1, 13].

The correlations that were used in the development of the spreadsheet were based on Shewen et al recommendations [1] and will be discussed in the following sections.

4.3.1 PRESSURE DROP

When dealing with pressure drop prediction, different types of models were achieved [18]. In this research the rocks that are investigated are crushed dolerite rocks, whose specific properties are not easily quantified such as the shape factor, void fraction and the sphericity. These factors are used in most correlations developed for pressure drop predictions. Shewen et al. (1978) recommended the equation of Dunkle and Ellul (1972) when measurements of the void fraction (ε) and the surface area shape factor (α) of the rock are not known, this is the method that was used in the pressure drop prediction in this research [1,18].

$$\Delta p = \frac{LG_\circ^2}{\rho_{air} D_e}\left(21 + 1750\frac{\mu}{G_\circ D_e}\right) \tag{4.1}$$

Where $G_\circ$ is the mass velocity (air mass flow rate divided by the bed frontal area), L is the length of the bed in the air flow direction and D_e is the average particle diameter (diameter of a spherical particle having the same volume as the rock sample) from which it is calculated [1]:

$$D_e = \left(\frac{6m}{\pi \rho_{rock} n}\right) \tag{4.2}$$

Where (m) represents the mass of rocks and n the number of rocks sample.

4.3.2 THERMAL ANALYIS

The method pursued in this research for the prediction of the thermal energy is the Effectiveness NTU method of Hughes (1975) which was recommended by Duffie and Beckmann (1991) [1]. In his thesis Kenneth Guy Allen found that the NTU-method correlates well with the measured results. The difference in the prediction and actual results was about 15 % [18]. As discussed in Chapter 2, the use of baffles in the storage tank to reduce the problem of the wall effect will lead to a better agreement between the experimental and the predicted results.

4.3.2.1 VOLUMETRIC HEAT TRANSFER COEFFICIENT

It describes the ability of a given volume of rocks to store internal energy while undergoing a temperature change and is used to compute the number of transfer units (NTU) from the air to the rocks. Shewen et al. recommend the Lof and Hamley (1948) equation [1, 18]:

$$h_v = 650\left(\frac{G_\circ}{D_e}\right)^{0.7} \tag{4.3}$$

Where $G_\circ$ is the mass velocity, D is the average particle diameter h_v the volumetric heat transfer coefficient.

4.3.2.2 THE EFFECTIVENESS-NTU METHOD OF HUGHES

The “Effectiveness-NTU” numerical method developed by Hughes (1975) for solar system simulation was used in this analysis to predict the thermal performance of the packed bed storage [1].

In this approach the bed is divided into N segments of length Δx as shown in Figure (4.2). The bed temperature is considered to be uniform across each segment. The air temperature is assumed to have an exponential profile and the air temperature leaving the bed element i is found from the ”effectiveness-NTU” equation of a heat exchanger operating as an evaporator (Duffie and Beckman , 2006) [1].

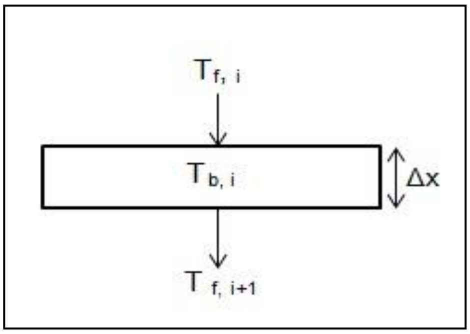

Figure 4.2: Packed bed divided into N segments [1].

The working fluid temperature is given by equation (4.4) [1, 18]:

$$T_{f,i+1} = T_{f,i} - (T_{f,i} - T_{b,i})(1 - e^{-\phi}) \tag{4.4}$$

Where:

$$\phi = \frac{NTU}{N} \;; \tag{4.5}$$

$$NTU = \frac{h_v AL}{\left(\dot{m} c_p\right)_f} \;; \tag{4.6}$$

$$N = \frac{L}{\Delta x} \;; \tag{4.7}$$

As the " NTU "is applied for the whole system, it is divided by N to give the " NTU "that applies to a single segment.

An energy balance on the rock within the region Δx in Figure (4.2) can then be expressed by equation (4.8) [1, 18]:

$$m_{seg} C_s \frac{dT_b}{dt} = \dot{m}_f \, C_{pf} \, (T_{f,i} - T_{b,i})(1 - e^{-\phi}) \tag{4.8}$$

Where m_{seg} is the mass of solid within the region Δx . Rearranging the equation and expression the segment mass with respect to the total mass, we have equation (4.9) [1, 18]:

$$\frac{dT_b}{dt} = N \frac{\dot{m}_f \, C_f}{m_s C_s} (T_{f,i} - T_{b,i})(1 - e^{-\phi}) \tag{4.9}$$

To solve equations (4.8) and (4.9): The process starts at node 1 so that the inlet temperature is known. A new bed temperature is calculated from equation (4.9) and an outlet temperature from equation (4.8). The new fluid temperature becomes the inlet temperature to node (2) in this iterative calculation.

4.3.3 GENERAL EQUATIONS USED TO ANALYSE THE RESULTS

The mass flow rate of the air:

$$\dot{m} = \dot{V} \times \rho \tag{4.10}$$

Energy supply by the heating element:

$$Q_{Supply} = \dot{m} C_p \times (T_{\text{Air in}} - T_{ambient}) \tag{4.11}$$

Energy absorbed by the rocks:

$$Q_{Ansorbed} = \dot{m} C_p \times (T_{Air\,in} - T_{Air\,out}) \tag{4.12}$$

Energy dumped by the storage tank:

$$Q_{Dumped} = \dot{m} C_p \times (T_{Air\,out} - T_{ambient}) \tag{4.13}$$

Energy stored by the rocks:

$$Q_{Stored\ \text{by rocks}} = m_{Rocks} C_{p(rocks)} \times (T_{rocks} - T_{ambient}) \tag{4.14}$$

As the tank is divided into six different sections where heat stratification is recorded, the total stored energy is the sum of the energy stored by all the layers.

4.4 DEVELOPMENT OF THE SPREADSHEET

4.4.1 SAMPLES CALCULATION FROM THE SPREADSHEET:

The heat transport fluid is air and the storage material is crushed dolerite rocks. Each layer carries 53 kg of dolerite. Hot air at temperature ‘T_a’ enters layer ‘m’ which contains dolerites at temperature ‘T_b’, transfer the hot energy to the rocks and leaves at temperature ‘$T_{a,m+1}$’ where $T_a < T_{a,m+1}$. The schematic of the scenario is shown in Figure (4.3).

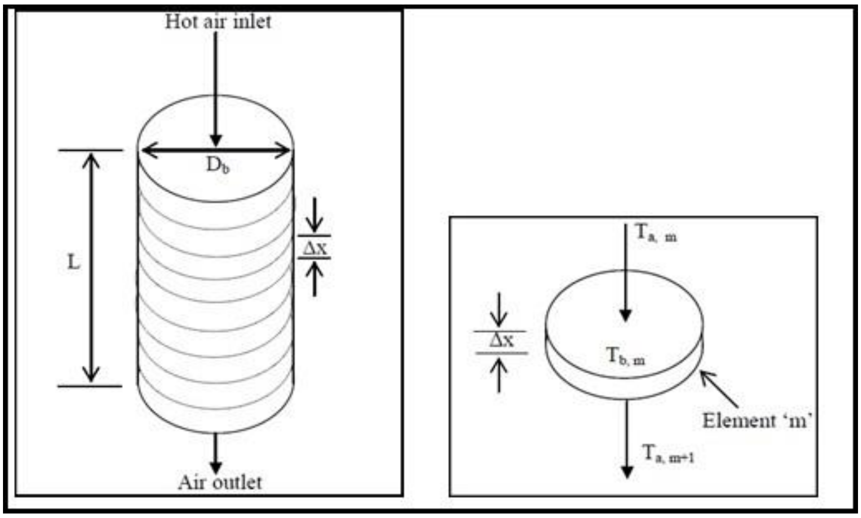

Figure 4.3: Packed bed and element 'm' of a packed bed [12].

4.4.1.1 CALCULATION OF THE PRESSURE DROP AND THE HEAT TRANSFER PARAMETERS:

The pressure drop and the heat transfer parameters are computed to see the effect of mass flow rates and rocks size applying the proposed equations. The results are shown in Table (4.2**).**

Table 4.2: Pressure drop and heat transfer parameters.

	5 l/s	10 l/s	10l/s
Mass flow(Kg/s)	**0.00602**	**0.01204**	**0.01204**
Mass velocity(Kg/m^2.s)	**0.0244715**	**0.048943**	**0.048943**
volumetric efficiency	**394.18248**	**640.3513**	**915.614**
rock size (m)	**0.05**	**0.05**	**0.03**
NTU	**14.442477**	**11.73094**	**16.774**
φ	**2.4070795**	**1.955156**	**2.795**
Pressure drop (Pa)	**1.10**	**2.95**	**6.53**

4.4.1.2 CALCULATION OF THE BED AND FLUID TEMPERATURES:

At initial condition (t=0), the temperature of the rocks was assumed to be $T_b = 20°C$. The predictions were made assuming the heating element delivered a constant temperature of 300°C throughout the duration of the test. The time internal for the recording of the results was 60s.

To solve equations (4.4) and (4.9) to determine the temperature at the inlet, outlet and the bed temperature of each Δx segment: The process starts at node 1 so that the inlet temperature is known. A new bed temperature is calculated from equation (4.9) and an outlet temperature from equation (4.4). The new fluid temperature becomes the inlet temperature to node (2).

Table **(**4.3) shows a sample computation of the temperature profile for the first two layers at a flow rate of 10 l/s.

Table 4.3: Air and Rocks temperatures for the first two layers.

Layer 1			
Bed Temp (^{0}C)	**Exit Temp(1) &Inlet(2) (^{o}C)**	**Inlet Temp (^{0}C)**	**Time (s)**
20	**0**	**0**	**0**
21.3566	**41.9519**	**250**	**60**
22.7052	**43.1791**	**250**	**120**

Layer 2		
Bed Temp (^{o}C)	**Exit Temp(2) &Inlet(3) (^{o}C)**	**Time (s)**
20	**0**	**0**
20.129	**22.09517**	**60**
20.266	**22.32941**	**120**

4.4.2 OPERATION OF SPREADSHEET

The operation of the spreadsheet is shown in the flow diagram in Figure (4.4).

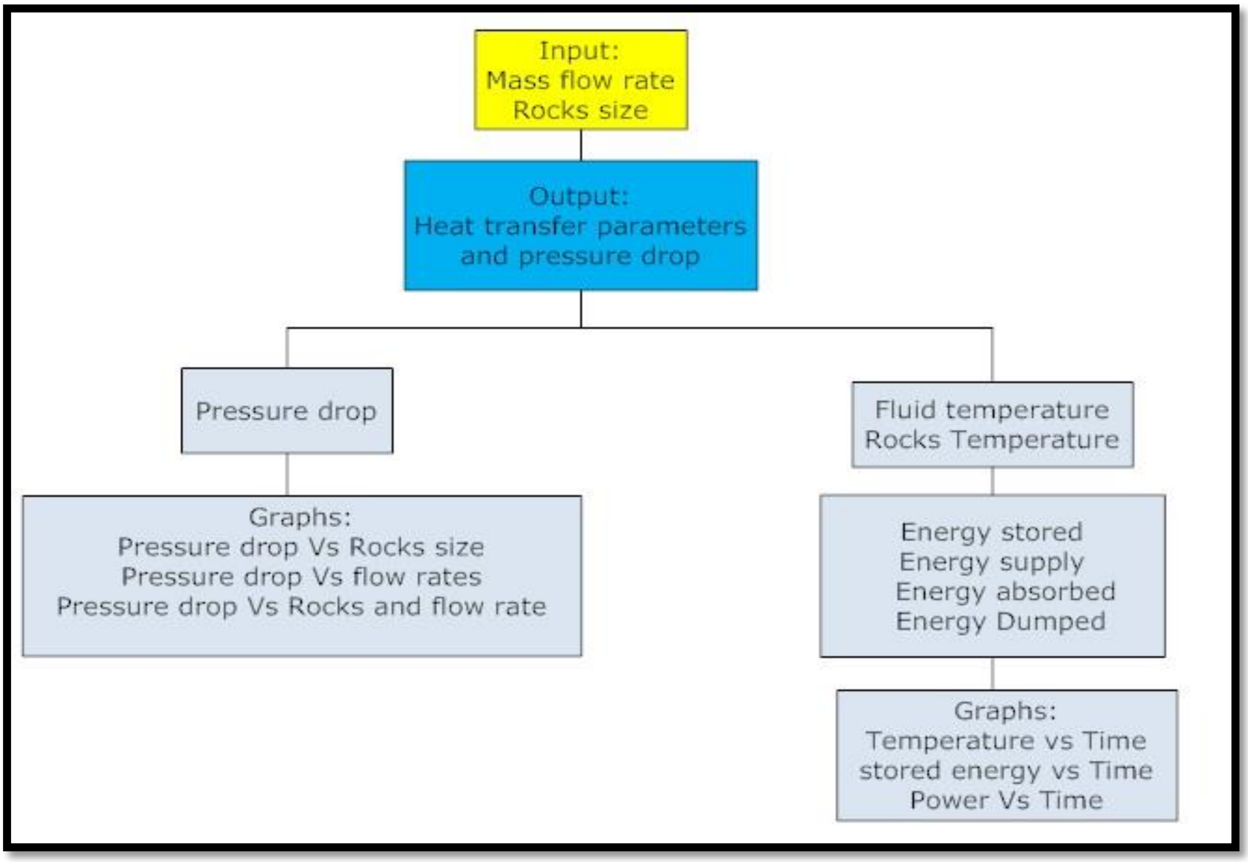

Figure 4.4: Flow diagram of spreadsheet operation.

- PRESSURE DROP: Tab (4 and 5) of the spreadsheet gives information on the pressure drop through the rocks.

This tab gives information on the pressure drop though the packed-bed rock. It shows the relationship between pressure drop and rocks size and also the variation of pressure drop at different flow rates. The user will only input rocks size and flow rates and the pressure drop will be displayed. Graphs showing the variation of pressure drop with rocks size, flow rates and also a combination of the two will be displayed as shown in Figures (4.5 and 4.6).

Mass velocity(Kg/m^2.s)	Pressure drop (Pa)
0.01	0.216885246
0.02	0.522295082
0.03	0.916229508
0.04	1.398688525
0.05	1.969672131
0.06	2.629180328
0.07	3.377213115
0.08	4.213770492
0.09	5.138852459
0.1	6.152459016
0.11	7.254590164
0.12	8.445245902
0.13	9.72442623
0.14	11.09213115
0.15	12.54836066
0.16	14.09311475
0.17	15.72639344
0.18	17.44819672
0.19	19.25852459
0.2	21.15737705
0.21	23.1447541
0.22	25.22065574
0.23	27.38508197
0.24	29.63803279
0.25	31.9795082

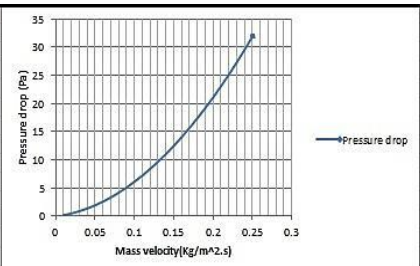

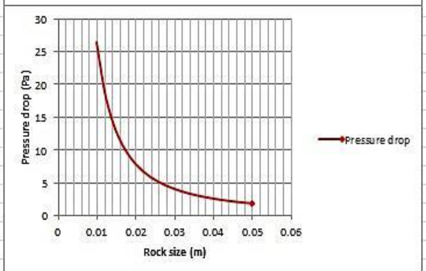

Rock size (m)	Pressure drop (Pa)
0.01	26.42310393
0.012	19.0856767
0.014	14.56308417
0.016	11.56402949
0.018	9.464254948
0.02	7.93111414
0.022	6.773703943
0.024	5.875867641
0.026	5.163501204
0.028	4.587441156
0.03	4.113978799
0.032	3.719343722
0.034	3.386362478
0.036	3.102362713
0.038	2.857817957
0.04	2.645447614
0.042	2.459605008
0.044	2.295852421
0.046	2.150660368
0.048	2.021191142
0.05	1.905140578

Mass flow(Kg/s)	0.01204	Input 1
Mass velocity(Kg/m^2.s	0.04894309	
volumetric efficiency	640.351335	
rock size (m)	0.05	Input 2
NTU	11.7309367	
ϕ	1.95515612	
Pressure drop (Pa)	1.90514058	

NB: Only inputs can be change in the spredsheets

Figure 4.5: Screen shot of Pressure drop vs Flow rates & Pressure drop vs Rocks size

Mass velocity(Kg/m^2.s)	Pressure drop (Pa)		
	0.05 m	0.04 m	0.03 m
0.01	0.21689	0.32505	0.55328
0.02	0.5223	0.76076	1.2541
0.03	0.91623	1.30712	2.10246
0.04	1.39869	1.96414	3.09836
0.05	1.96967	2.73181	4.2418
0.06	2.62918	3.61014	5.53279
0.07	3.37721	4.59913	6.97131
0.08	4.21377	5.69877	8.55738
0.09	5.13885	6.90907	10.291
0.1	6.15246	8.23002	12.1721
0.11	7.25459	9.66163	14.2008
0.12	8.44525	11.2039	16.377
0.13	9.72443	12.8568	18.7008
0.14	11.0921	14.6204	21.1721
0.15	12.5484	16.4946	23.791
0.16	14.0931	18.4795	26.5574
0.17	15.7264	20.5751	29.4713
0.18	17.4482	22.7813	32.5328
0.19	19.2585	25.0981	35.7418
0.2	21.1574	27.5256	39.0984
0.21	23.1448	30.0638	42.6025
0.22	25.2207	32.7126	46.2541
0.23	27.3851	35.4721	50.0533
0.24	29.638	38.3422	54
0.25	31.9795	41.323	58.0943

Mass flow(Kg/s)	0.01204		
Mass velocity(Kg/m^2.s)	0.048943		
volumetric efficiency	640.3513		
rock size (m)	0.05	0.04	0.03
NTU	11.73094		
ϕ	1.955156		
Pressure drop (Pa)	1.905141		

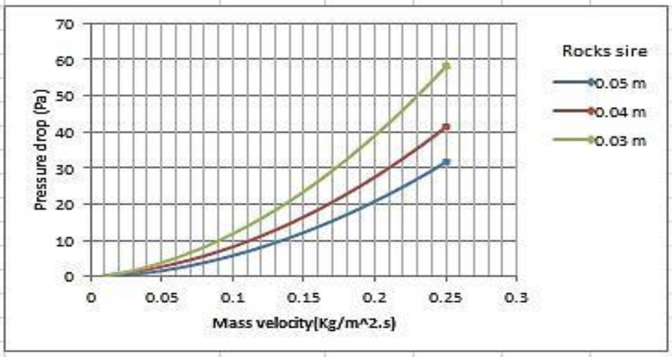

Figure 4.6: Screen shot of Pressure drop vs Flow rate & Rocks size

- THERMAL PERFORMANCE: Tab (2 and 3) of the spreadsheet gives information on the thermal performance.

The thermal analyses of the packed-bed rock during the charging cycle are performed in this tab.

This analysis consists of three stages of computation, namely:

Step 1: Computation of the heat transfer and pressure drop parameters

Step 2: Computation of the inlet and output temperature across each layer and the energy stored

Step 3: Computation of the total energy stored and the thermal energy analysis over the entire tank.

These steps will now be discussed in the following sections:

Step 1: Heat transfer and pressure drop parameters

The user is required to insert two inputs namely the rocks' size and the flow rate. The temperature of the air entering and exiting each layer and the average temperature of the rocks across the same layer will be computed for the duration of the charging cycle. Table (4.4) shows the input required and the properties used to compute the pressure drop and the temperature profiles.

Table 4.4: Screen shot of Heat transfer parameters and pressure drop table.

Mass flow(Kg/s)	0.01204	←	Input 1
Mass velocity(Kg/m^2.s)	0.048943089		
volumetric efficiency	640.3513353		
rock size (m)	0.05	←	Input 2
NTU	11.73093672		
ϕ	1.95515612		
Pressure drop (Pa)	1.905140578		
NB: Only inputs can be change in the spredsheets			

Step 2: Computation of the inlet and output temperature across each layer and the energy stored

The temperature profile and the thermal energy stored across each layer are computed for the duration of the charging cycle. Figure (4.7) shows a screen print temperature profile of the rocks and air and the thermal energy stored across the six layers for a set period of charging cycle.

Layer 1				
Bed Temp	Exit Temp(1)&Inlet(2)	Inlet Temp	Time(s)	Energy stored (MJ)
20	0	0	0	0
23.116185	62.30646619	300	60	0.173415694
26.197689	64.95181268	300	120	0.344901404
29.244899	67.5677185	300	180	0.51447861
32.258195	70.1545113	300	240	0.682168552
35.237956	72.71251508	300	300	0.847992234
38.184554	75.24205024	300	360	1.011970426
41.098359	77.74343362	300	420	1.174123666
43.979735	80.21697853	300	480	1.334472265
46.829044	82.66299477	300	540	1.493036307
49.646642	85.08178874	300	600	1.649835653
52.432883	87.47366338	300	660	1.804889944
55.188115	89.8389183	300	720	1.958218598
57.912683	92.17784975	300	780	2.109840823
60.606929	94.49075068	300	840	2.259775609
63.27119	96.77791081	300	900	2.408041735
65.9058	99.0396166	300	960	2.554657774
68.511089	101.2761513	300	1020	2.699642089
71.087383	103.4877952	300	1080	2.843012839
73.635004	105.6748251	300	1140	2.984787984
76.154273	107.8375151	300	1200	3.124985279
78.645504	109.9761359	300	1260	3.263622287
81.109009	112.0909556	300	1320	3.400716371
83.545098	114.182239	300	1380	3.536284703
85.954075	116.250248	300	1440	3.670344264
88.336242	118.2952416	300	1500	3.802911845
90.691897	120.317476	300	1560	3.93400405
93.021335	122.3172045	300	1620	4.0636373
95.324849	124.2946776	300	1680	4.191827831

Layer 2			
Bed Temp	Exit Temp(2)&Inlet(3)	Time(s)	Energy stored (MJ)
20	0	0	0
20.4708	26.39227529	60	0.026202161
20.9659	27.19167002	120	0.053751086
21.4845	28.00716045	180	0.082613553
22.0262	28.8382893	240	0.112756911
22.5903	29.68460748	300	0.144149075
23.1763	30.54567396	360	0.176758515
23.7835	31.42105563	420	0.210554249
24.4116	32.31032721	480	0.245505832
25.0599	33.2130711	540	0.28158335
25.7279	34.1288773	600	0.318757413
26.4151	35.05734323	660	0.356999146
27.1209	35.99807368	720	0.396280178
27.845	36.95068066	780	0.436572641
28.5867	37.9147833	840	0.477849156
29.3456	38.89000774	900	0.520082828
30.1212	39.875987	960	0.563247241
30.9131	40.87236091	1020	0.607316447
31.7208	41.87877598	1080	0.65226496
32.5439	42.89488529	1140	0.698067749
33.3819	43.92034842	1200	0.744700232
34.2343	44.9548313	1260	0.792138269
35.1008	45.99800615	1320	0.840358154
35.9809	47.04955139	1380	0.889336607
36.8742	48.10915147	1440	0.939050772
37.7804	49.17649688	1500	0.989478206
38.699	50.25128398	1560	1.040596876
39.6296	51.33321491	1620	1.09238515
40.5718	52.42199755	1680	1.144821791

Layer 3			
Bed Temp	Exit Temp(3)&Inlet(4)	Time(s)	Energy stored (MJ)
20	0	0	0
20.0711	20.96583778	60	0.003959003
20.1504	21.14701403	120	0.008369044
20.2378	21.33750254	180	0.013235072
20.3335	21.53730973	240	0.018561697
20.4376	21.74643807	300	0.024353202
20.5501	21.96488622	360	0.030613546
20.6711	22.19264918	420	0.037346377
20.8006	22.42971832	480	0.04455504
20.9388	22.67608156	540	0.052242584
21.0856	22.93172347	600	0.060411768
21.2411	23.19662531	660	0.069065073
21.4053	23.47076521	720	0.078204707
21.5783	23.75411823	780	0.087832613
21.7601	24.04665646	840	0.097950477
21.9508	24.34834913	900	0.108559734
22.1503	24.65916269	960	0.119661576
22.3586	24.9790609	1020	0.13125696
22.5759	25.30800493	1080	0.14334661
22.802	25.64595343	1140	0.155931031
23.037	25.99286266	1200	0.169010509
23.281	26.3486865	1260	0.182585121
23.5338	26.71337661	1320	0.19665474
23.7955	27.08688246	1380	0.211219041
24.0661	27.4691514	1440	0.226277506
24.3455	27.86012879	1500	0.241829435
24.6339	28.25975804	1560	0.257873942
24.931	28.66798068	1620	0.274409972
25.237	29.08473642	1680	0.291436297

Layer 4			
Bed Temp	Exit Temp(4)&Inlet(5)	Time(s)	Energy stored (MJ)
20	0	0	0
20.0107	20.1459328	60	0.000598184
20.0234	20.18243245	120	0.00130192
20.038	20.22194927	180	0.002115802
20.0547	20.2645543	240	0.003044375
20.0735	20.31031723	300	0.004092135
20.0946	20.35930647	360	0.005263529
20.1179	20.41158908	420	0.006562949
20.1437	20.46723076	480	0.007994735
20.1718	20.52629587	540	0.009563168
20.2026	20.58884743	600	0.011272476
20.2359	20.65494706	660	0.013126828
20.2719	20.72465502	720	0.015130324
20.3106	20.79803021	780	0.017287018
20.3522	20.87513012	840	0.01960089
20.3967	20.95601088	900	0.022075861
20.4441	21.04072723	960	0.024715788
20.4946	21.1293325	1020	0.02752446
20.5482	21.22187867	1080	0.030505603
20.6049	21.31841628	1140	0.033662874
20.6649	21.41899453	1200	0.036999862
20.7281	21.5236612	1260	0.040520089
20.7947	21.63246271	1320	0.044227006
20.8648	21.74544406	1380	0.048123996
20.9383	21.86264892	1440	0.05221437
21.0153	21.98411953	1500	0.05650137
21.0959	22.10989679	1560	0.060988167
21.1802	22.24002022	1620	0.065677858
21.2682	22.374528	1680	0.07057347

Layer 5			
Bed Temp	Exit Temp(5)&Inlet(6)	Time(s)	Energy stored (MJ)
20	0	0	0
20.0016	20.02204965	60	9.03823E-05
20.0036	20.02894327	120	0.000202364
20.0061	20.03662226	180	0.000337575
20.0089	20.04512219	240	0.000497667
20.0123	20.05447883	300	0.000684321
20.0162	20.06472812	360	0.000899239
20.0206	20.07590617	420	0.001144145
20.0255	20.08804922	480	0.001420787
20.0311	20.10119363	540	0.001730932
20.0373	20.11537589	600	0.002076366
20.0442	20.13063256	660	0.002458893
20.0518	20.14700027	720	0.002880337
20.0601	20.16451571	780	0.003342534
20.0691	20.18321561	840	0.003847339
20.079	20.20313673	900	0.004396619
20.0897	20.22431582	960	0.004992254
20.1013	20.24678962	1020	0.005636136
20.1137	20.27059486	1080	0.006330171
20.1272	20.29576823	1140	0.007076271
20.1415	20.32234634	1200	0.007876361
20.1569	20.35036575	1260	0.00873237
20.1733	20.37986294	1320	0.009646237
20.1908	20.41087428	1380	0.010619909
20.2094	20.44343602	1440	0.011655333
20.2292	20.47758432	1500	0.012754467
20.2501	20.51335515	1560	0.013919266
20.2723	20.55078437	1620	0.015151694
20.2957	20.58990766	1680	0.016453711

Layer 6			
Bed Temp	Exit Temp	Time(s)	Energy stored (MJ)
20	0	0	0
20.0002	20.00333	60	1.36563E-05
20.0006	20.00458	120	3.14301E-05
20.001	20.00601	180	5.3762E-05
20.0015	20.00764	240	8.11097E-05
20.002	20.00947	300	0.000113948
20.0027	20.01152	360	0.000152769
20.0036	20.0138	420	0.00019808
20.0045	20.01633	480	0.000250408
20.0056	20.01911	540	0.000310295
20.0068	20.02217	600	0.000378299
20.0082	20.02551	660	0.000454995
20.0097	20.02915	720	0.000540974
20.0114	20.03311	780	0.000636845
20.0134	20.0374	840	0.000743231
20.0155	20.04203	900	0.00086077
20.0178	20.04702	960	0.000990119
20.0203	20.05239	1020	0.001131947
20.0231	20.05815	1080	0.00128694
20.0262	20.06432	1140	0.001455799
20.0295	20.07091	1200	0.001639239
20.033	20.07794	1260	0.001837992
20.0369	20.08543	1320	0.002052801
20.041	20.0934	1380	0.002284427
20.0455	20.10185	1440	0.002533641
20.0503	20.11081	1500	0.002801232
20.0555	20.1203	1560	0.003087999
20.061	20.13033	1620	0.003394755
20.0669	20.14092	1680	0.003722329

Figure 4.7: Screen shot of Temperature profile and energy stored table across the layers

The graphs of the rocks’ temperature versus time and the thermal energy stored versus time across the six layers for the duration of the test are generated by the software as shown in Figure (4.8).

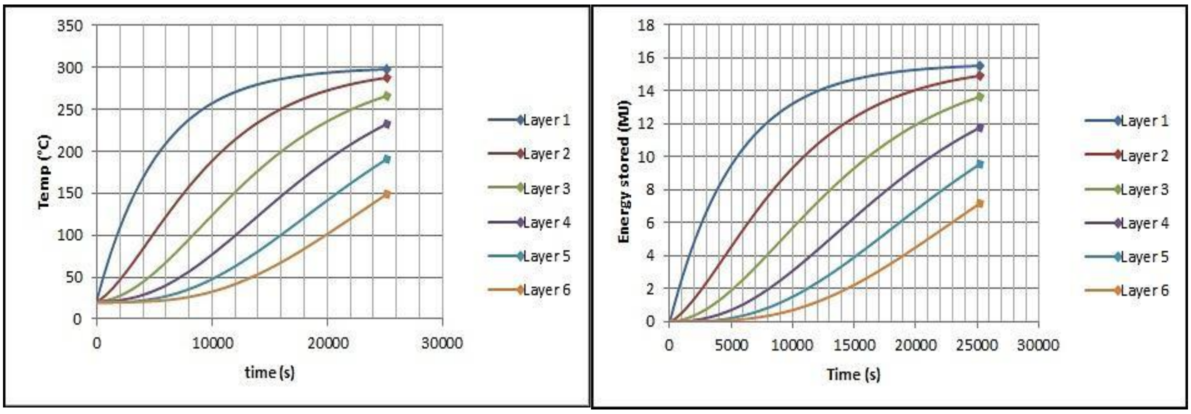

Figure 4.8: Screen shot of Rocks vs time and Energy stored vs time across each layer.

Step 3: Computation of the total energy stored and the thermal energy analysis over the entire tank

The total thermal energy stored by the rocks and the energy interaction between the air and the rocks are computed for the duration of the test as shown in Figure (4.9).

∑(energy stored by all the layers)	Energy analysis (W)		
Energy stored (MJ)	Supply	Absorbed	Dumped
0	0	0	0
0.204279081	3388.06	3388.02	0.04031
0.408557249	3388.06	3388	0.05544
0.612834373	3388.06	3387.98	0.07276
0.817110312	3388.06	3387.96	0.09242
1.021384915	3388.06	3387.94	0.11457
1.225658023	3388.06	3387.92	0.13937
1.429929466	3388.06	3387.89	0.16698
1.634199067	3388.06	3387.86	0.19754
1.838466636	3388.06	3387.82	0.23123
2.042731975	3388.06	3387.79	0.26821
2.246994876	3388.06	3387.75	0.30866
2.451255119	3388.06	3387.7	0.35274
2.655512474	3388.06	3387.66	0.40063
2.859766701	3388.06	3387.6	0.45252
3.064017548	3388.06	3387.55	0.50858
3.268264752	3388.06	3387.49	0.56899
3.472508039	3388.06	3387.42	0.63396
3.676747123	3388.06	3387.35	0.70366
3.880981708	3388.06	3387.28	0.77829
4.085211483	3388.06	3387.2	0.85805
4.289436128	3388.06	3387.11	0.94314
4.493655309	3388.06	3387.02	1.03375
4.697868682	3388.06	3386.93	1.1301
4.902075887	3388.06	3386.82	1.23238
5.106276554	3388.06	3386.72	1.34082
5.3104703	3388.06	3386.6	1.45561
5.514656728	3388.06	3386.48	1.57697

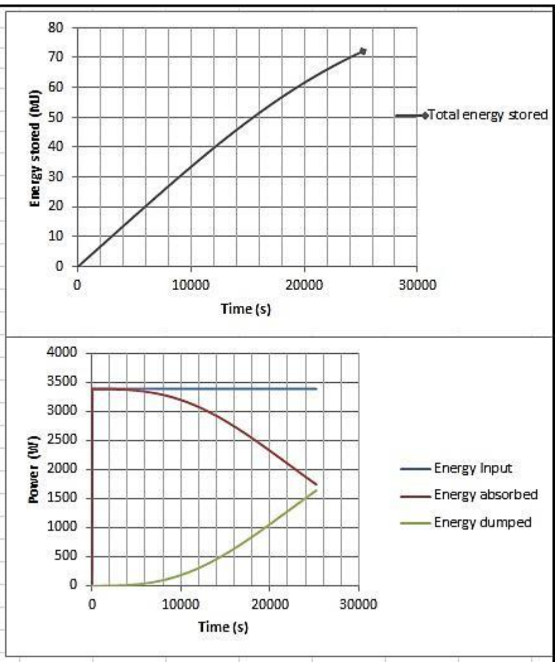

Figure 4.9: Screen shot of the tables and graphs displaying total energy stored and energy interaction between the air and rocks.

4.5 SUMMARY

The focus of this chapter was to discuss the stages developed in excel spreadsheet to predict the thermal performance and the pressure drop for packed-bed rock storage systems. Although many correlations were developed for the predictions of those systems [1, 18], most of those predictions are for small size rocks which depend on the knowledge of specific properties of rocks such as void fraction, shape and sphericity factor, so they cannot be utilized for the design of packed bed systems using large sized elements because fluid flow and heat transfer characteristics of such systems are different from those with small size materials.

The research scope was the development of a packed-bed rock storage system and the use of large size rocks was suggested [7, 16]. The major expenditure of packed rock storage systems is the fan energy to circulate air through the rocks. Therefore it was proposed to use crushed dolerite rocks having an equivalent diameter ranging between 4cm to 6 cm. Due to the complexity of determining shape factor and sphericity of crushed rocks, and also due to the relatively large size of the rocks, most of the previously developed correlations cannot be used in the prediction of the performance of this system.

The experimental results showed that the predicted results using this spreadsheet are in good agreement. The percentage error between the predicted and actual thermal performance is about 8% as will be discussed in Chapter 7.

This spreadsheet can be used by designers to predict thermal performance and pressure drop for packed bed systems. It does not restrict itself only to small size rocks but it can be used for any size rocks.

CHAPTER 5: MINIMIZING HEAT LOSS OF A PACKED-BED ROCK SYSTEM

5.1 INTRODUCTION

The objective of thermal insulation of the rock bed is the reduction of heat flux to the surroundings in order to decrease the drop in storage temperature. Effective insulation of a storage tank requires a tank design in order to reduce conduction heat loss across the tank structure and also applying the right insulation techniques. There are three insulation techniques used, which are conventional material insulation, vacuum insulation and vacuum super insulation [20, 45]. The super insulation approach is pursued in the development of this spreadsheet. Super insulation is achieved by making use of vacuum insulation and putting opaque materials in the evacuated space because radiation heat transfer (only mechanism of heat transfer in vacuum) can be significant at high temperatures; so the introduction of opaque materials has the objective of reducing radiation heat transfer. As discussed in Chapter 2, two types of opaque materials were used. The most common technique is the use of multilayers of reflective foils of low emissivity (aluminium foil) and also the use of powder insulation to slow radiation heat loss [20, 21].

The spreadsheet presents an analysis based on a vacuum super insulation technique: A comparison between the use of vacuum with multilayers of aluminium foil and the use of vacuum and expanded perlite powder insulation is investigated as shown in Figure (5.1).

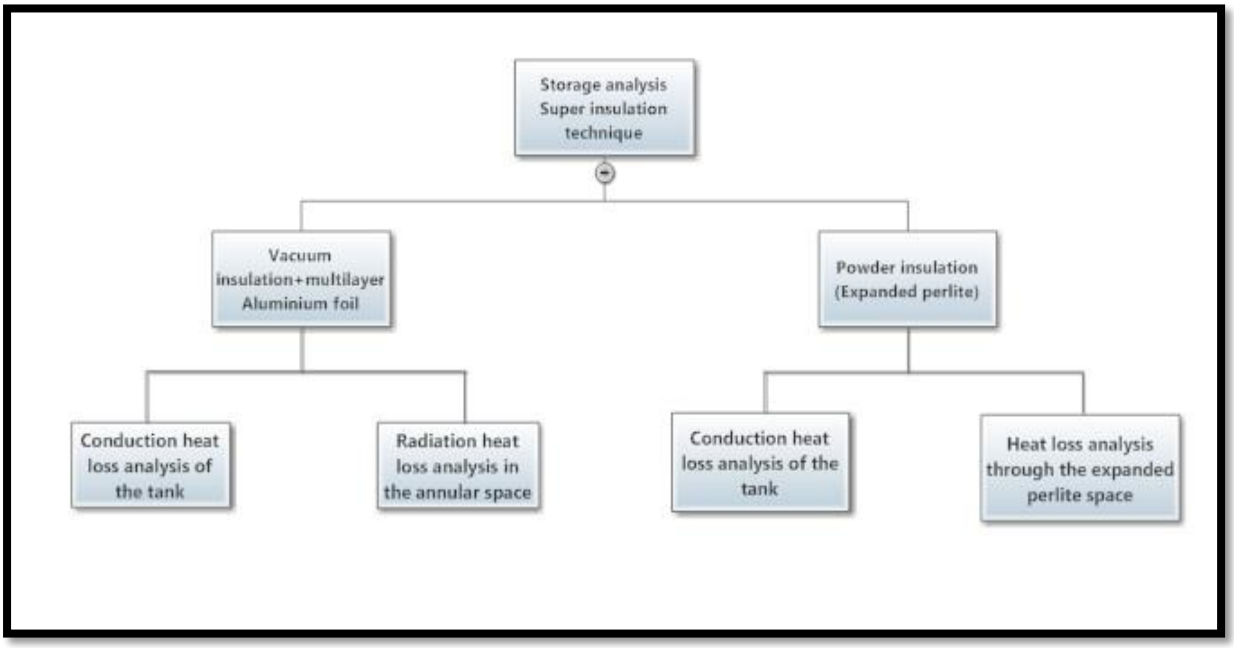

Figure 5.1: Storage analysis

5.2 TANK INSULATION USING EXPANDED PERLITE

The heat loss analysis of the storage tank is done in two stages. The first stage is the heat loss analysis through the cavity and the second stage will be the analysis of the conduction heat loss across the tank structure (occurs at the top and bottom because that is the area where the inside and outside tank are connected).

5.2.1 DEFINING HEAT LOSS TROUGH THE EXPANDED PERLITE REGION

The heated rocks are stored in the inner cylindrical container, which is fixed to the outer tank by a welded connection on the bottom as shown in Figures (5.2 and 5.3). Both containers are made of mild steel. The annular gap is filled with expanded perlite.

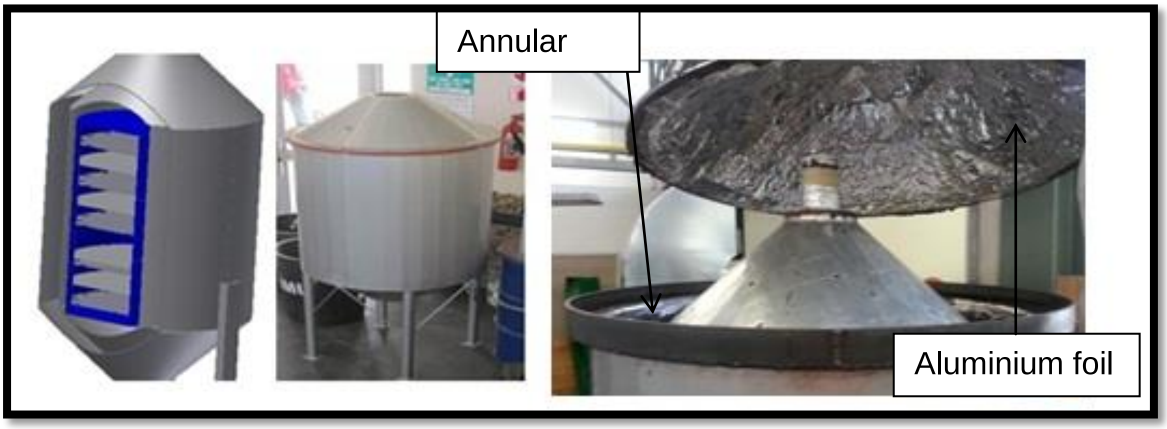

Figure 5.2: Storage tank.

Expanded perlite is supplied in a microscopic granular structure. The total thermal conductivity may be described by formula (5.1): [28]

$$\lambda tot = \lambda g + \lambda r + \lambda s \qquad (5.1)$$

Where λ*g:* thermal conductivity of free gas (air), λ*r:* describes the radiation transfer and λ*s:* the solid conduction within the material skeleton. All measured in (W/m.K)

Formulas are available for the computations of those parameters but in this spread sheet, the thermal conductivity from the expanded perlite data sheet has been selected [20].

The following factors are important to consider for a thermal energy storage process:

- The storage temperature (T) of the system (initial temperature T_0) decreases with time (t) due to the thermal losses ($\dot{Q}$) to the surrounding environment (ambient temperature Ta).
- Heat loss Q which is related to the temperature decrease dT/dt by the integral heat capacity ($C = c_p \rho V$) of the storage medium (c_p: specific heat capacity, ρ: density, V: storage volume). The heat loss $\dot{Q}$ can also be expressed by $\lambda A(T - T_a)/d$, (λ: heat conductivity of the insulation, A: tank surface area, d:

insulation thickness). The expression of the storage temperature as a function of time is derived from equating and solving the heat transfer equations [20]. The derivation is shown below:

$$\dot{Q} = \lambda \frac{A}{d}(T - T_a) \tag{5.2}$$

$$or$$

$$\dot{Q} = -C\frac{dT}{dt} = -c_p \rho V \frac{dT}{dt} \tag{5.3}$$

$$Equating \dot{Q}:$$

$$\frac{dT}{T - T_a} = -\frac{A\lambda}{c_p \rho V d} dt$$

$$\ln(\frac{T - T_a}{T - T_0}) = -\frac{A\lambda}{c_p \rho V d} dt$$

$$T(t) = (T_0 - T_a)\exp(-\frac{A\lambda}{c_p \rho V d} t) + T_a \tag{5.4}$$

Equation (5.4) represents the drop in the storage temperature through the expanded perlite and was used in this spreadsheet to predict the drop in temperature of the rocks.

5.2.2 CONDUCTION HEAT LOSS ACROSS THE TANK STRUCTURE

The conduction heat occurs in two regions. The first region is at the bottom of the tank where the inside and outside tank are welded together and the second region is from the top teflon fitting to the storage tank that conducts the hot air into the tank.

5.2.2.1 Bottom conduction heat loss

The inside tank is welded to the outside tank at the bottom of the tank. In order to reduce heat loss that occurs in this region, a 3mm thick stainless steel 304 sheet was rolled into a cylindrical form. This cylinder was welded to the inside and the outside tank. The length of the cylinder is 100mm. Figure (5.3) shows the stainless steel cylinder and where it is welded to the storage tank.

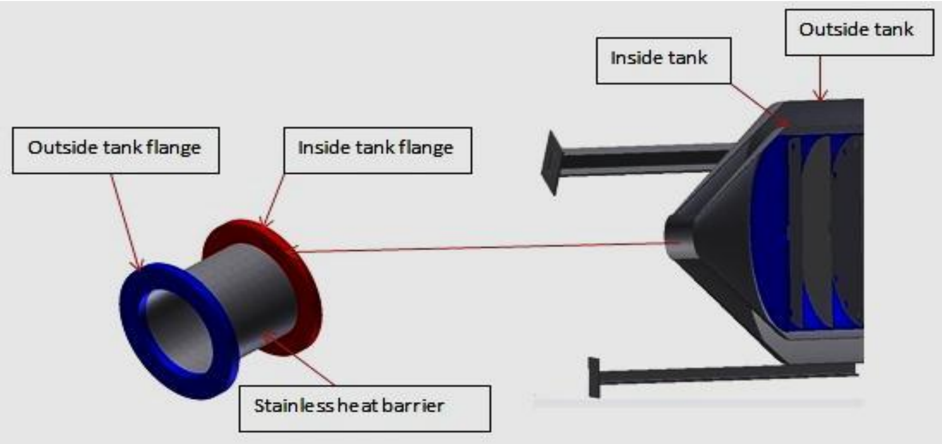

Figure 5.3: Stainless steel heat barrier

The drop in the storage temperature caused by the conduction heat loss through the stainless steel barrier can be determined from equation (5.5).

$$T(t) = (T_0 - T_a)\exp(-\frac{Ak}{c_p \rho VL}t) + T_a \tag{5.5}$$

Where: A: cross sectional area of the stainless steel, K: stainless steel thermal conductivity and L: the length of the stainless steel cylinder.

5.2.2.2 Conduction heat loss through Teflon fittings

The Teflon fitting is screwed on the top of the inside tank. The hot air is pumped through it. Figure (5.4) shows the fitting and where it is applied.

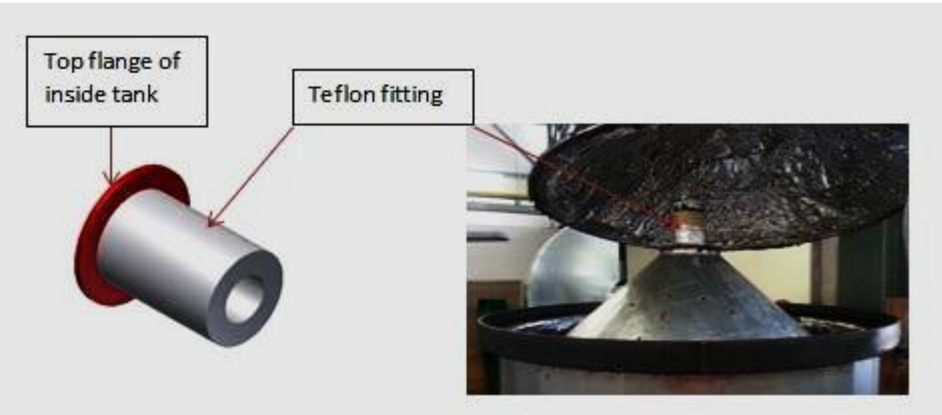

Figure 5.4: Teflon fitting

The heat loss analysis through the Teflon is the same as that for the stainless steel connection; however, A: cross section area of the Teflon, K: Teflon thermal conductivity and L: the length of the Teflon.

$$T(t) = (T_0 - T_a)\exp\left(-\frac{Ak}{c_p \rho VL}t\right) + T_a \tag{5.6}$$

5.3 INSULATION OF THE TANK USING VACUUM AND ALUMINIUM FOIL:

The procedure followed in this analysis is the same as that in section (5.1). The first stage is the heat loss analysis through the vacuum space (cavity) and the second stage is the analysis of the conduction heat losses across the tank structure; however this analysis is the same as in section (5.1.2).

5.3.1 HEAT LOSS TROUGH THE VACUUM SPACE WITH MULTILAYERS OF ALUMINIUM FOIL:

In this approach vacuum insulation is achieved by evacuating the annular space between the inside and the outside tank. Evacuating a space suppresses the possibility of conduction and convection heat transfer because these heat transfer mechanisms require a material medium. So radiation heat is the only mechanism of heat transfer in a vacuum space [20, 28].

The use of multilayers of aluminium foil results in the reduction of radiation heat losses as illustrated in Figure (5.5). The foil absorbs the radiation heat loss until the amount of energy absorbed by the foils equals the energy emitted by them. So, the irradiation of the foil happens homogeneously in both directions. As a consequence, only half of the radiation heat loss occurs by the insertion of the foil. If two foil layers were used only a third of the energy would be lost and if N foils were used, the reduction factor would be given by (N + 1) [20, 21].

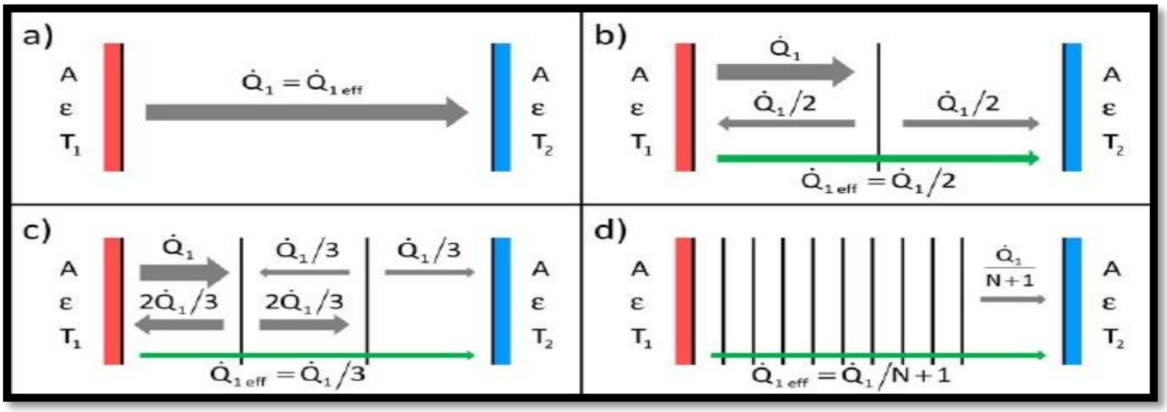

Figure 5.5: Foil insulation principle [20].

The radiation heat analysis on the storage tank is given by equations (5.7 and 5.8). The view factor is 1 because all the irradiations leaving the inner tank are intercepted by the outer tank [3, 20].

$$\dot{Q}_{Radiation} = \frac{\sigma A_1 (T_o^4 - T_a^4)}{(\frac{1}{\varepsilon}(1+\frac{A_1}{A_2}) - \frac{A_1}{A_2})*(N+1))} = \frac{\sigma A_1}{(\frac{1}{\varepsilon}(1+\frac{A_1}{A2}) - \frac{A_1}{A_2})*(N+1))}(T_o^2 + T_a^2)(T_o + T_a)(T_o - T_a)$$

$$\dot{Q}_{Radiation} = h_{rad} A(T_o - T_a) \quad (5.7)$$

$$h_{rad} = \frac{\sigma A_1}{(\frac{1}{\varepsilon}(1+\frac{A_1}{A_2}) - \frac{A_1}{A_2})*(N+1))}(T_o^2 + T_a^2)(T_o + T_a) \quad (5.8)$$

The drop in storage temperature caused by radiation heat loss is given by this equation (5.9): [20]

$$T(t) = (T_0 - T_a)\exp(-\frac{Ah_{rad}}{c_p \rho V}t) + T_a \quad (5.9)$$

5.4 PARAMETERS USED IN THE SPREADSHEET

In the previous section equations were derived that will be used in the thermal energy storage prediction. The parameters used in these equations are defined and listed in Table 5.1:

- Conduction through Teflon fitting:

The length, cross-sectional area and the thermal conductivity of the Teflon.

- Conduction through stainless steel barrier

The cross-sectional area, the length and the thermal conductivity of the stainless steel barrier.

- Heat loss through the expanded perlite

The surface area of the inside tank, the thickness of the perlite insulation and the thermal conductivity.

- Heat loss trough the vacuum space

The Boltzmann constant and the number of the aluminium layers used. The radiation heat transfer coefficient is computed using the derived equation (5.8) [3, 20]:

The parameters used in the prediction of the results are given in table 5.1.

Table 5.1: Parameters used in the spreadsheet analysis [[3, 30, 31]].

Inside tank area (A_1)	2 m^2
Outside tank area (A_2)	3.3 m^2
Teflon area (A_t)	0.0029 m^2
Teflon length (L)	0.1 m
Stainless steel area (A_s)	0.00125 m^2
Stainless steel length (L)	0.1 m
Thermal conductivity of Teflon (k_T)	0.25 W/m.K
Thermal conductivity of stainless steel (k_S)	19 W/m.K
Emissivity of inside tank	0.32
Stefan Boltzmann constant	5.67×10^{-8} $W/m^2.K^4$
Number of aluminium foil (x)	5
Thickness of expanded perlite insulation (d)	40 mm
Storage volume (V)	0.25 m^3
Specific heat of rocks C_p (W/m.K)	1050
Thermal conductivity of expanded perlite	0.057 W/m.K at at DT of 38°C

The manufactured storage tank is not only made of an inside and outside tank. A 200 L drum where the rocks are packed was inserted inside the inner tank. There is a 20 mm gap annular space between the drum and the inside tank. As the purpose of this spreadsheet was the investigation of two insulation techniques (Vacuum insulation and powder insulation), the effect of the calcium silicate is accounted for by the method described below:

I. Accounting for calcium silicate in the expanded perlite insulation region:

Thermal conductivity of calcium silicate is: k=0.05 W/m.K at room temperature and the thermal conductivity of expanded perlite is k=0.057 W/m.K at the same temperature.

K (calcium silicate) / K (perlite) = 0.05/0.057

= 0.9

The assumption that follows from this analysis is that calcium silicate and expanded perlite insulation of the same thickness will produce almost the same effect. So in the spreadsheet the 20 mm of calcium silicate is added to the thickness of the expanded perlite as a combined effect.

II. Taking consideration of calcium silicate in the vacuum region:

To take consideration of the calcium silicate effect in the vacuum region, the heat transfer coefficient through the calcium silicate and the radiation heat transfer coefficient should be combined in order to predict the storage temperature. Heat analysis was done in this way and it was found that if 3 foil layers of aluminium were added in the vacuum region the effect would be similar.

The assumption that follows is that to account for the 20 mm of calcium silicate insulation, 3 extra imaginary aluminium foils are used.

5.4 PRESENTATION OF THE NUMERICAL ANALYSIS

In this section the graphs obtained from the prediction are presented. Discussion and interpretation of the results are done in Chapter 7.

Figure (5.6) shows a screen print of the input parameters to the excel spreadsheet. In this figure two parameters are varied, the insulation thickness and the number of aluminium foil layers to investigate their effects on the storage temperature.

Storage Temperature (°C)	300
Ambient Temperature (°C)	18

Inputs	
Insulation thickness (m)	0.06
Surface area of tank outside (m^2)	3.3
Surface area of tank inside (m^2)	2
Cprocks (J/Kg.K)	1050
Rocks density	2800
Volume of storage	0.25
Teflon cross sec Area (m^2)	0.004
Teflon length (m)	0.1
Stainless steel C-area (m^2)	0.00125
Length of stainless steel (m)	0.1
Thermal con teflon (W/m.K)	0.27
Thermal con stainless (W/m.K)	19
Thermal expan perlite (W/m.K)	0.043
Boltzmann constant(W/m^2.K^4)	5.67E-08
Steel emissivity	0.2
Number of aluminium foil	5
Rad heat transfer coeff(Hrad)[W/m^2.K)	0.9084143

Figure 5.6: Input parameters

The storage temperature of the rock bed of dolerite as a function of time for a period of three days is shown in Figures (5.7) and (5.8). Figure (5.7) shows the storage temperature as a combined effect of the conduction heat loss through the tank (teflon and stainless steel) and heat loss through the expanded perlite region, whereas Figure (5.8) shows the effect of conduction heat loss through the tank (teflon and stainless steel) and in the vacuum space (5 Al foil).

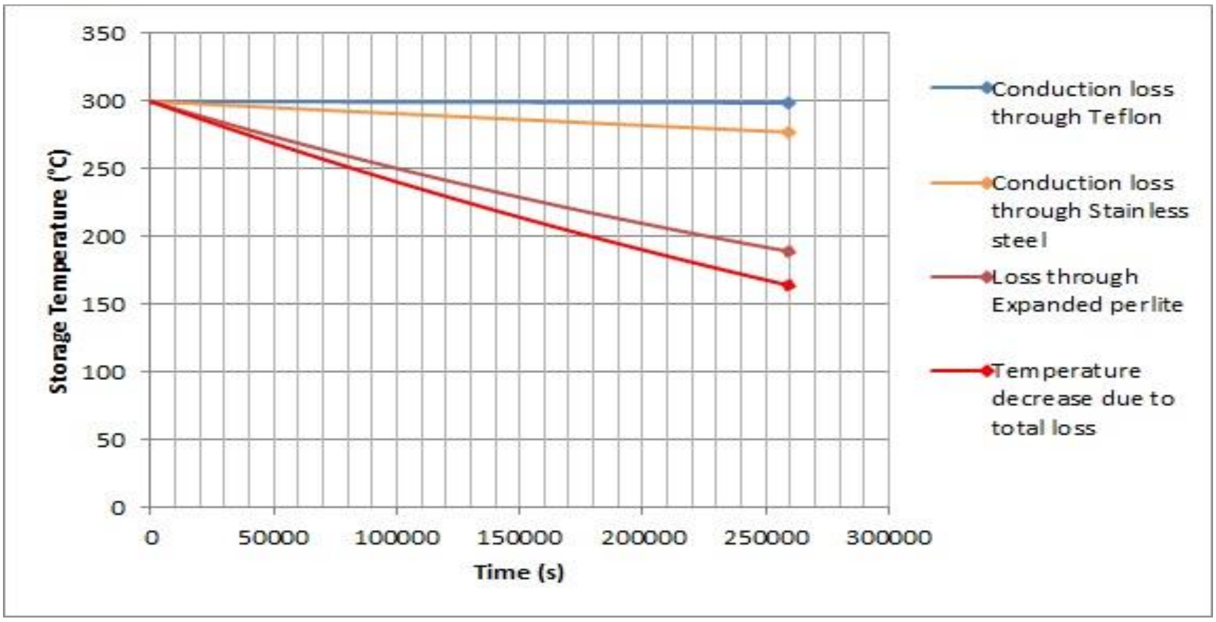

Figure 5.7: Storage temperature as a function of time using expanded perlite insulation.

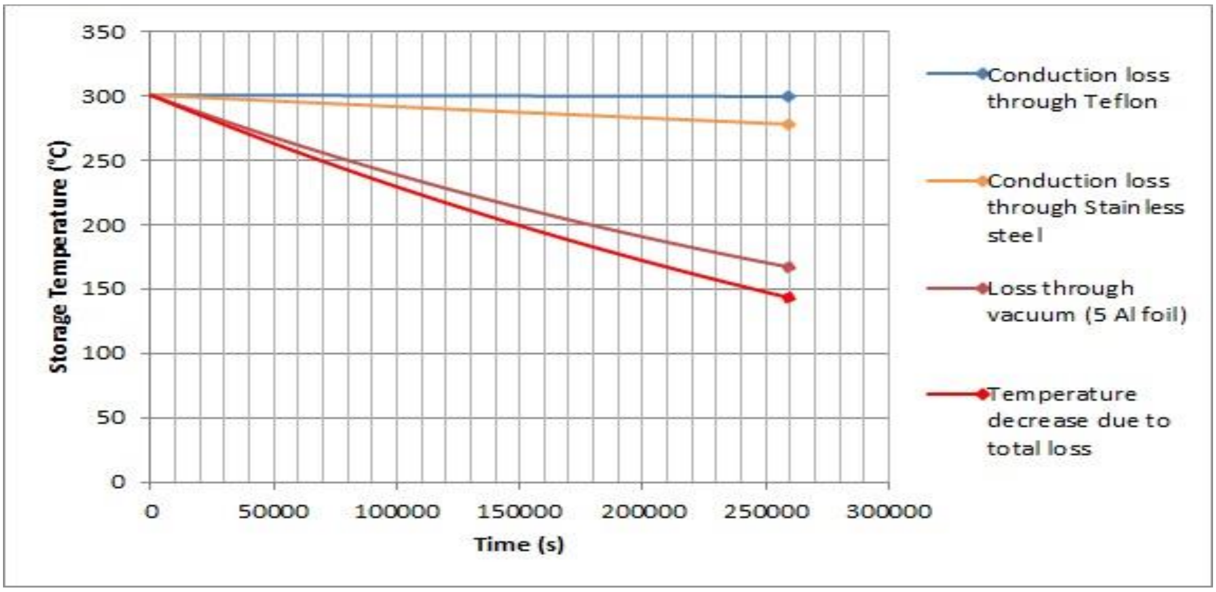

Figure 5.8: Storage temperature as a function of time using vacuum insulation.

Figure (5.9) illustrates the storage temperature effect when inserting aluminium foil layers in the vacuum space.

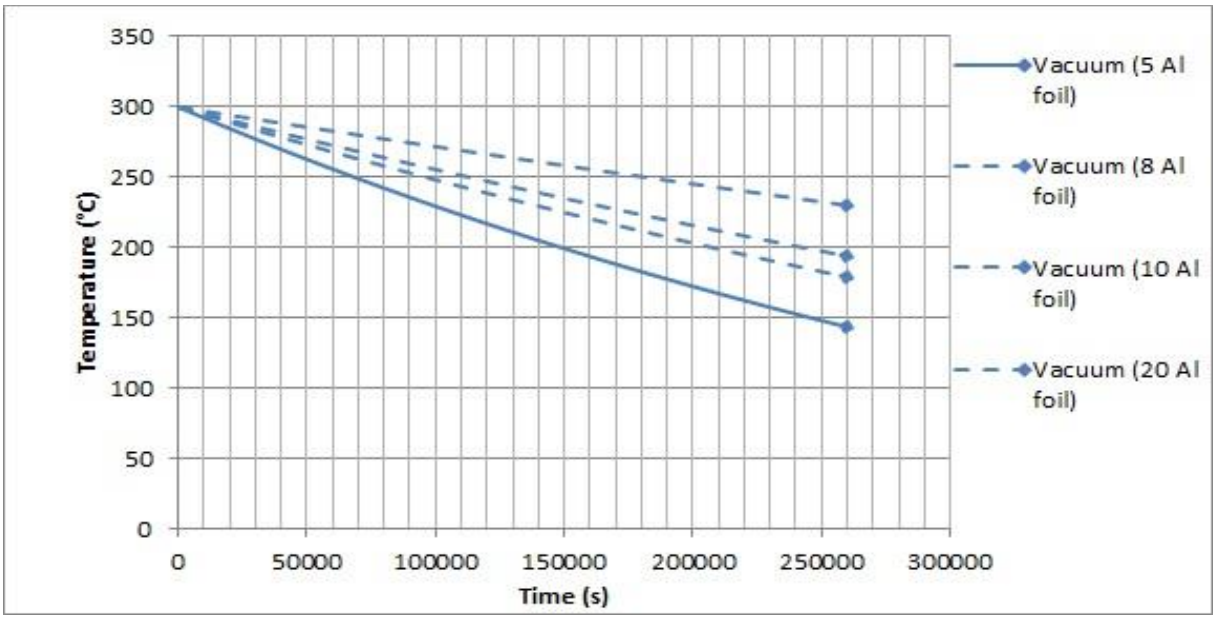

Figure 5.9: The effect of aluminium foil on storage time.

Figure (5.10) shows the effect of increasing the thickness of perlite insulation on the storage.

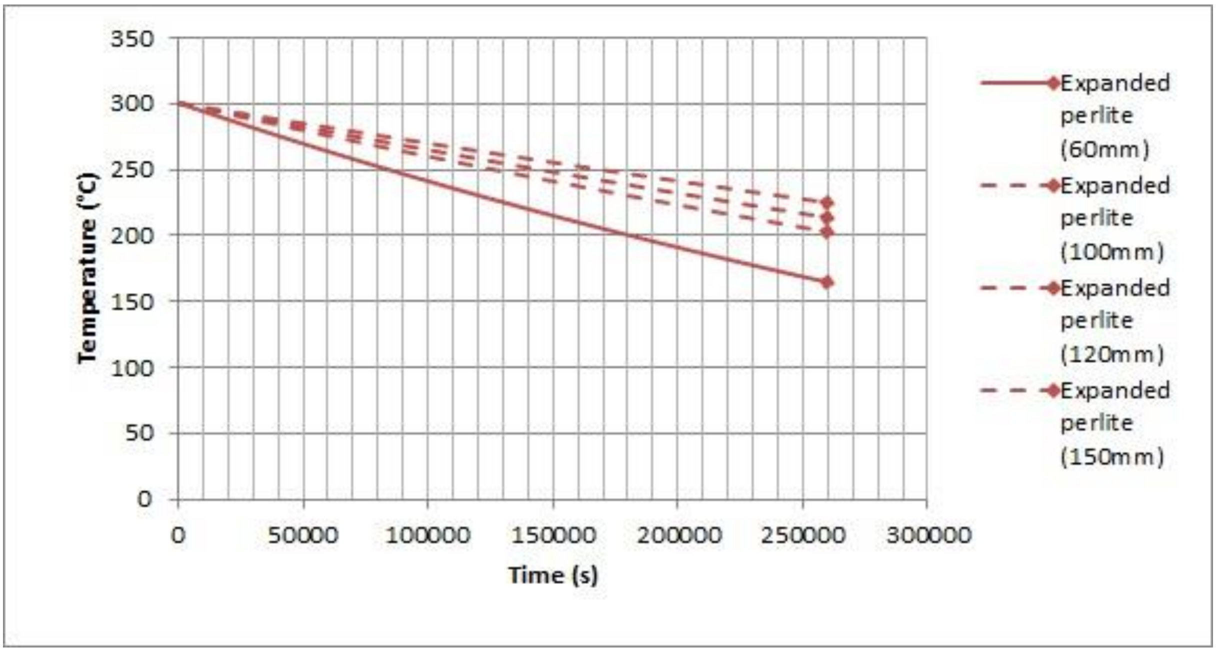

Figure 5.10: The effect of expanded perlite thickness on storage temperature

Figure (5.11) shows the actual predicted comparison where the perlite thickness cannot be changed but the aluminium layers are varied.

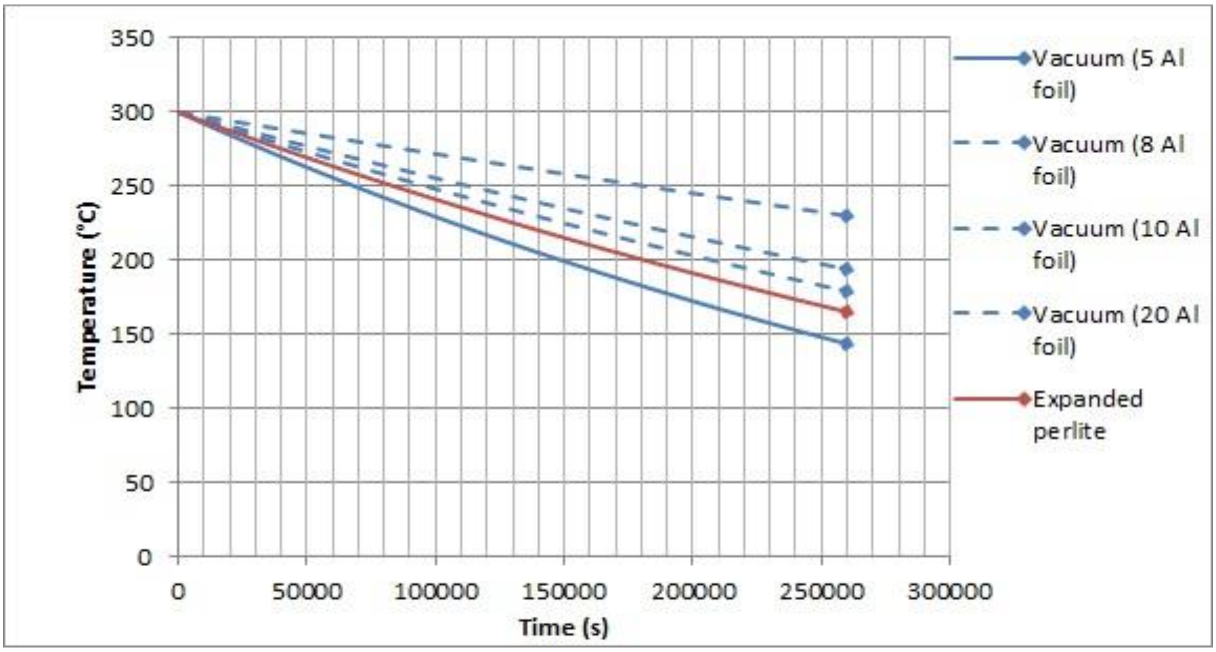

Figure 5.11: Storage temperature as function of time for Vacuum insulation vs perlite insulation.

5.5 SUMMARY

The purpose of this chapter was the development of a spread sheet to analyse thermal energy storage based on the two insulation techniques that were pursued in this dissertation. The optimization of the storage temperature was investigated using the spread sheet.

If high temperature storage is to be done using vacuum insulation techniques, the use of multilayers of aluminium foil will lead to increased storage time and effective insulation of the tank as shown in the results. Increasing the number of aluminium foil layers from 5 to 20 has increased the storage temperature from 142 °C to 233°C as shown in Figure (5.9).The objective of using the foil was to reduce radiation heat loss as this is the only way of losing heat in a vacuum space. The technique of vacuum insulation plus the use of multilayer aluminium foil leads to a compact design of a tank compared to the conventional insulation techniques where very thick insulation material is required. A special property of vacuum insulation is the fact that the radiation heat transfer is independent of the thickness of the space to be vacuumed; hence the thickness of the vacuum space needs only to be a few millimetres thick. Vacuum insulation also has economic advantages as no insulation material is required. Vacuum insulation is only effective at pressures below 0.01 bar [20, 28, 29]. Hence the tank design should minimize the chances of leaks.

One important aspect to consider when designing a vacuum insulated storage tank is the conduction heat loss that occurs where the inside and outside tank are joined. A material having low thermal conductivity should be used in this juncture region to reduce conduction heat loss.

Expanded perlite has shown to be a possible insulation technique for high temperature storage. By increasing the thickness of expanded perlite, effective insulation can be achieved. A comparable test showed the storage temperature had increased from 163°C to 232°C by increasing the insulation thickness from 60mm to 150mm as shown in Figure (5.10).

New research has shown that the combination of vacuum insulation and expanded perlite is the more effective and bankable option than vacuum insulation with multilayers foil. Matthias Demharter tested such a tank using those techniques and obtained favourable results [20]. In this spread sheet this combination has been analysed, but the actual testing will be discussed in Chapter 7.

The experimental results showed that the predicted results using this spread sheet are in good agreement. The percentage error between the predicted and actual thermal performance is approximately 19%. (Chapter7).

CHAPTER 6: NUMERICAL APPROACH PREDICTING THERMAL PERFORMANCE OF A PROPOSED LOW COST PARABOLIC TROUGH COLLECTOR FOR AIR HEATING SYSTEMS

6.1 INTRODUCTION

The purpose of this chapter is to design a numerical approach that will predict the performance of a designed parabolic trough solar collector. This dissertation evaluates the use of air as a heat transfer mechanism in a low cost parabolic trough collector. The main focus of the previous research was the use of liquid fluid such as water, brine water, oil, liquid salt as the working medium [34, 35, 40]. Liquid fluid has a higher thermal capacity than air but due to its chemical instability such high expansion pressure makes the system expensive. The use of air allows a simple and cheap design because air does not have the problem of high pressure because it remains a gas at all possible operating temperatures (20-500˚C) [40].

6.2 BASIC THEORY AND CONCEPT

The incoming solar irradiation in the form of electromagnetic waves reaches the earth's atmosphere with an energy flux of about 1365 W/m^2 [39, 40]. Some of that energy is absorbed by the atmosphere and also reflected back to the space and only 1000 W/m^2 [35, 40] reaches the earth's surface. Solar collectors are used to convert this energy to heat.

A parabolic trough collector concentrates optically solar energy and converts it to heat. Concentration is obtained by reflection of solar radiation using mirrors or high reflective surfaces. The reflected light is concentrated in a focal zone, thus increasing the energy flux in the receiving target as seen in Figure (6.1).

Parabolic trough collectors are made by bending a sheet of reflective material into a parabolic shape [4]. A metal black tube covered with a glass tube to reduce heat losses is placed along the focal line of the receiver [4]. When the parabola is pointed towards the sun, parallel rays incident on the reflector are reflected onto the receiver as seen in Figure (6.1). An evacuated receiver tube is placed at the focal line of the collector so that all the sun energy that strikes onto the collector is directed towards it as seen in Fgure (6.1). It absorbs solar energy and converts it into heat for use in the air heating system. The working fluid (air) that flows inside the hot receiver tube is heated by the solar irradiation absorbed [40].

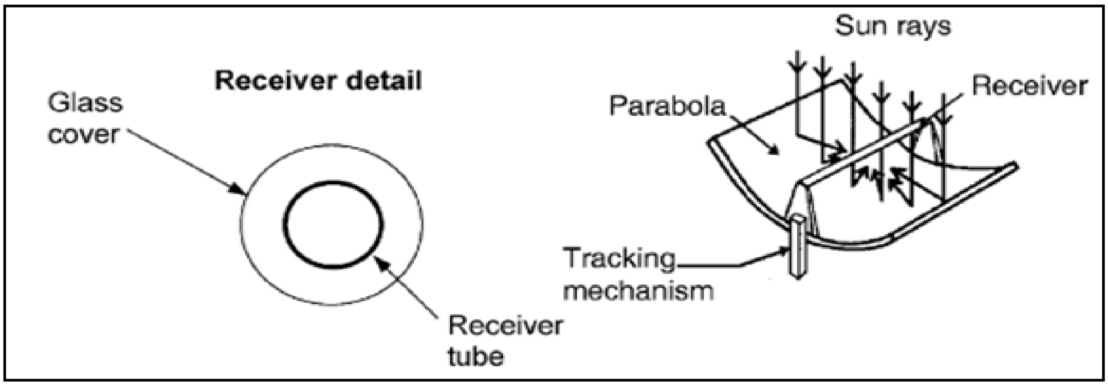

Figure 6.1: Parabolic Trough Details [40].

The parabolic trough collectors must always face the sun; therefore the need of a tracking system is required.

Figure (6.2) shows the CAD model of the designed parabolic trough collector and the way the system operates is shown in Figure (6.3). The collectors are at any time oriented towards the sun by an electronic tracking device so that the incoming solar irradiations that are reflected by the mirrors are directly oriented to the evacuated solar geyser tube. The entire system can be tilted according to the sun's position. Figure (6.2) shows the CAD model of the collectors' tracking in the summer position.

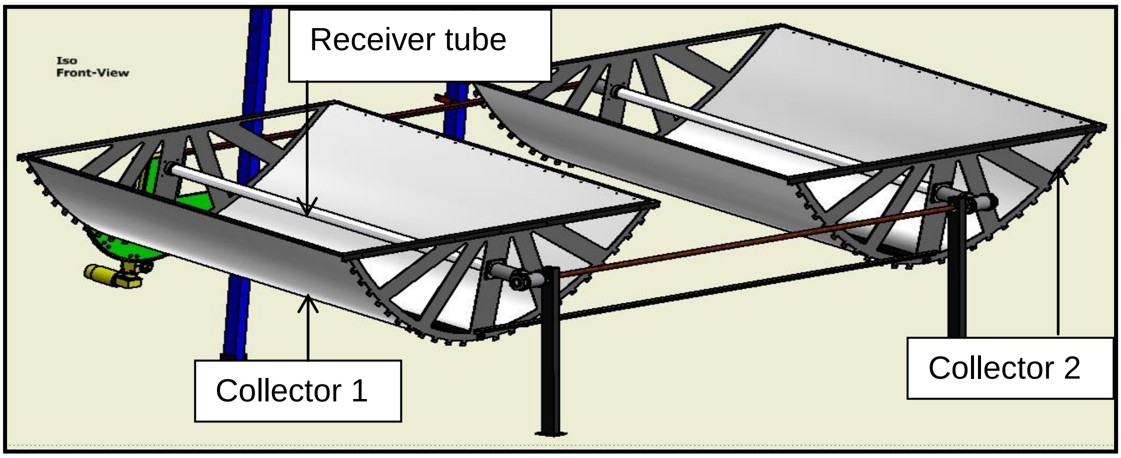

Figure 6.2: CAD Model of Parabolic Trough Collectors.

The principle of operation of the collectors is shown in Figure (6.3). The ambient air is pumped through the collectors. The incoming solar irradiation intercepted by the solar collectors heats the air to the operating temperature.

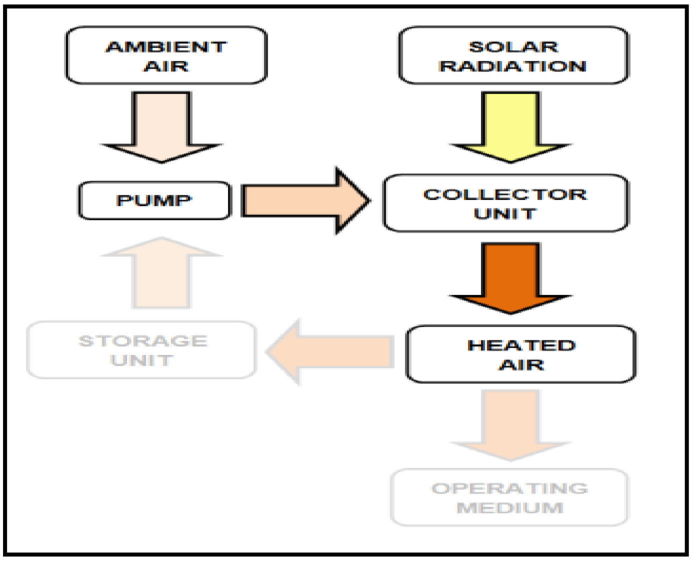

Figure 6.3: Flow Chart of the parabolic trough solar collector [40].

6.3 THEORY USED TO DEVELOP THE NUMERICAL SOLUTION

This section describes the procedure followed and the equations used to solve the mathematical developed to predict the thermal performance of the parabolic trough solar collector. The diagram explaining the thermal analysis of the collectors is shown in Figure (6.4). The following sections discuss in detail the analysis shown in Figure (6.4).

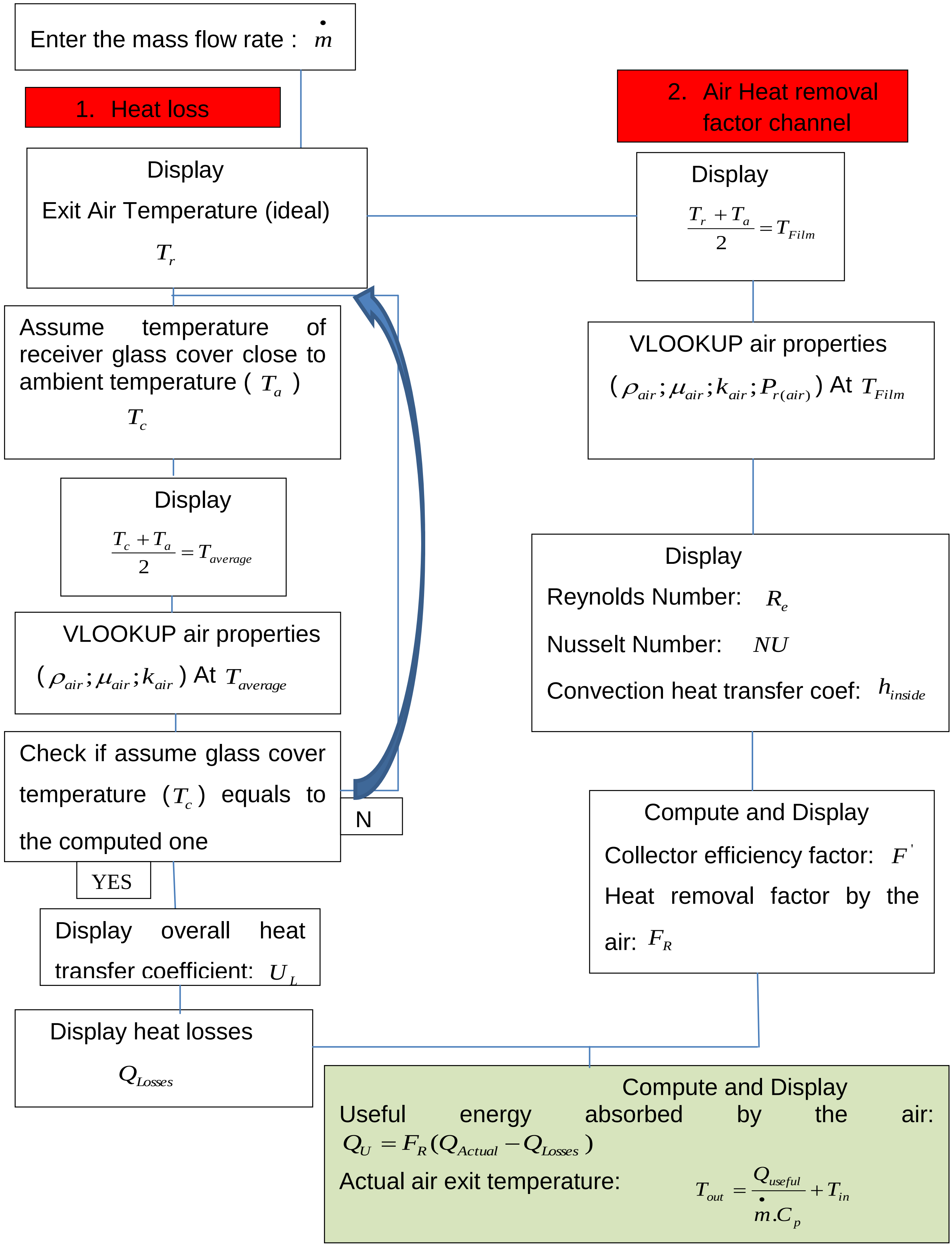

Figure 6.4: Operating diagram of the spread sheet.

The solar energy available is given by equation (6.1). An important parameter in this equation is the length of the day which is not a constant value. The length of the day depends on the location and also the time of the year on under consideration. Figure (6.5) shows the length of the day in Port Elizabeth for the month of December [41].

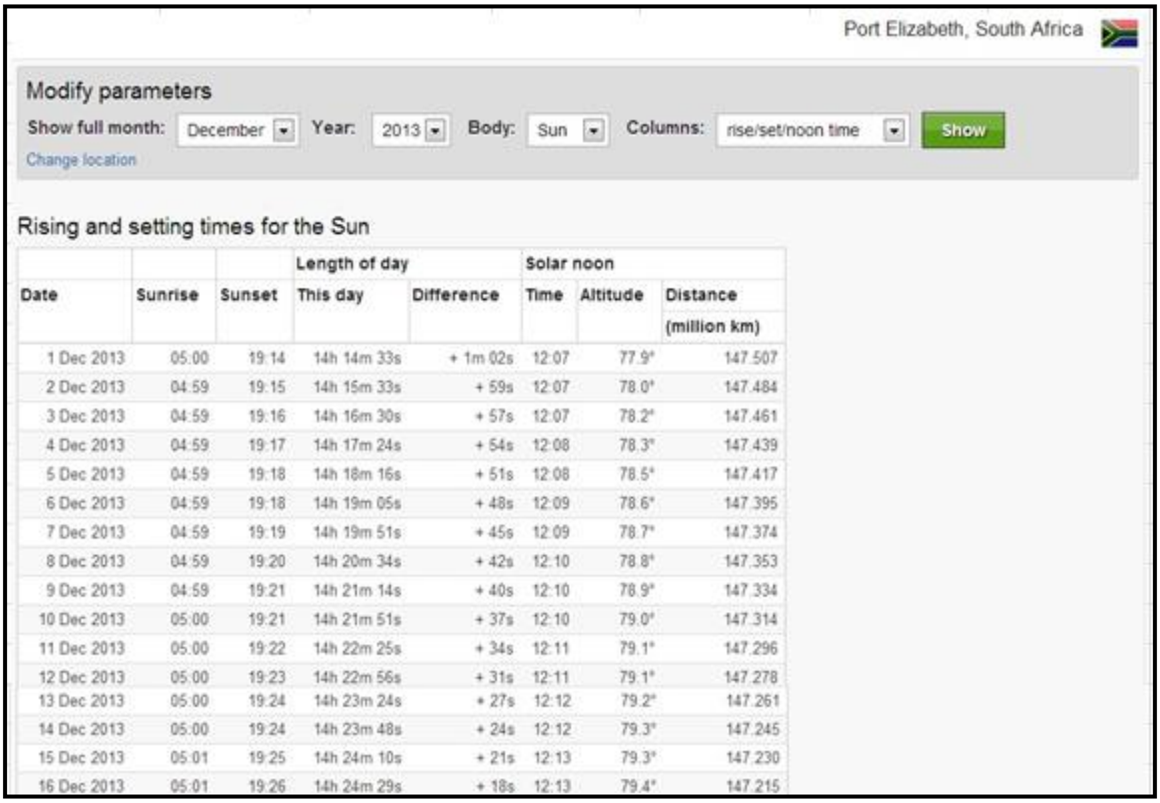

Port Elizabeth, South Africa

Modify parameters

Show full month: December Year: 2013 Body: Sun Columns: rise/set/noon time Show

Change location

Rising and setting times for the Sun

			Length of day		Solar noon		
Date	Sunrise	Sunset	This day	Difference	Time	Altitude	Distance (million km)
1 Dec 2013	05:00	19:14	14h 14m 33s	+ 1m 02s	12:07	77.9°	147.507
2 Dec 2013	04:59	19:15	14h 15m 33s	+ 59s	12:07	78.0°	147.484
3 Dec 2013	04:59	19:16	14h 16m 30s	+ 57s	12:07	78.2°	147.461
4 Dec 2013	04:59	19:17	14h 17m 24s	+ 54s	12:08	78.3°	147.439
5 Dec 2013	04:59	19:18	14h 18m 16s	+ 51s	12:08	78.5°	147.417
6 Dec 2013	04:59	19:18	14h 19m 05s	+ 48s	12:09	78.6°	147.395
7 Dec 2013	04:59	19:19	14h 19m 51s	+ 45s	12:09	78.7°	147.374
8 Dec 2013	04:59	19:20	14h 20m 34s	+ 42s	12:10	78.8°	147.353
9 Dec 2013	04:59	19:21	14h 21m 14s	+ 40s	12:10	78.9°	147.334
10 Dec 2013	05:00	19:21	14h 21m 51s	+ 37s	12:10	79.0°	147.314
11 Dec 2013	05:00	19:22	14h 22m 25s	+ 34s	12:11	79.1°	147.296
12 Dec 2013	05:00	19:23	14h 22m 56s	+ 31s	12:11	79.1°	147.278
13 Dec 2013	05:00	19:24	14h 23m 24s	+ 27s	12:12	79.2°	147.261
14 Dec 2013	05:00	19:24	14h 23m 48s	+ 24s	12:12	79.3°	147.245
15 Dec 2013	05:01	19:25	14h 24m 10s	+ 21s	12:13	79.3°	147.230
16 Dec 2013	05:01	19:26	14h 24m 29s	+ 18s	12:13	79.4°	147.215

Figure 6.5: Length of the day in Port Elizabeth for December [41].

The solar energy intercepted by the parabolic trough collectors is the product of the solar energy delivered times the projected area of the collectors and the computation of the energy available at the focal line is given by equation (6.2). This is the actual solar energy reaching the glass tube (receiver). The computation of this energy takes into consideration the optical losses of the collectors. If the heat losses were not taken into consideration, the energy at the focal point would be entirely absorbed by the air. The actual energy absorbed by the working fluid takes into consideration the heat losses and also the heat removal factor by the working fluid (air). The actual air exit temperature is computed using equation (6.6).

6.3.1 AVAILABLE SOLAR AT THE RECEIVER TUBE

The energy delivered by the sun on a clear day is approximately a sinusoidal function of time with a maximum near noon and a minimum at sun rise and sunset [5]. The useful energy delivered is given by equation (6.1) [5]:

$$Q_U = Q_{U\circ}.\sin(\frac{\pi t}{\tau}) \tag{6.1}$$

Where:

t : Time (s) (measured from sunrise); τ : the length of day (from sun rise to sunset) and $Q_{U\circ}$ is the peak delivery rate of solar energy.

The amount of solar energy reaching the focal line of the collectors is given by equation (6.2) [4].

$$Q_{actual(sune-energy)} = Q_{U\circ} \times Area_{projected} \times \tau \times \alpha \times \rho \times \lambda \tag{6.2}$$

The net energy absorbed by the working fluid (Air) is given by equation (6.3) [8].

$$Q_{Net} = (Q_{Actual} - \Sigma(Heat-loss)) \tag{6.3}$$

The useful energy from the working fluid is the net energy absorbed multiplied by the heat removal factor. Equation (6.4) shows the useful energy delivered by the air [4]. The heat removal factor is the ratio of the energy delivered by a solar collector to the energy that would be delivered if the entire absorber were at the fluid inlet temperature [4]. It is used to express the total useful energy gained by the collectors in terms of the fluid inlet temperature [4].

$$Q_{Useful} = F_R Q_{Net} \tag{6.4}$$

$$Q_{Useful} = \dot{m} C_p \times (T_{out} - T_{in}) \tag{6.5}$$

From equation (6.4) and (6.5) we derive equation (6.6)

$$T_{out} = \frac{Q_{useful}}{\dot{m}.C_p} + T_{in} \tag{6.6}$$

Where T_{in} and T_{out} representing the air temperature entering and exiting the collectors respectively. The temperature is measured in (°C).

6.3.2 HEAT LOSS ANALYSIS

The analysis of heat loss requires knowledge of the overall heat loss coefficient (U_L). Assuming no temperature gradients along the receiver, the heat loss coefficient considering radiation (h_r) and convection (h_w) from the surroundings and conduction (h_c) through the support structure is given by equation (6.7) [4]:

$$U_L = h_w + h_r + h_c \tag{6.7}$$

The Nusselt number for wind loss coefficient is given by equation (6.8), (6.9) [4]:

- For $0.1 \le \mathrm{Re} \le 1000$, we have: $Nu = 0.4 + 0.54(\mathrm{Re})^{0.52}$ (6.8)
- For $1000 \le \mathrm{Re} \le 50000$, we have: $Nu = 0.3(\mathrm{Re})^{0.6}$ (6.9)

To reduce heat loss, an evacuated solar geyser glass tube is used around the receiver. The vacuum makes the convection losses of the receiver negligible.

The heat loss coefficient based on the receiver area is given by equation (6.10) [4]:

$$U_L = \left[\frac{A_r}{(h_W + h_{r,c-a} + h_{r,r-c})A_c} + \frac{1}{h_{r,r-c}} \right]^{-1} \tag{6.10}$$

Where:

$h_{r,c-a}$= Linearized radiation coefficient from cover to ambient (W/m^2K), given by equation (6.11) [4]:

$$h_{r,c-a} = \varepsilon_c \sigma (T_c + T_a)(T_c^2 + T_a^2) \tag{6.11}$$

A_r : Receiver area and A_c ,the glass tube area.

$h_{r,r-c}$: Linearized radiation coefficient from receiver to cover (W/m^2K), given by equation (6.12) [4]:

$$h_{r,r-c} = \frac{\sigma(T_r^2 + T_c^2)(T_r + T_c)}{\frac{1}{\varepsilon_r} + \frac{A_r}{A_c}(\frac{1}{\varepsilon_c} - 1)} \quad (6.12)$$

In order to investigate heat losses, the glass tube temperature must be known. This temperature is closer to the ambient temperature than the receiver temperature. The energy balance while ignoring the radiation absorbed by the glass cover is [4]:

$$A_c(h_{r,c-a} + h_w)(T_c - T_a) = A_r h_{r,c-a}(T_r - T_c) \quad (6.13)$$

From equation (6.13), T_c can be solved as shown by equation (6.14)

$$T_c = \frac{A_r h_{r,r-c} T_r + A_c(h_{r,c-a} + h_w)T_a}{A_r h_{r,r-c} + A_c(h_{r,c-a} + h_w)} \quad (6.14)$$

The procedure to find the glass tube temperature is by iteration as shown in Figure (6.4): Estimate U_L by considering a random T_c (close to T_a). Then if T_c differs from the original value, iterate. Usually no more than 2 iterations are required [4].

The total heat loss is given by equation (6.15) [4]:

$$Heat-losses = A_r U_l(T_r - T_a) \quad (6.15)$$

The collector efficiency factor, which is defined as the ratio of the energy collected by a solar collector to the radiant energy incident on the collector, is used to compute heat removal factor [4].

The collector efficiency factor is given by equation (6.16) [4]:

$$F' = \frac{1/U_L}{\frac{1}{U_L} + \frac{D_\circ}{h_{fi} D_i} + (\frac{D_\circ}{2k}\ln\frac{D_\circ}{D_i})} \quad (6.16)$$

Where:

$D_\circ$ And D_i :The outside and inside diameter of the receiver tube.

h_{fi} : Convective heat transfer coefficient inside the receiver tube (W/m^2K).

When the thickness of the receiver tube is negligible, the collector efficiency factor becomes [4]:

$$F' = \frac{1/U_L}{\frac{1}{U_L} + \frac{1}{h_{fi}}} \tag{6.17}$$

The convective heat transfer coefficient h_{fi} is obtained from the standard pipe flow equation [4]:

- Turbulent flow ($\mathrm{Re} \geq 2300$) , $Nu = 0.023(\mathrm{Re})^{0.8}(\mathrm{Pr})^{0.4}$ (6.18)
- laminar flow ($\mathrm{Re} \leq 2300$), $Nu = 4.364$ (6.19)

Where:

$\mathrm{Re} = \frac{\rho V D_i}{\mu}$, is the Reynolds number.

$\mathrm{Pr} = \frac{C_p \mu}{k_f}$, is the Prandtl number.

μ = Fluid viscosity ($Kg/m.s$)

k_f = Thermal conductivity of fluid ($W/m.K$).

The heat removal factor is given by equation (6.20) [4]:

$$F_R = \frac{\dot{m} C_p}{A_r U_L}\left[1 - \exp\left(-\frac{U_L F' A_r}{\dot{m} C_p}\right)\right] \tag{6.20}$$

The solar energy conversion efficiency of the parabolic trough collector is given by equation (6.21) [4]:

$$\eta_{Solar-conversion} = \frac{Q_{Useful}}{Q_{Solar}} \tag{6.21}$$

6.4 PARAMETERS USED IN THE NUMERICAL APPROACH

The parameters used in the thermal predictions of the proposed low cost parabolic trough collectors for air heating system shown in Figure (6.3) are presented in Table (6.1) below.

Table 6.1: Operating parameters required to perform the analysis.

Parameters used in the design of the excel spread sheet	
Collector length (L)	1800mm
Collector width (W)	2000mm
Collector depth (D)	625mm
Number of collectors (B)	2
Solar glass tube diameter (OD;ID)	OD=43mm and ID=57mm
Solar glass tube length (L)	1800mm
Copper receiver tube diameter (d)	22mm
Copper receiver tube length (l)	1900mm
Copper absorptivity coefficient: (α)	0.95
Glass tube transmittance: (τ)	0.91
Mirror reflectivity: (λ)	0.96
Reflectivity percentage: (ρ)	1-57/2000 = 0.97
Emissivity of receiver copper: (ε)	0.19
Actual projected area ($A_{projected}$)	6.8 m^2
Stefan Boltzmann constant: (σ)	5.67×10^{-8} W/m^2.K^4
Peak sun irradiation: ($Q_{U\circ}$)	1000 W/m^2

The assumptions used in this prediction are:

- Steady flow operation exists;
- Air is an ideal gas with constant specific properties;
- Local atmospheric pressure;
- Average ambient temperature throughout the year in PE: $T_a = 20$;
- An average wind speed of 8 m/s is assumed;

- Because the two collectors are connected in series, to simplify the analysis the two collectors are assumed to be one collector having an equal length of twice of the single collector;.
- The emissivity of the pure copper tube used is assumed to be constant. This assumption is valid because the emissivity of pure copper does not vary much with temperature;
- The glass tube transmittance is also assumed to be constant.

6.5 PRESENTATION OF THE EXCEL SPREADSHEET RESULTS

Figures (6.6) and (6.7) show the actual print screen of the spread sheet. Figure (6.6) shows the heat transfer parameters used to compute the exit air temperature and the efficiency of the collector. The thermal results of the spread sheet when the heating is done in December for an airflow rate of 10 l/s are given in Figure (6.7). Figure (6.7) shows the air exit temperature for a heating that occurs from 8am to 4pm.

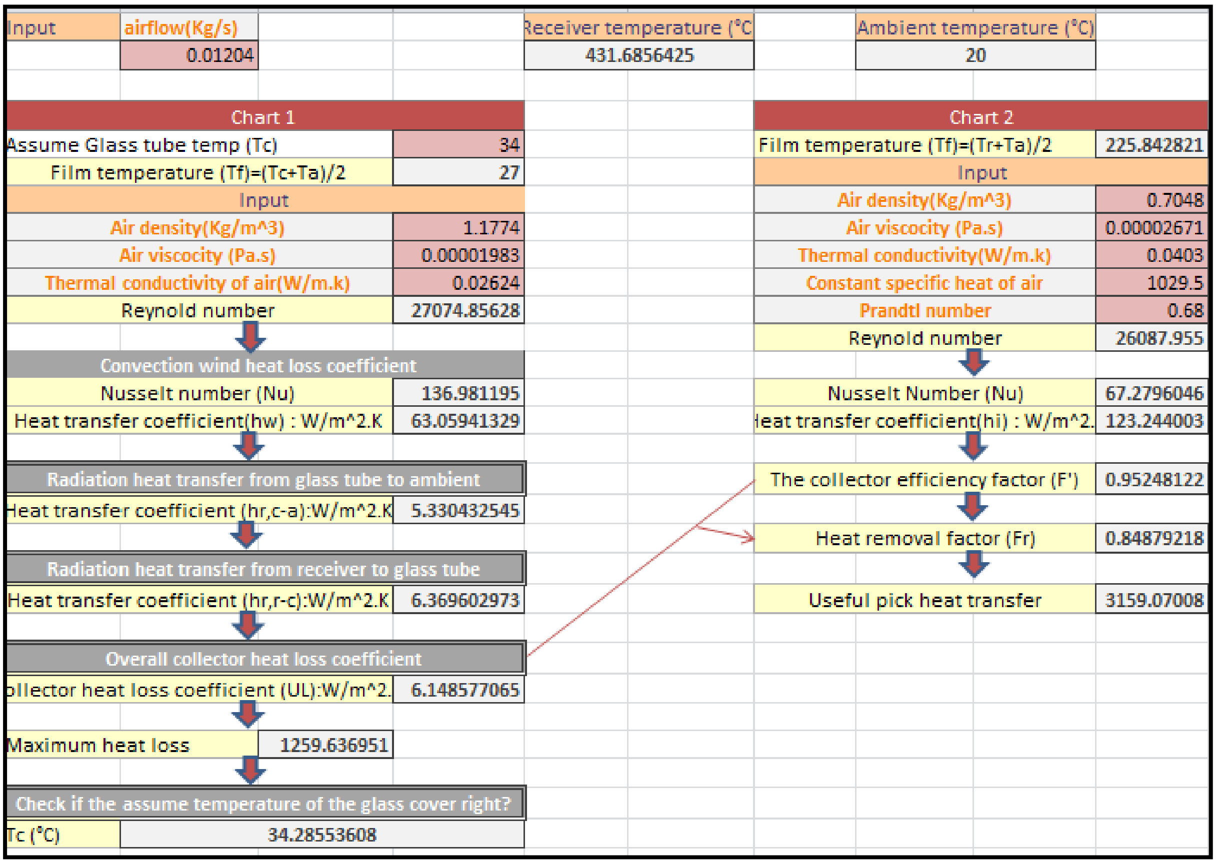

Figure 6.6: Heat transfer parameters.

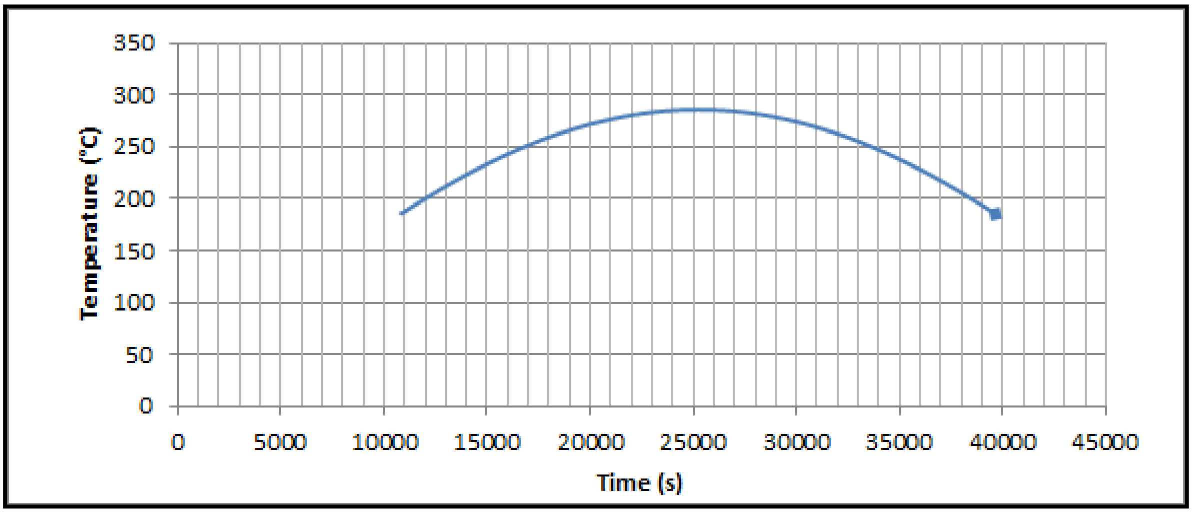

Figure 6.7: Output temperature from the collectors at a flow rate of 10 l/s.

The analysis of heat losses across the collector receiver tube is time consuming because of the iterative procedure required to obtain the glass tube receiver surface temperature as shown in Figure (6.6). To simplify the spread sheet and to hasten the iterative procedure, the heat losses across the receiver tube of the proposed PTSC were analysed for the operating flow rate range. A correlation of the heat losses with respect to the air flow rate was derived as shown in Figure (6.8). Figure (6.9) shows the simplified heat transfer parameters without the iterative procedure.

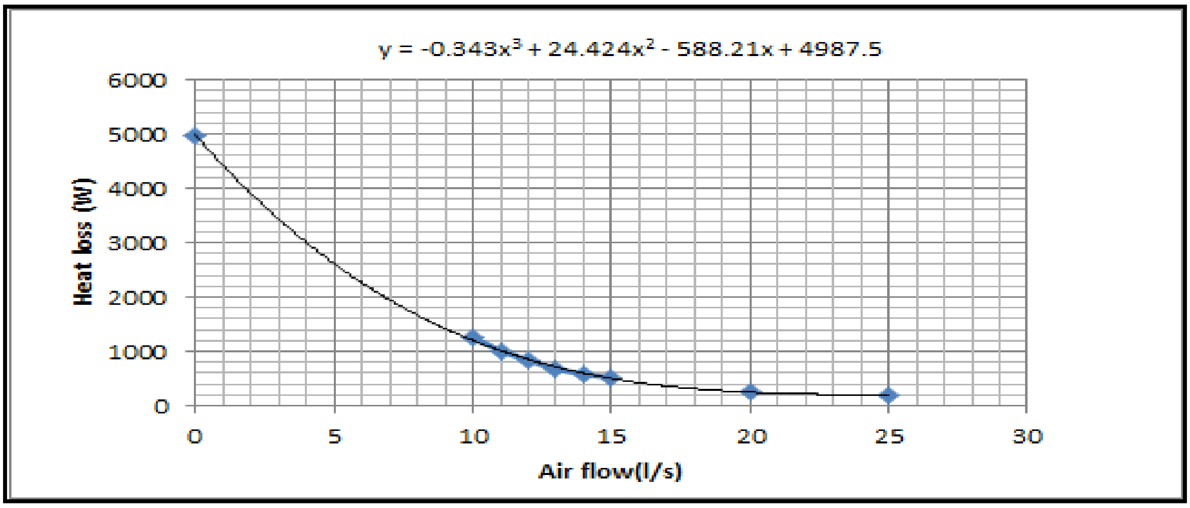

Figure 6.8: Variation of receiver tube heat losses with air flow rate

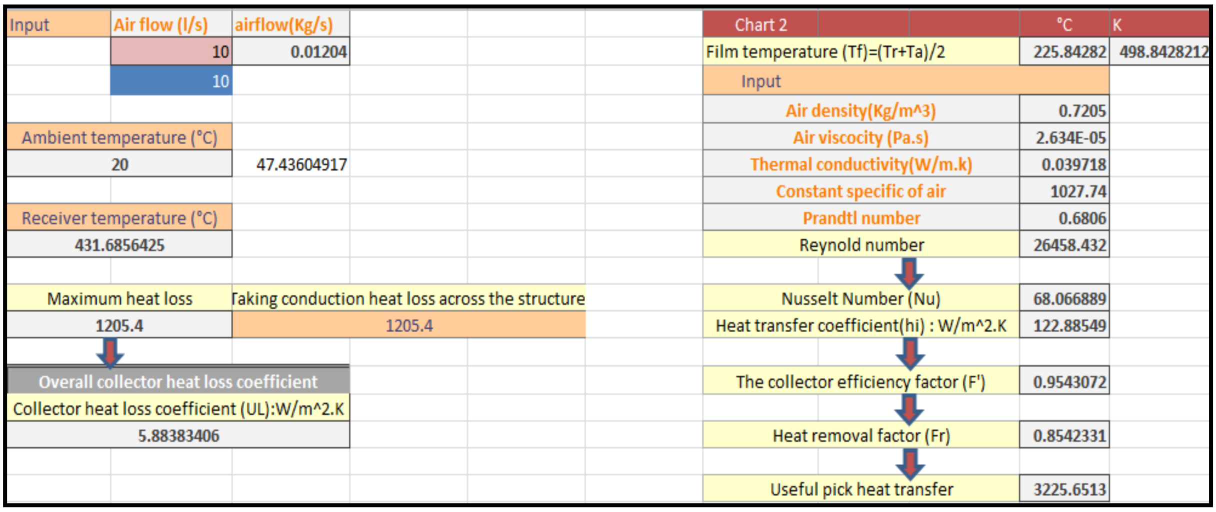

Input	Air flow (l/s)	airflow(Kg/s)
	10	0.01204
	10	
Ambient temperature (°C)		
20		47.43604917
Receiver temperature (°C)		
431.6856425		
Maximum heat loss		Taking conduction heat loss across the structure
1205.4		1205.4
Overall collector heat loss coefficient		
Collector heat loss coefficient (UL):W/m^2.K		
5.88383406		

Chart 2	°C	K
Film temperature (Tf)=(Tr+Ta)/2	225.84282	498.8428212
Input		
Air density(Kg/m^3)	0.7205	
Air viscocity (Pa.s)	2.634E-05	
Thermal conductivity(W/m.k)	0.039718	
Constant specific of air	1027.74	
Prandtl number	0.6806	
Reynold number	26458.432	
Nusselt Number (Nu)	68.066889	
Heat transfer coefficient(hi) : W/m^2.K	122.88549	
The collector efficiency factor (F')	0.9543072	
Heat removal factor (Fr)	0.8542331	
Useful pick heat transfer	3225.6513	

Figure 6.9: Simplified heat transfer parameters.

The predictions presented in Figures (6.10, 6.11, 6.12) are for a summer application where the heating occurs from 8am to 4 pm which represents 8 hours of heating cycle. The detailed discussion of the results is presented in Chapter 7.

Figure (6.10) shows the effect of increasing the flow rate of air on the amount of the energy extracted by the air. As the flow rate is increased, the amount of energy absorbed by the working fluid (Air) also increases. Figure (6.11) illustrates the effect of air flow on the temperature profile of the air; the increase in the airflow leads to a decrease of the air exit temperature from the parabolic trough collector. Figure (6.12) demonstrates the effect of flow rate onto the solar energy conversion efficiency of the collectors.

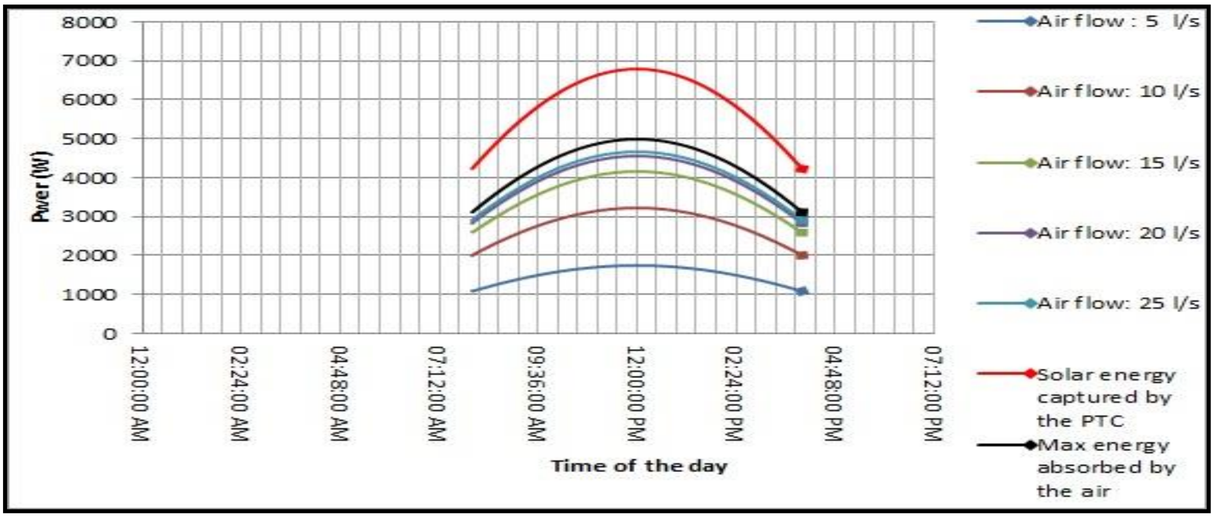

Figure 6.10: PTC solar power graph

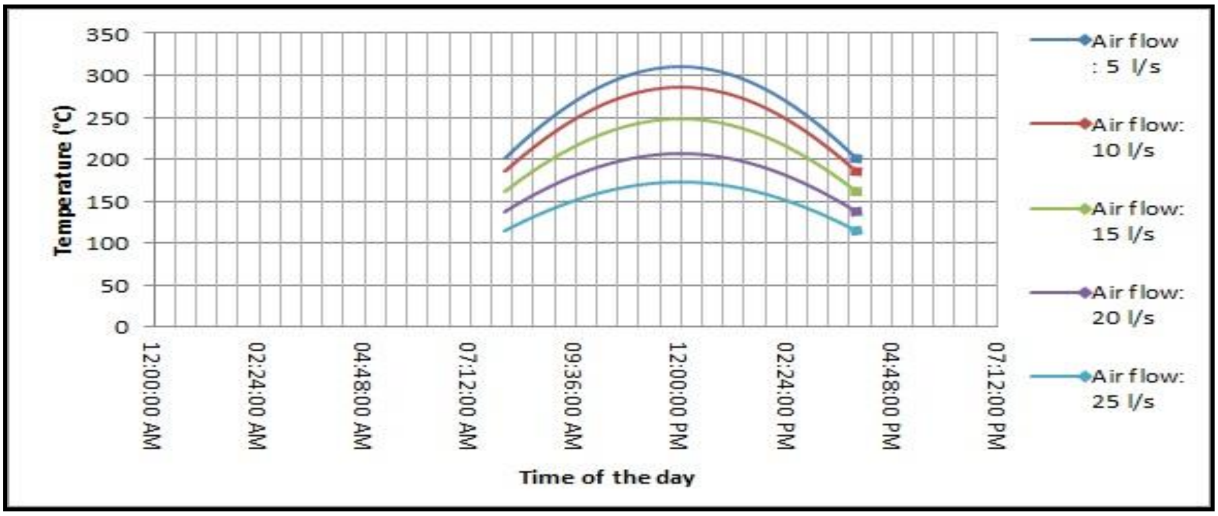

Figure 6.11: Air exit temperature of the PTC at different flow rates.

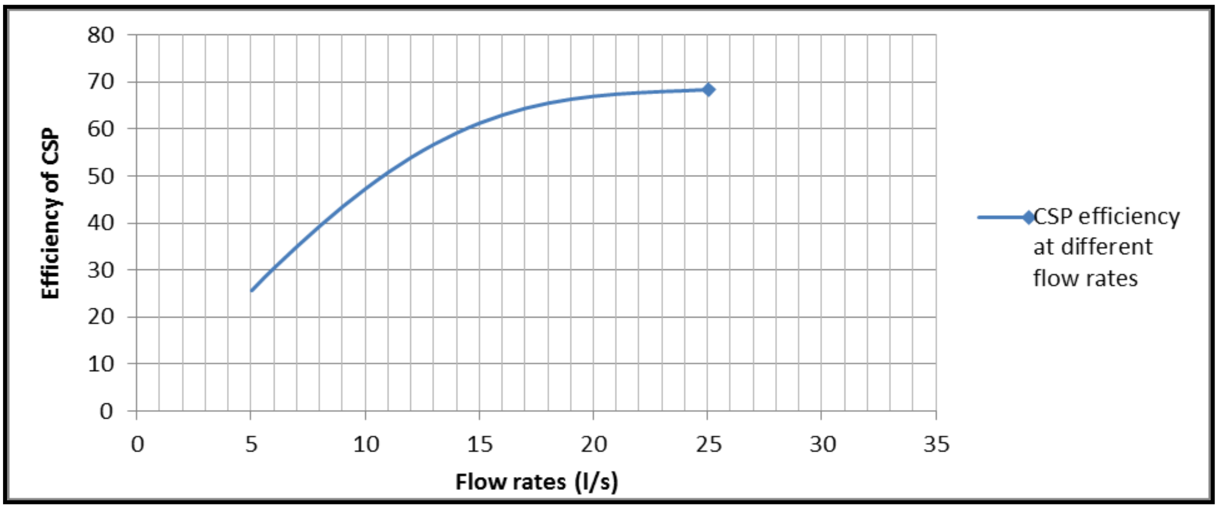

Figure 6.12: Efficiency of solar energy conversion of the CSP at different flow rates

6.6 SUMMARY

The objective of this chapter was the development of a spread sheet to predict the thermal performance of the proposed parabolic trough solar collectors for air heating systems. The spread sheet can be used as an operational manual to predict the thermal performance of the collectors. The experimental results showed that the predicted results correlate well with the experimental results. The percentage error between the predicted and actual thermal performance is in the range of (4-20) % as discussed in Chapter 7.

CHAPTER 7: ANALYSIS OF THE RESULTS AND DISCUSSIONS

7.1 INTRODUCTION

The development of a low cost parabolic trough solar collector for air heating systems and a packed-bed rock thermal energy storage system for high temperature storage was investigated in this dissertation. This chapter discusses a comparison between the experimental and the numerical results. The first section of this chapter presents the results of the packed rock thermal energy storage system where the predictions and the actual experimental test results are compared. The effect of flow rate, rock sizes and temperature on the pressure drop and thermal energy storage is investigated. The effect of adding baffles for better air flow distribution through the rocks on the pressure drop and thermal energy stored is also investigated. In the second part of this chapter, the results of the proposed low cost CSP are analysed. The third part of this chapter investigates the effect of varying the air flow rate using the proposed low cost PTC to heat the rocks on the thermal energy stored. The effect of air recirculation is also investigated. Finally a brief economic analysis of the designs and the recommendations for further work are presented.

7.2 PACKED-BED ROCK THERMAL ENERGY RESULTS

The investigations of these results are discussed in this section. The development of a numerical approach to predict the performance of the packed-bed rock storage system handled in Chapters 4 and 5 showed a good agreement between the predicted and actual results. The operating parameters of the tests conducted are discussed in Chapters 4 and 5 and the experimental set up of the testing with all the equipments used to record the results is shown in Chapter 3.

7.2.1 CHARGING CYCLE

7.2.1.1 PRESSURE DROP

The variation of pressure drop was investigated as a function of mass velocity, rock size and temperature in this section.

7.2.1.1.1 PREDICTED ANALYTICAL RESULTS:

Figures (7.1) and (7.2) indicate the effect of particle size and the mass velocity on the pressure drop in the rock bed. The increase in mass velocity results in an increase in pressure drop and also as the particle size decreases, the pressure drop increases [6, 16].

As the pressure drop correlation is dependent on the dynamic viscosity of the working fluid, the rise in temperature of the working fluid leads to an increase in pressure drop through the rock bed as shown in Figure (7.3). [1].

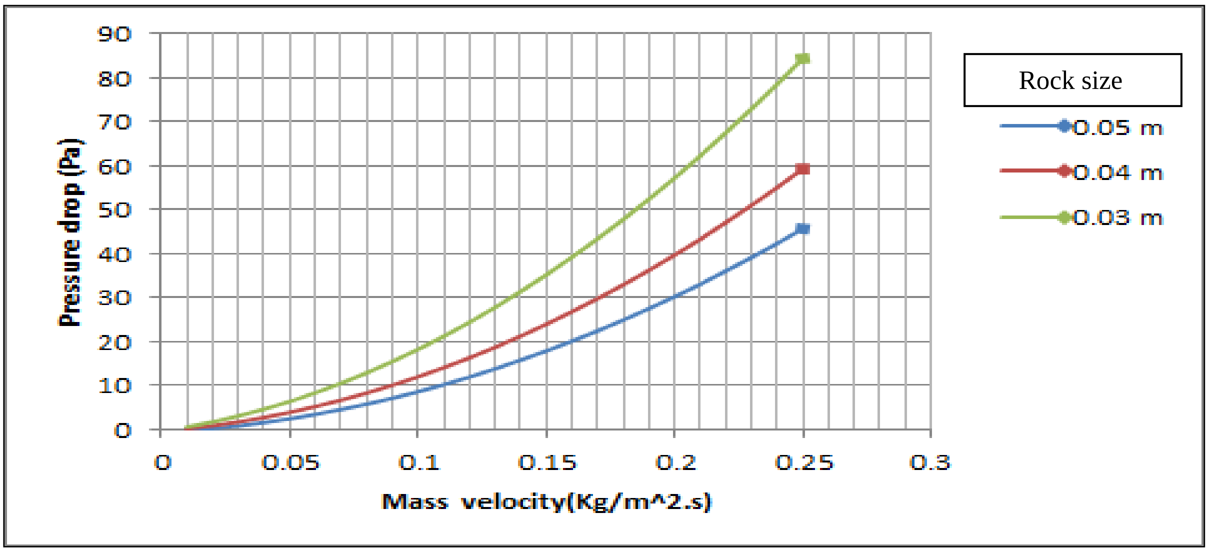

Figure 7.1: The relation between pressure drop, mass velocity and rock size.

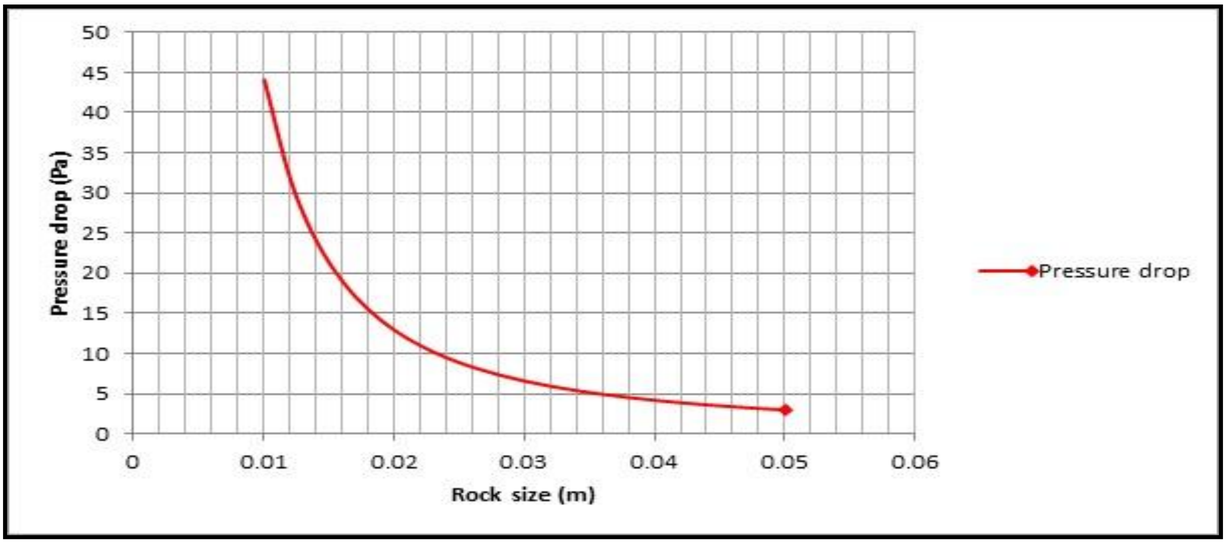

Figure 7.2: The relation between pressure drop and rock size.

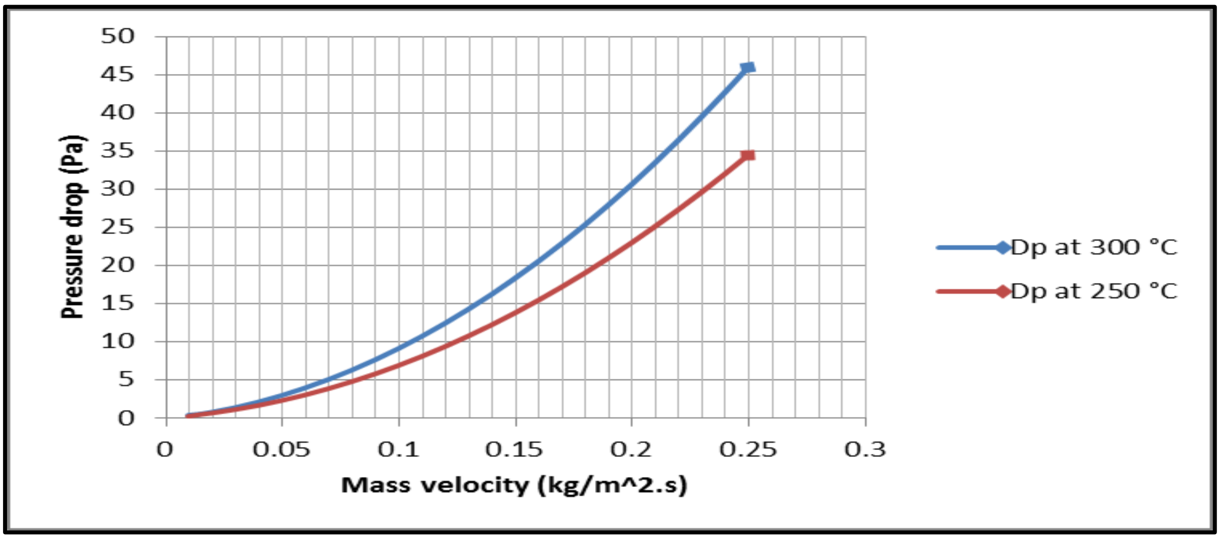

Figure 7.3: Influence of temperature on pressure drop.

7.2.1.1.2 ACTUAL RESULTS:

The actual pressure drop through the rock storage tank was recorded using a pressure sensor. This pressure measured is the total pressure through the bed system. It includes pressure drop through the rocks, the pressure drop through the piping system in the tank and the pressure drop caused by the air diffusing system in the tank (baffles). In this analysis the rock diameter was constant at 50mm and the flow rate was varied. The result of the measured pressure drop is shown in Figure (7.4).

Figure (7.5) shows the total predicted pressure drop through the storage tank without accounting for the baffling system. At a flow rate of 5 l/s the predicted pressure drop is 7 Pa, whereas the pressure drop recorded from Figure (7.4) is 120 Pa at the same flow rate. The difference in the pressure values implies that the baffles create a significant pressure drop through the system.

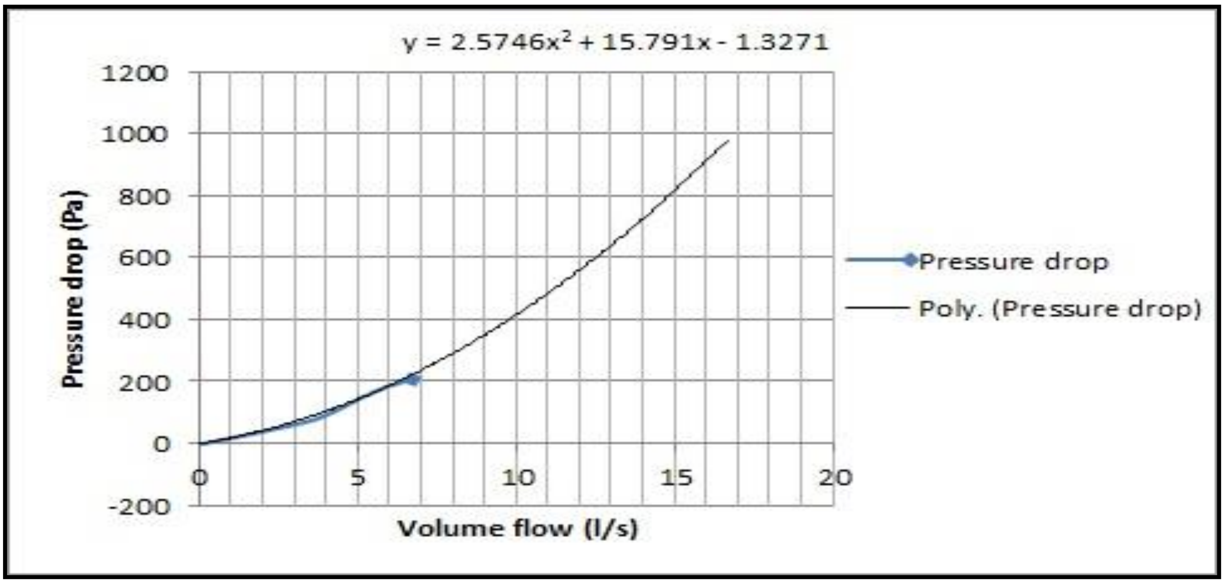

Figure 7.4: The relation between pressure drop and the flow rate.

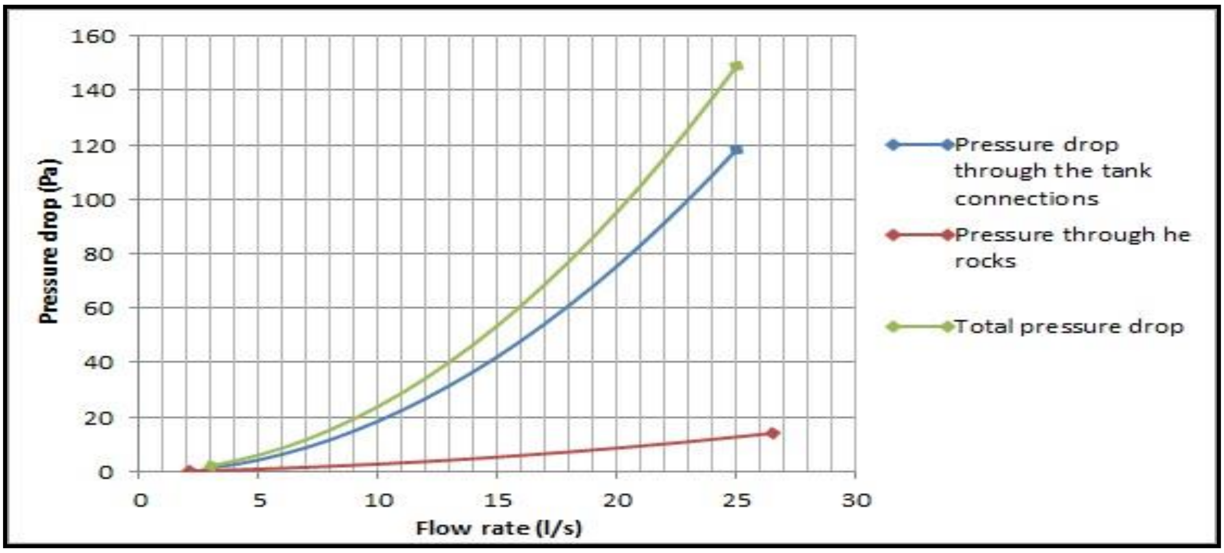

Figure 7.5: Predicted pressure drop as a function of flow rate (without taking baffles into consideration).

7.2.1.2 THERMAL ANALYSIS:

7.2.1.2.1 PREDICTED ANALYTICAL RESULTS

Figures (7.6) and (7.7) show the temperature distribution of the rocks for each layer along the packed bed. At the start of the charging heat cycle (time=0s) there was a steep temperature gradient and as the time increased the packed bed temperature became asymptotic to the inlet temperature [12, 16].

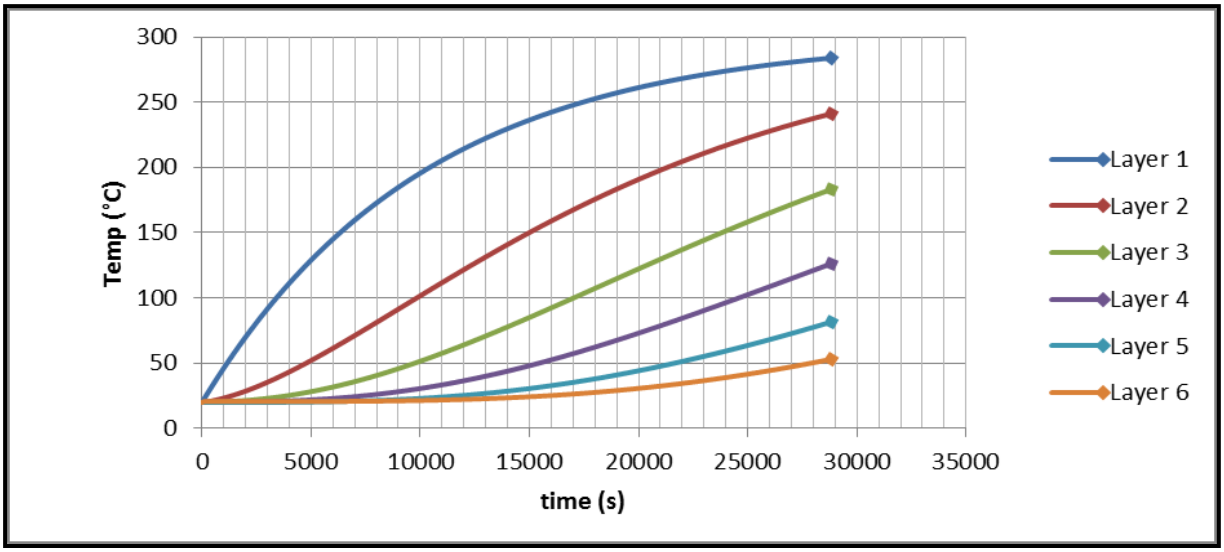

Figure 7.6: Temperature predicted over the 8h of charging cycle at 5 l/s.

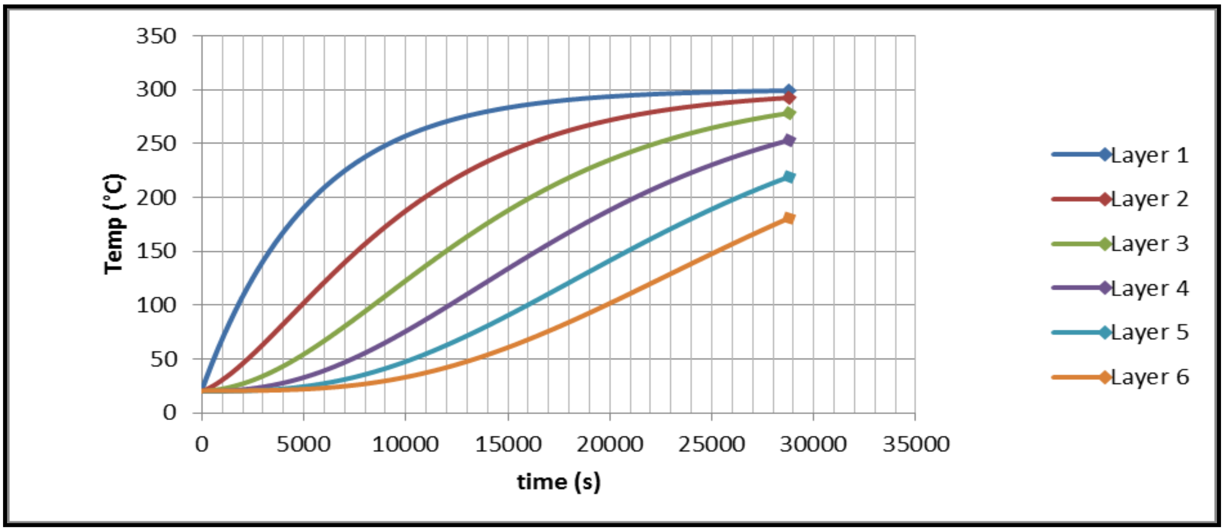

Figure 7.7: Temperature predicted over the 8h of charging cycle at 10 l/s.

Figure (7.8) demonstrates the mass velocity effect on the thermal energy stored. The increase in mass flow rate of air leads to an increase in energy stored and to a fast arrival to steady state because of the fast charging of the rocks [13, 16].

Figure (7.9) shows the amount of the energy stored by the system as a function of the flow rate. The figure shows that the relation between the energy stored and the flow rate is not linear but exponential. At flow rates higher than 20 l/s, the energy stored graph is asymptotic to the maximum energy that can be stored by the tank. There is no substantial energy storage gained by increasing the flow from 10 l/s to 20 l/s [12, 16, 18].

The effect of particle size on the energy stored is shown in Figure (7.10).The smaller the rock size, the more energy is stored by the rocks because there is an increase in the heat transfer surface area and also the mass of the rocks [6, 16].

The amount of energy stored is dependent on the thermal capacity of the packed bed storage material. The increase of the thermal capacity causes the increase in the ability of the storage medium to absorb more thermal energy as shown in Figure (7.11) [16].

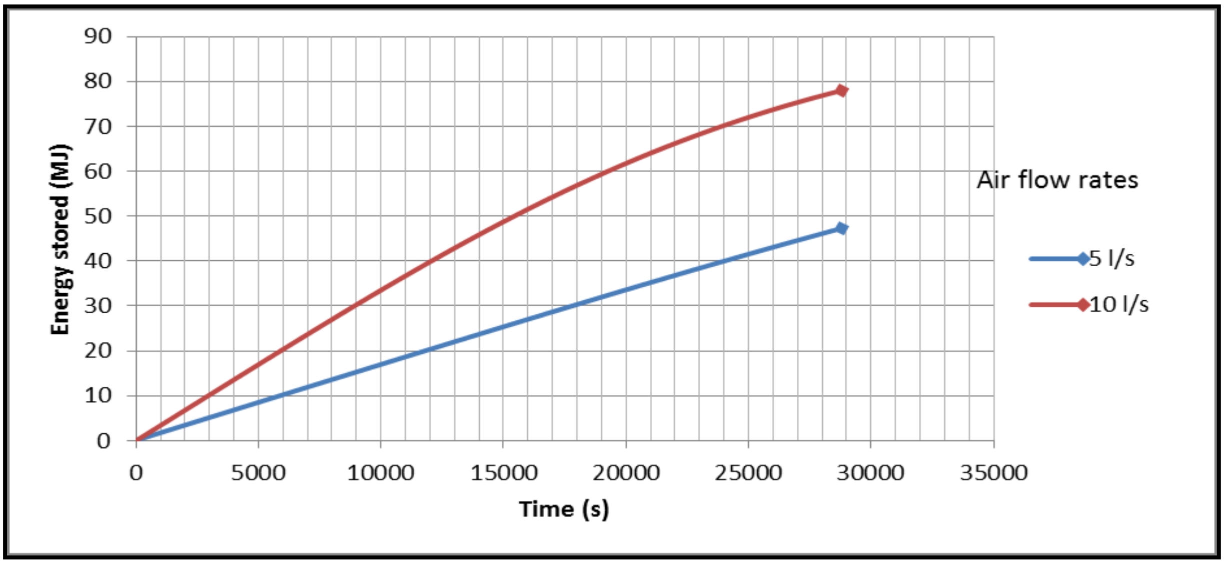

Figure 7.8: The change of the total energy stored predicted with time at different flow rates.

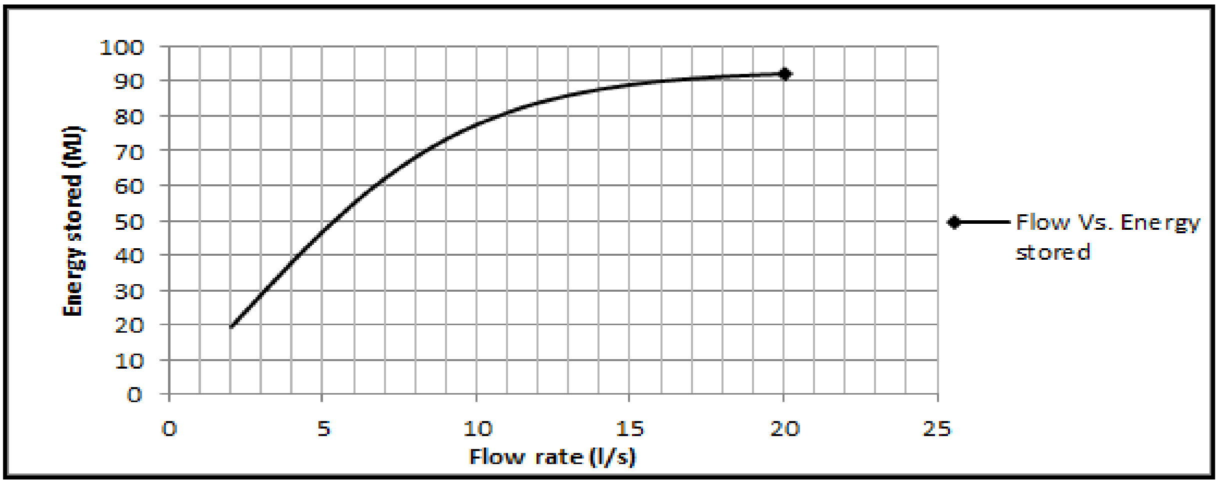

Figure 7.9: Relation between flow rates and energy stored.

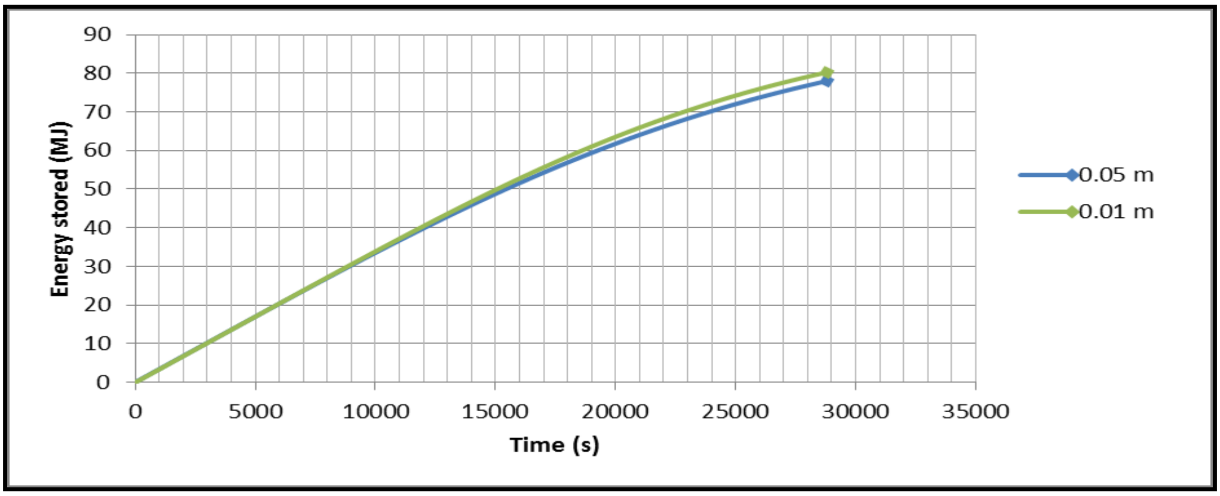

Figure 7.10:: The change of the total energy stored with time for different rock sizes.

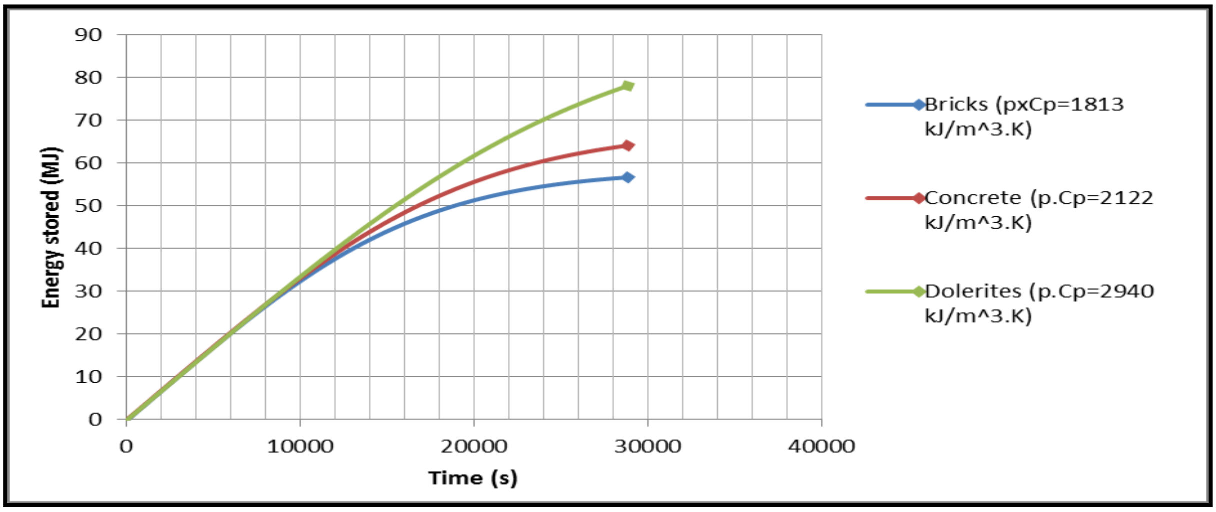

Figure 7.11: Change of energy stored with time for different thermal capacities.

Figure (7.12) illustrates the interaction between the input energy to the system (hot air), the energy absorbed by the rocks and the energy that is dumped by the system. This graph shows the importance of recirculating the air. By recirculating the air, power can be saved because if for example it takes 3.6 kW to raise the air temperature from ambient to 300°C, it will only take half of that power to raise the temperature from a recirculated air of 150°C to 300°C. Recirculation is very important in solar collectors because the solar energy is not constant throughout the day. Making use of recirculation means in the afternoon when the solar energy is low we can still maintain high temperature inlet to the storage tank because the recirculated air will be at high temperature, which means it only requires a small amount of energy to heat it to the required temperature.

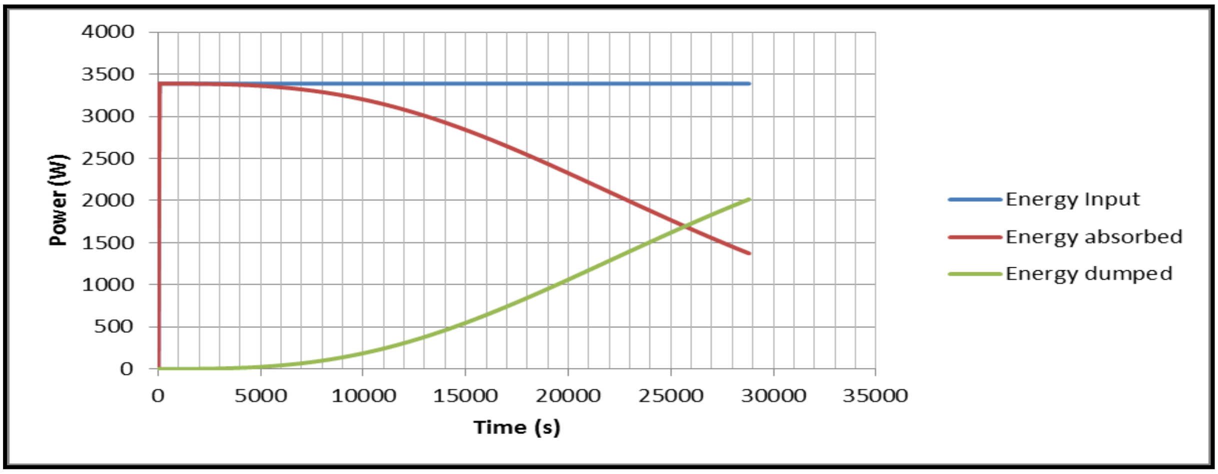

Figure 7.12: Predicted power graphs at 10 l/s.

7.2.1.2.2 ACTUAL EXPERIMENTAL RESULTS:

The results presented are for a 7-hour heat charging cycle at a constant flow rate of 10 l/s. The actual and predicted results are compared. The results show a good agreement between the two methods as shown in Figures (7.13-7.17).

Figure (7.18) shows the comparison between the predicted and the actual thermal energy stored. There is a good correlation as the difference between the actual and predicted is less than 4%. The correlation between the practical and predicted method is an indication that the incorporation of the baffles has allowed even distribution of air flow through the rocks because the prediction assumed even distribution of air flow. Therefore the baffles have allowed effective heating of the rocks and solved the problem of air channeling through the path of least resistance.

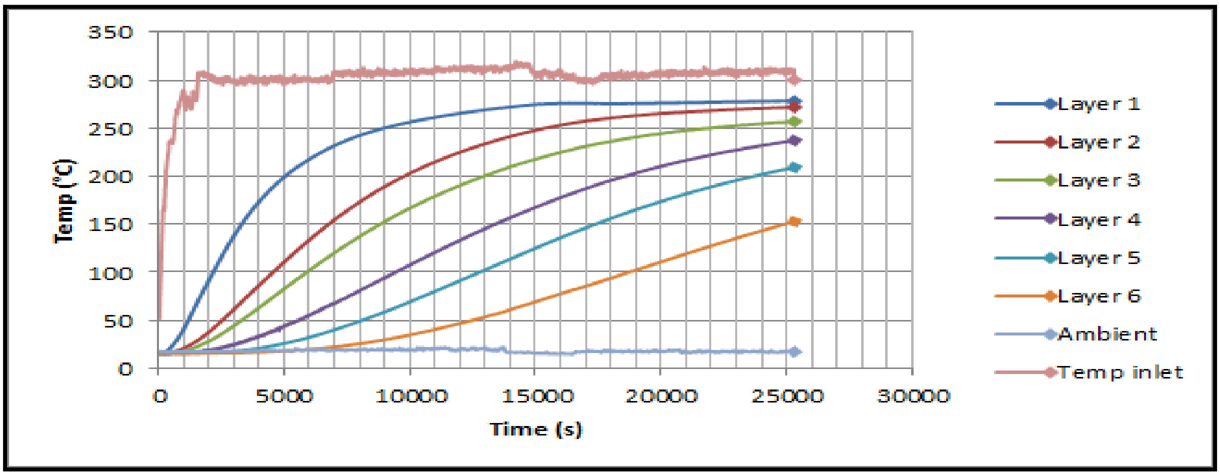

Figure 7.13: Temperature recorded over 7h of charging cycle at 10 l/s.

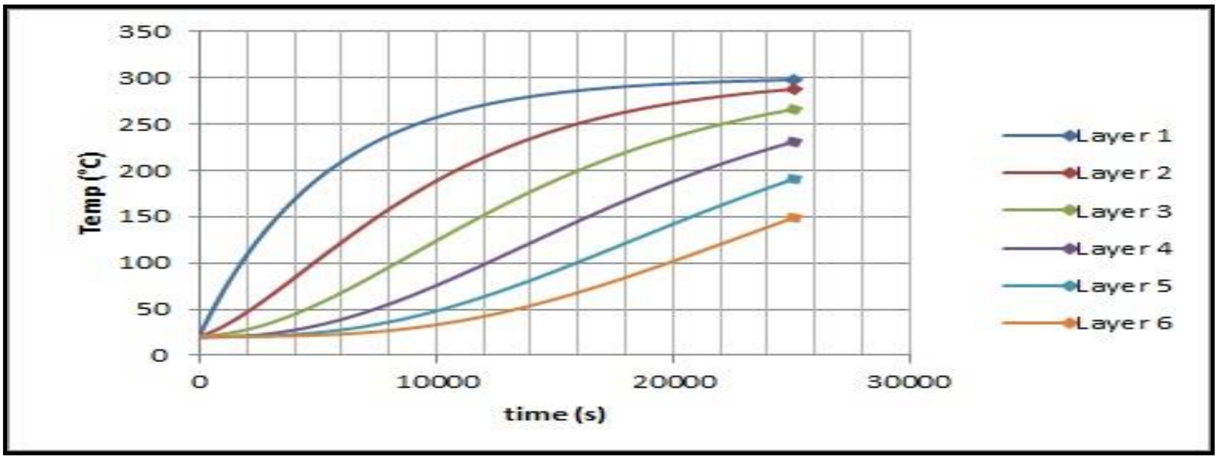

Figure 7.14: Temperature predicted over the 7 hours of charging cycle at 10 l/s.

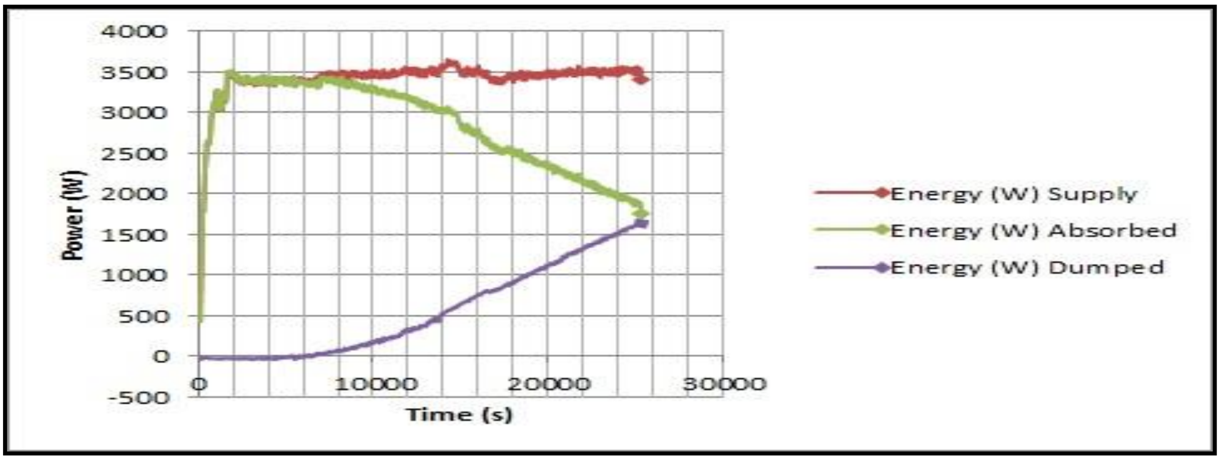

Figure 7.15: Actual power graphs at 10 l/s for 7- hours' charging cycle

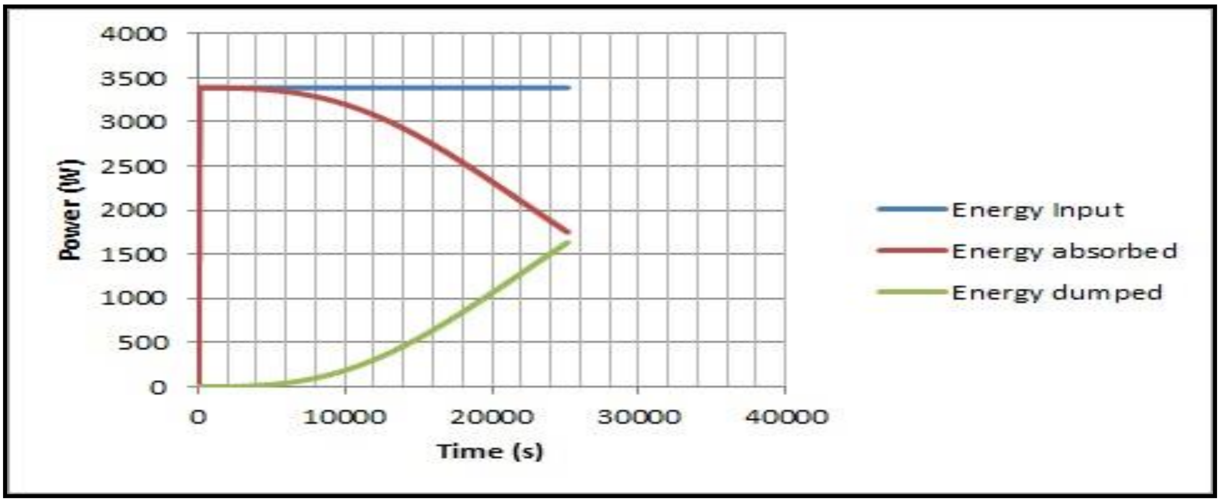

Figure 7.16: Predicted power graphs at 10 l/s for 7- hours' charging cycle

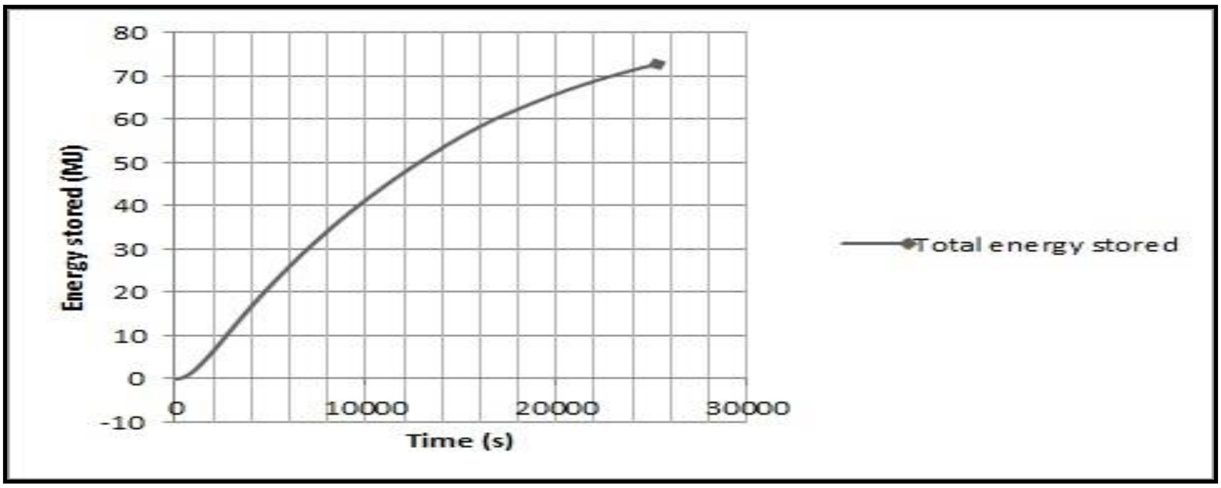

Figure 7.17: Actual total thermal energy stored at 10 l/s.

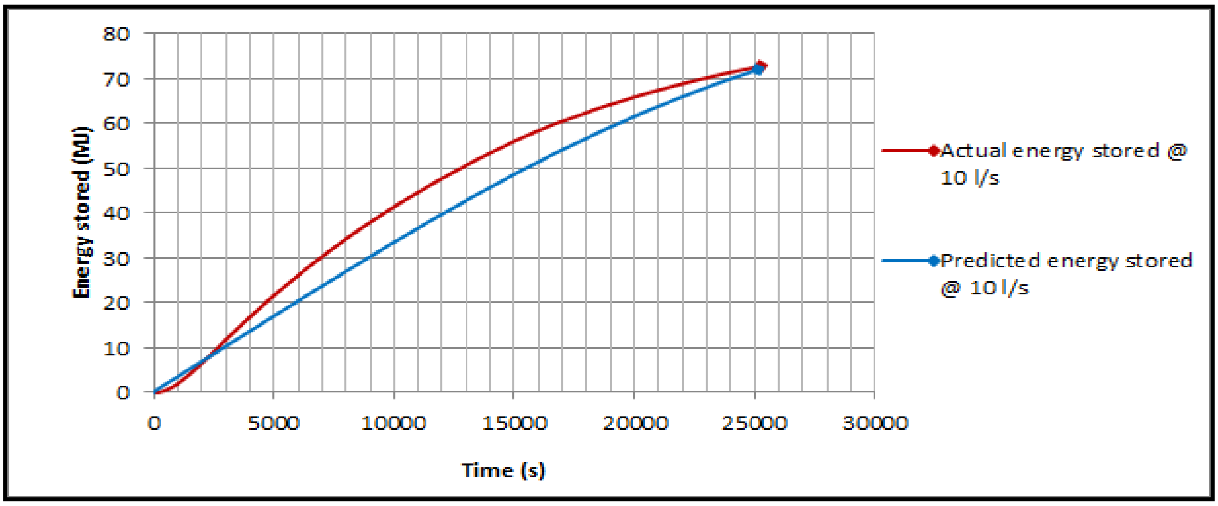

Figure 7.18: Actual vs Predicted total energy stored for 7- hours' charging cycle.

7.2.2 HEAT STORAGE ANALYSIS:

The storage results based on the insulation techniques that were used are discussed in this section. The predicted and the actual results of the storage temperature for a 3-day period are investigated. The vacuum storage tank is designed to reduce heat loss to a minimum. The prediction is that the tank will be able to store at least 80% of the total energy for a period of 3 days.

7.2.2.1 PREDICTED RESULT

The predicted results of the different insulation techniques used are discussed in this section. The results are based on a 300°C storage temperature for a period of three days and an ambient of 18°C was assumed. Figure (7.19) shows a screen print of the input parameters to the spreadsheet. In this figure two parameters are varied, the insulation thickness and the number of aluminium foil layers to investigate their effect on the storage temperature.

Storage Temperature (°C)	300
Ambient Temperature (°C)	18

Inputs	
Insulation thickness (m)	0.06
Surface area of tank outside (m^2)	3.3
Surface area of tank inside (m^2)	2
Cp rocks (J/Kg.K)	1050
Rocks density	2800
Volume of storage	0.25
Teflon cross sectional Area (m^2)	0.004
Teflon length (m)	0.1
Stainless steel Cross sectioanl area (m^2)	0.00125
Length of stainless steel (m)	0.1
Thermal conductivity of teflon (W/m.K)	0.27
Thermal conductivity of stainless steel (W/m.K)	19
Thermal conductivity of perlite (W/m.K)	0.043
Boltzmann constant(W/m^2.K^4)	5.67E-08
Steel emissivity	0.2
Number of aluminium foil layers	5
Radiation heat transfer coeff(Hrad)[W/m^2.K)	0.908414

Figure 7.19: Input parameters

The storage temperature of the rock bed of dolerite as a function of the time for a period of three days is shown in Figures (7.20) and (7.21). Figure (7.20) shows the storage temperature as a combined effect of the conduction heat loss through the tank (teflon and stainless steel) and heat loss through the expanded perlite region, whereas Figure (7.21) shows the effect of conduction heat loss through the tank (Teflon and stainless steel) and in the vacuum space (5 aluminium foil layers). The decrease in temperature due to the conduction heat transfer from the teflon and stainless steel fitting is the same for both cases. The combined effect of conduction heat loss through the fittings is minimal; 86% of the storage temperature decrease occurs in the annular space between the inner and the outer tank.

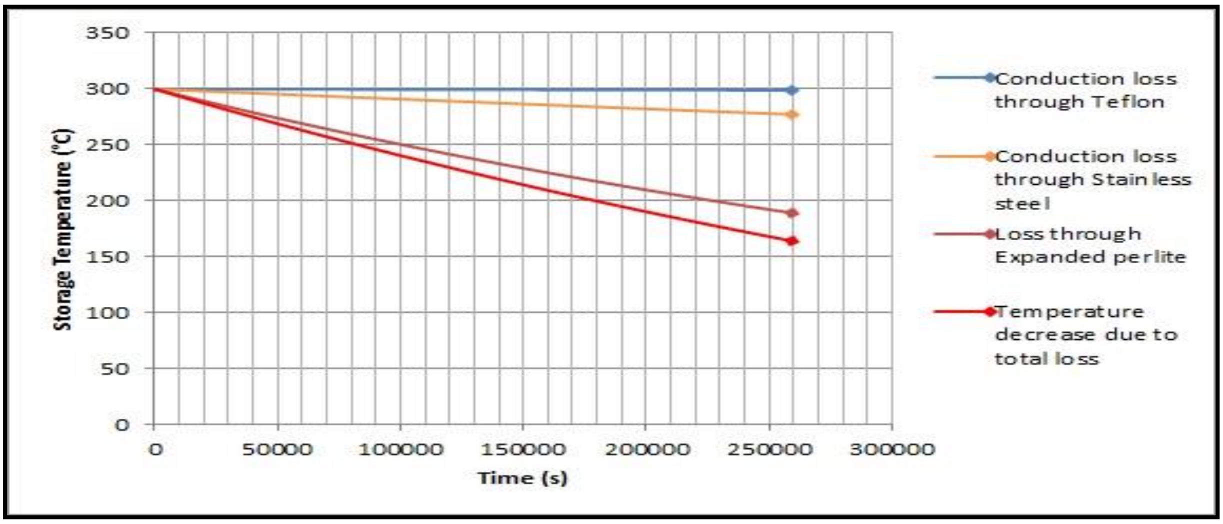

Figure 7.20: Storage temperature as a function of time using expanded perlite insulation.

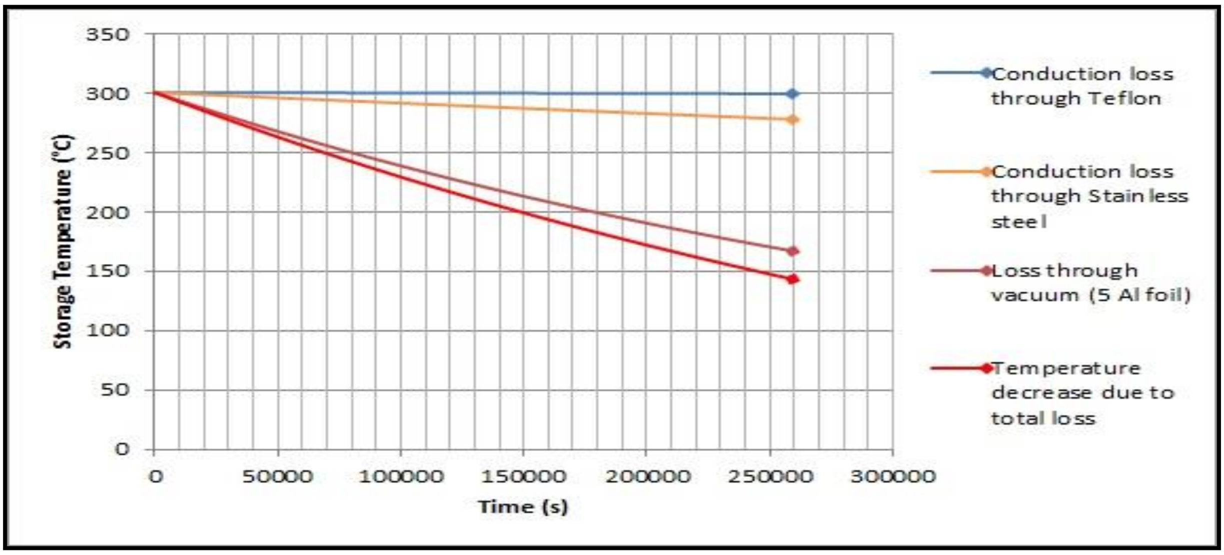

Figure 7.21: Storage temperature as a function of time using vacuum insulation.

Figure (7.22) illustrates the effect of inserting aluminium foil layers in the vacuum space on the storage temperature. Increasing the number of aluminium foil layers increases the storage temperature significantly. As shown in Figure (7.22) going from 5 aluminium foil layers to 20 has the effect of increasing the storage temperature from 142 °C to 233°C.

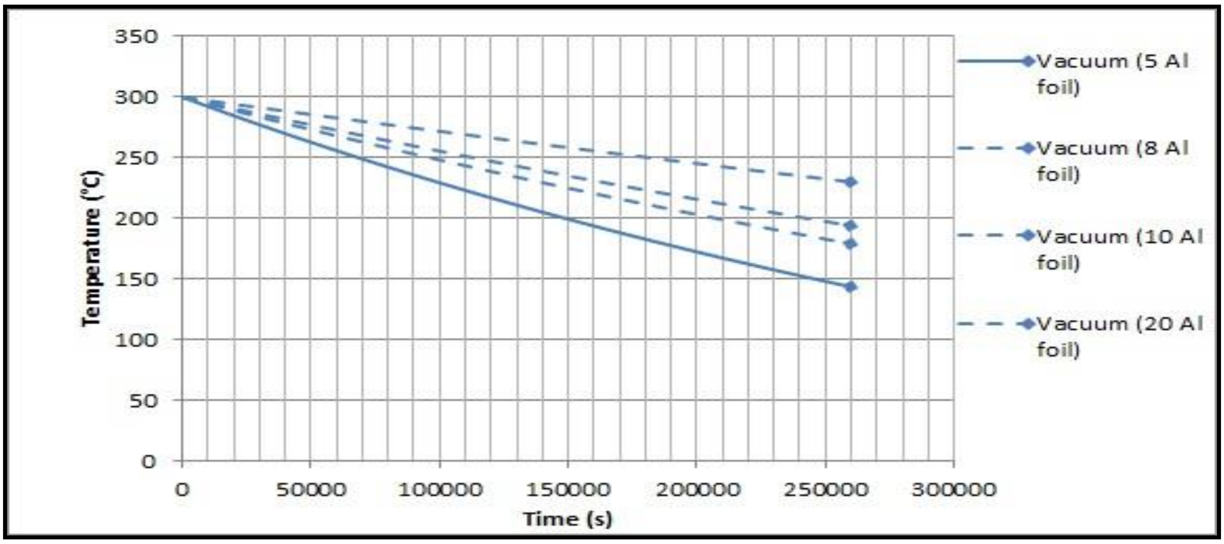

Figure 7.22: The effect of aluminium foil layers on storage time.

Figure (7.23) shows the effect of increasing the thickness of perlite insulation on the storage time (increasing insulation thickness means increasing annular space between the inside and outside tanks). The increase of the expanded perlite insulation thickness leads to an increase of the storage temperature. The storage temperature increased from 163°C to 232°C by increasing the insulation thickness from 60mm to 150mm.

The prediction of the storage temperature based on the expanded perlite insulation was performed at atmospheric pressure (without vacuum). In the actual testing, the investigation of the combination of vacuum and expanded perlite will be investigated. The analysis showed that if only expanded perlite insulation was used, 180 mm of insulation thickness would lead to 15% heat loss in the storage for a three-day storage time and bearing in mind that conduction heat loss through the connections accounts for about 10% of the total energy loss as shown in Figures (7.20) and (7.21), implies that only 5% of the energy would be lost through the expanded perlite insulation. The reason why a 60 mm annular space between the inside and outside tank (filled with expanded perlite) was selected is that a combined effect of expanded perlite and vacuum insulation will be used. The vacuum lowers the thermal conductivity of the perlite which leads to a reduction in the insulation thickness required. Due to equipment constraints a vacuum of up to 80 % was used. Figure (7.24) shows the actual predicted comparison where the expanded perlite (without vacuum) thickness cannot be changed but the aluminium layers are varied. When fewer than 7 layers of aluminium foil are used, the expanded perlite insulation performs better than the vacuum insulation, but when more layers are used the vacuum insulation becomes more effective than the perlite insulation.

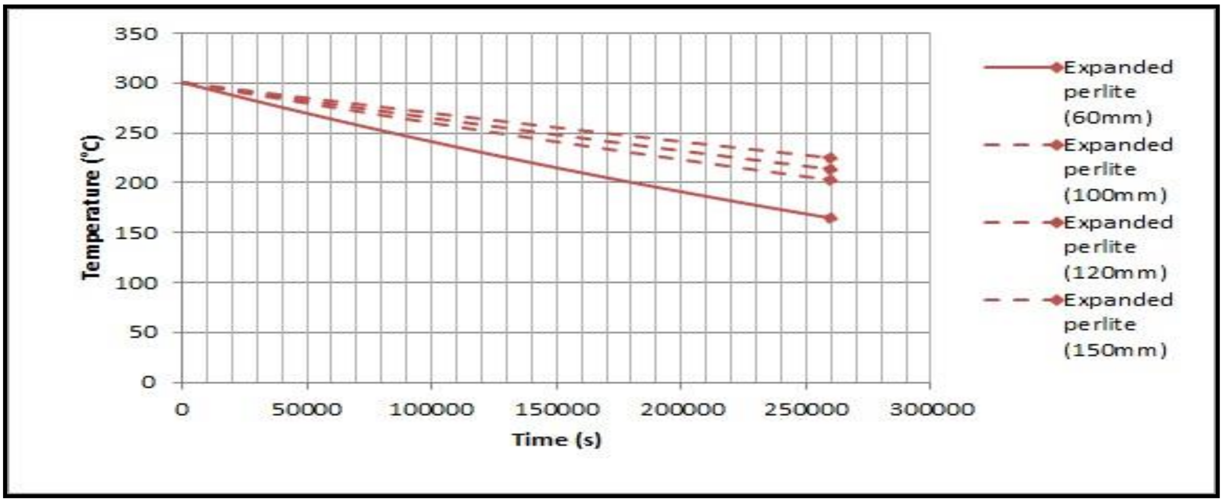

Figure 7.23: The effect of expanded perlite thickness on storage temperature.

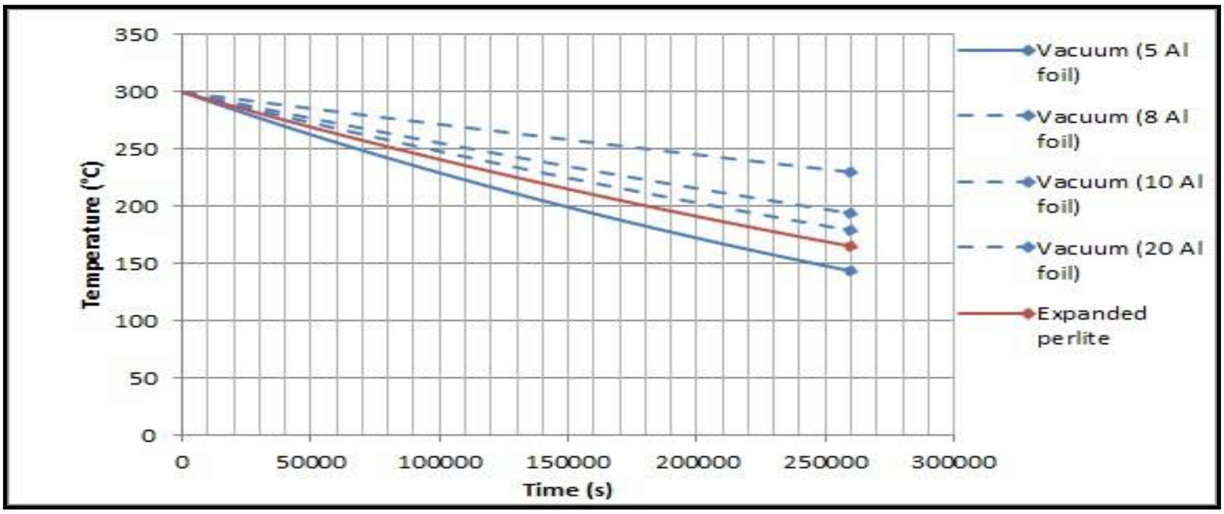

Figure 7.24: Storage temperature as function of time for vacuum insulation vs. perlite insulation.

7.2.2.2 ACTUAL RESULTS:

The two insulation techniques that were used are tested and the comparison between the two techniques are presented in this section

7.2.2.2.1 VACUUM INSULATION PLUS THE USE OF MULTILAYER ALUMINIUM FOIL:

To understand the effect of a vacuum on the heat loss, the system is tested without the vacuum first. The results show an average daily heat loss efficiency of about 42%. The results of the test are shown in Figures (7.25) and (7.26).

Energy stored (kw.h)			
Day	Energy	Efficiency	Average daily heat loss efficiency
Start	19		
Day 1	9.2	51.57895	
Day 2	5.1	44.56522	
Day 3	3.5	31.37255	42.50557126

Figure 7.25: Energy stored over 3 days of storage without vacuum.

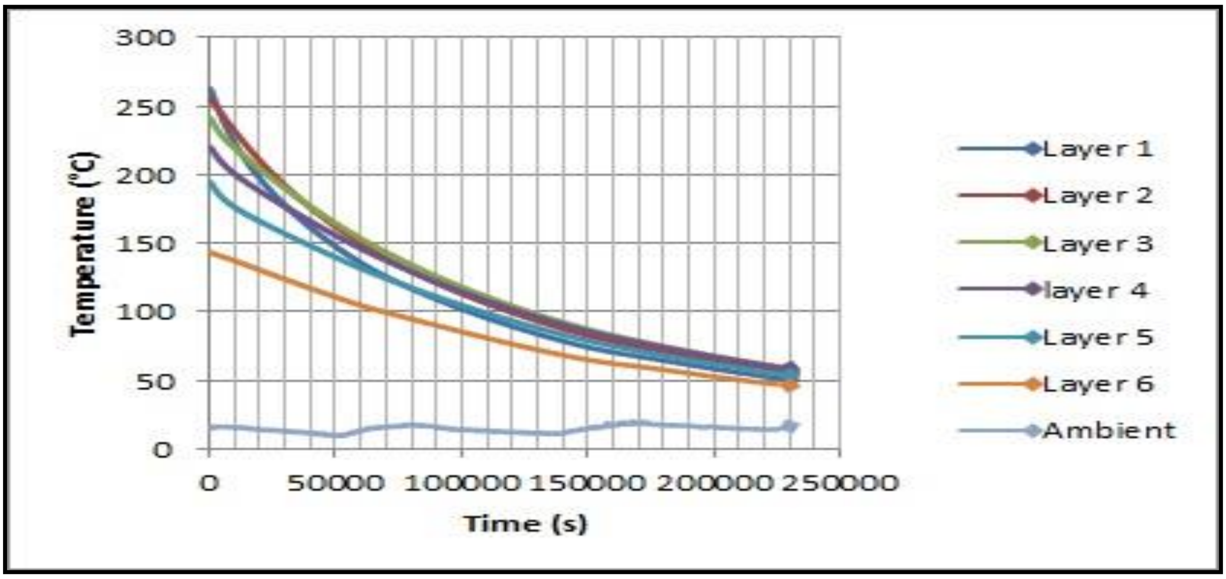

Figure 7.26: Variation of the stored temperature over 3 days of storage (no vacuum)

The results presented in Figures (7.28) and (7.29) show the effect of an 80% vacuum of the system on the heat loss. The average daily heat loss efficiency has improved from 42% to 39%. The comparison between the two results is presented in Figure (7.30).

The comparison between the prediction of the storage temperature based on a full vacuum and the 80% vacuum is shown in figure (7.31). At the end of the 3-day storage the prediction showed 158°C, whereas in the actual testing the recorded temperature was 64°C. The result shows that the effect of the vacuum on the heat loss is not linear; a 100% vacuum is 2.5 times more effective than an 80 % vacuum and 2.93 times more effective than no vacuum. This result confirms that vacuum insulation is only effective at pressures below 0.01 bar (beyond 90% vacuum). This statement is demonstrated in Figure (7.27) where the effect of vacuum pressure on the thermal conductivity of materials is shown [28]. Figure (7.27) shows that the decrease of thermal conductivity is considerable when the vacuum pressure is less than 10 kPa (Beyond 90%). From atmospheric pressure (0 % vacuum) to 10 kPa (90 % vacuum) the thermal conductivity is reduced slightly but from 10kPa to 0kPa, the thermal conductivity is reduced by a factor of around 3.

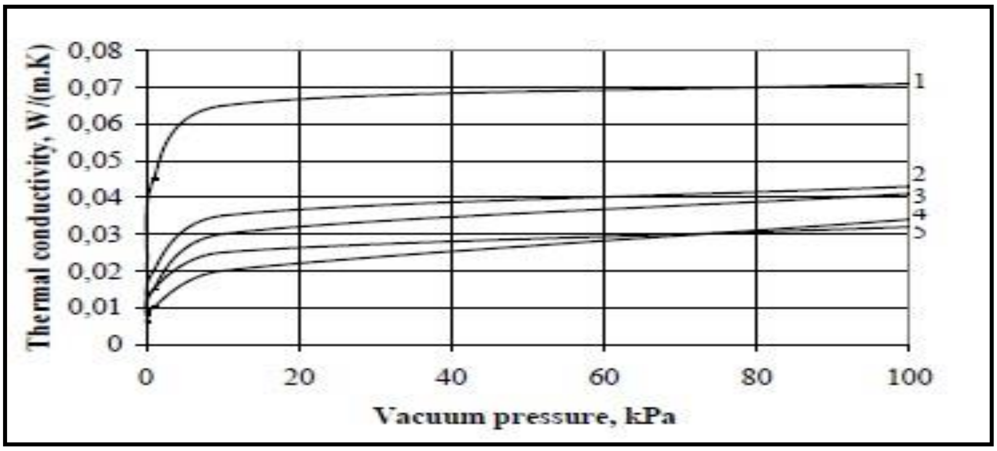

Figure 7.27: Dependence of thermal conductivity on vacuum pressure for different materials [28].

Energy stored (kw.h)			
Day	Energy	Efficiency	Average daily heat loss efficiency
Start	20.3		
Day 1	11.8	41.87192	
Day 2	7.2	38.98305	
Day 3	4.4	38.88889	39.91462031

Figure 7.28: Energy stored over 3 days of storage with 80% vacuum.

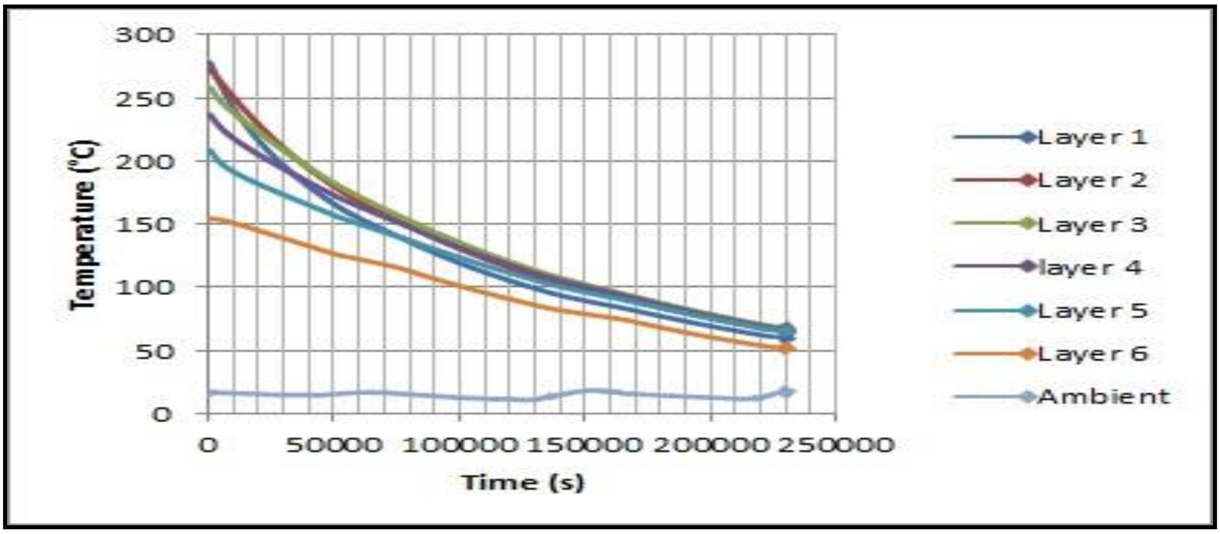

Figure 7.29: Variation of the storage temperature over 3 days with 80 %vacuum.

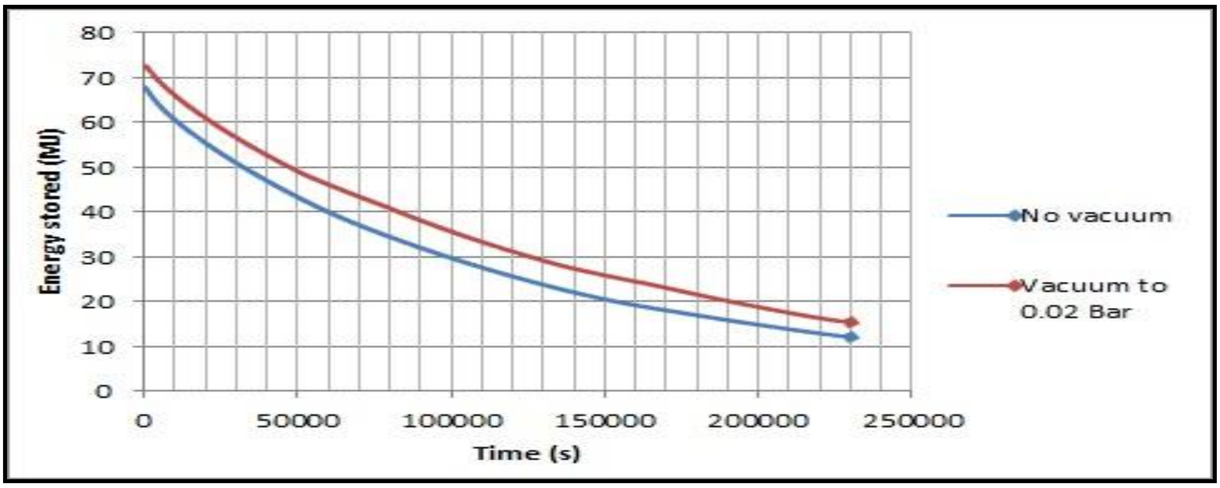

Figure 7.30: Effect of vacuum on heat storage.

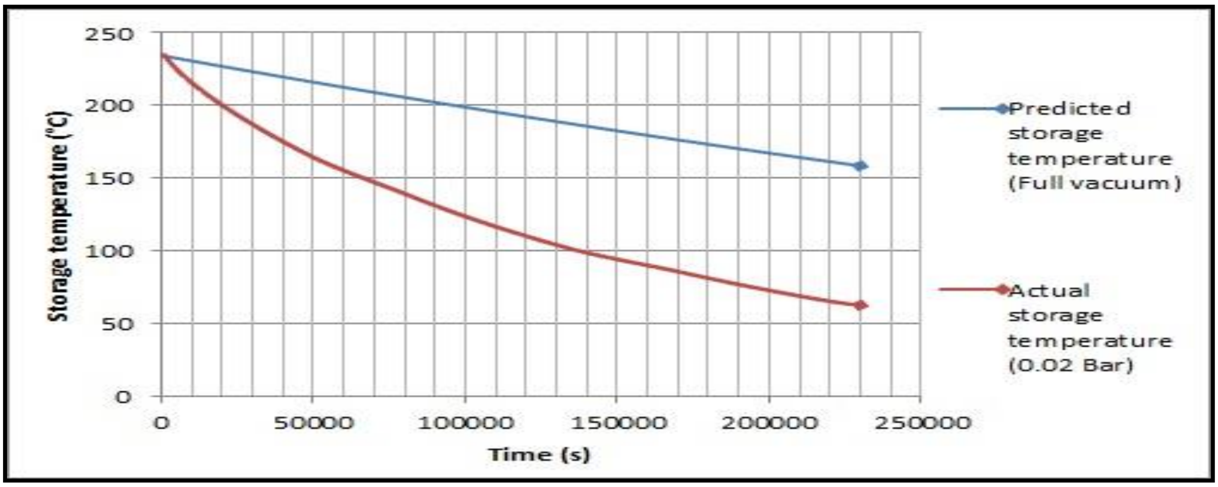

Figure 7.31: Predicted vs actual storage temperature.

7.2.2.2.2 VACUUM INSULATION PLUS THE USE EXPANDED PERLITE:

The procedure followed is the same as in the previous section. The first test conducted on the system insulated with expanded perlite was without any vacuum. The results shown in Figures (7.32) and (7.33) showed average daily efficiency heat loss of 29 % whereas the results from Figures (7.34) and (7.35) indicated a 27 % average daily heat loss efficiency from the test conducted at 70% vacuum. The results show only a 2 % improvement in the daily heat loss efficiency caused by a 70% vacuum. The comparison between the test conducted without a vacuum and the evacuated system is shown in Figure (7.36). This result once again showed that a partial vacuum has virtually no effect on the improvement of thermal insulation of a system; vacuum insulation is only effective at vacuum pressures below 10 kPa.

The comparison between the predicted and the actual results using expanded perlite insulation without vacuum is shown in Figure (7.37). The percentage difference between the two is about 18%. The difference between the results is probably due to the possible increase in moisture level in the perlite because the moisture level in Port Elizabeth is significant and it has been proven that moisture can drastically increase the thermal conductivity of a material [33].

Energy stored (kw.h)			
Day	Energy	Efficiency	Average daily heat loss efficiency
Start	20.04		
Day 1	13.2	34.13174	
Day 2	9.05	31.43939	
Day 3	7	22.65193	29.40768806

Figure 7.32: Energy stored over 3 days without vacuum.

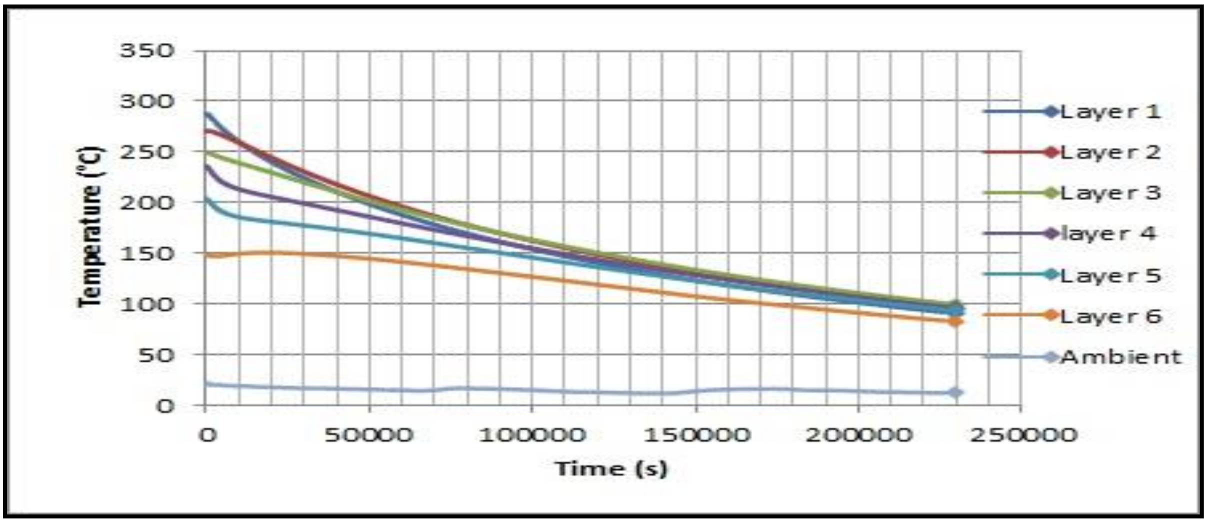

Figure 7.33: Variation of the stored temperature over 3 days of storage (no vacuum)

Energy stored (kw.h)			
Day	Energy	Efficiency	Average daily heat loss efficiency
Start	23		
Day 1	16	30.43478	
Day 2	11.5	28.125	
Day 3	8.7	24.34783	27.63586957

Figure 7.34: Energy stored over 3 days of storage with 70% vacuum.

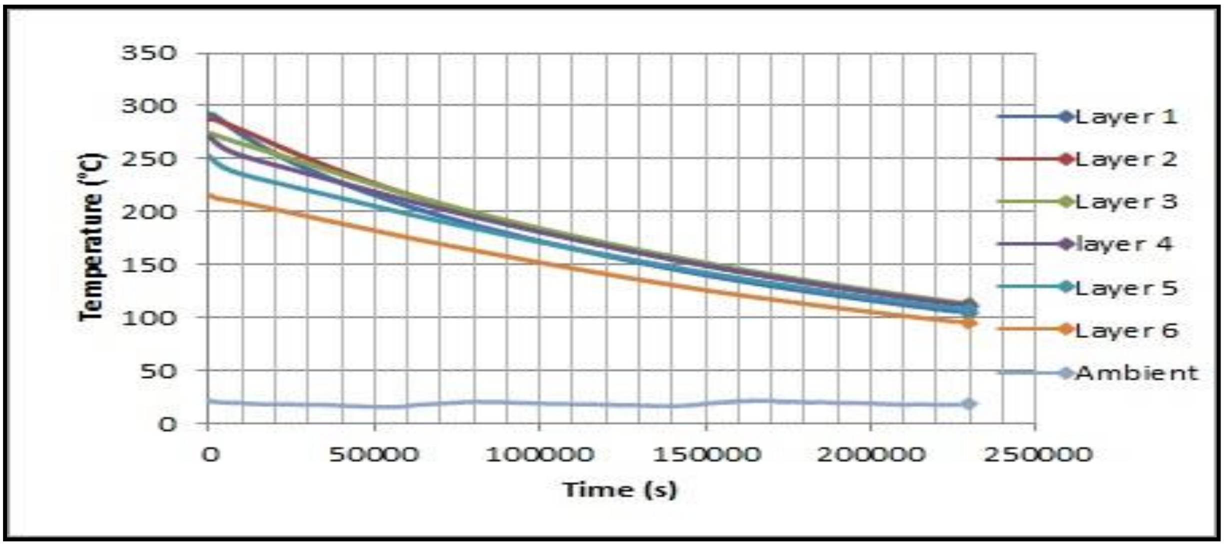

Figure 7.35: Variation of the stored temperature over 3 days of storage (70% vacuum)

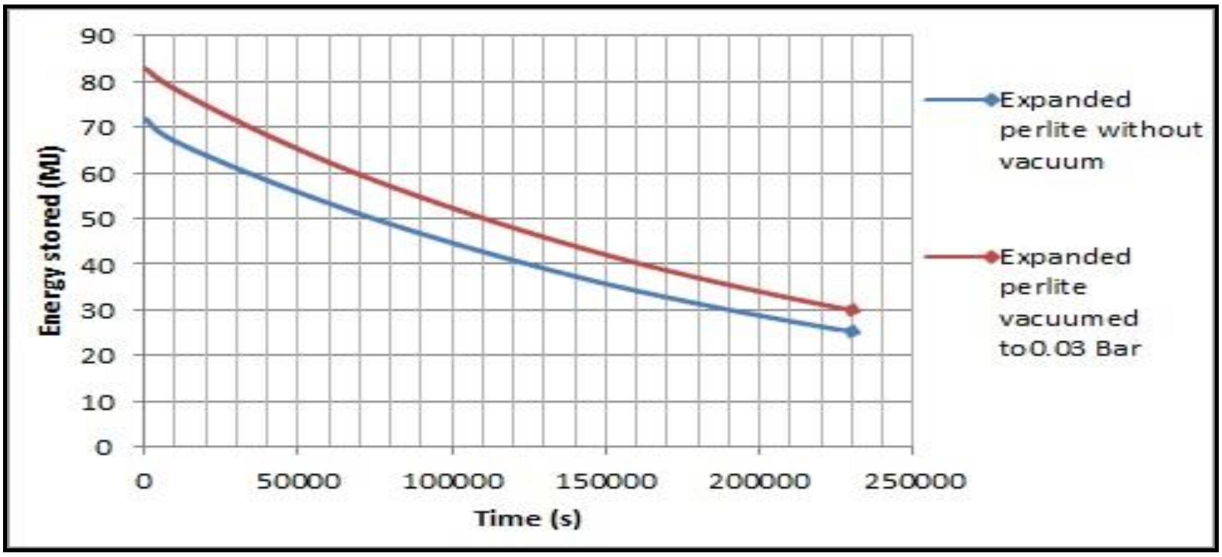

Figure 7.36: Effect of vacuum on heat storage.

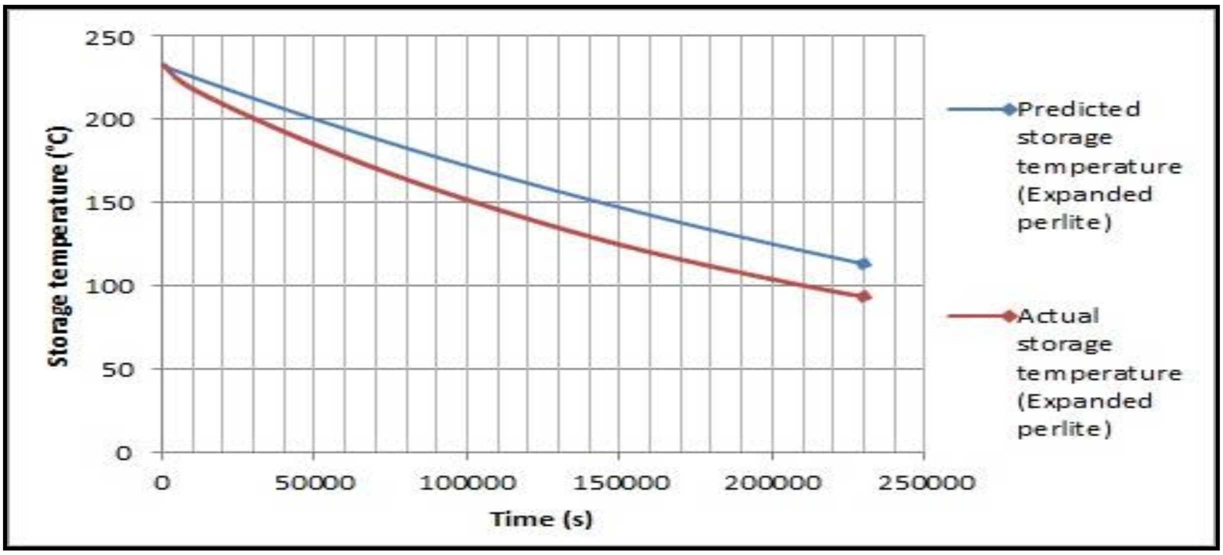

Figure 7.37: Predicted vs actual storage temperature (average thermal conductivity of the three days of storage).

7.3 PARABOLIC TROUGH SOLAR COLLECTORS RESULTS:

The test results of the proposed low cost parabolic trough collector for air heating are presented in this section. The prediction results are first discussed and in the second part the experimental results and the correlation of the results to predictions are made. A spread sheet was designed in Chapter 6 to predict the performance of the proposed CSP based on the steady state condition procedure which is known by ISO 9806-1:1994 [4] in which all the operating parameters are discussed.

The measured results are based on an experimental rig at the Renewable Energy Research Group (RERG) at Nelson Mandela Metropolitan University in South Africa which is detailed in chapter (3) [40].

As discussed in chapter (6), the predictions depend on the season of the year because the duration of the days changes according to the season under consideration but the efficiency of solar energy stays the same regardless of the change of the season. The predictions presented in Figures (7.38, 7.39, 7.40) are for a summer application where the heating occurs from 8am to 4 pm which represents 8 hours of heating cycle.

Figure (7.38) shows the effect of an increasing flow rate of air on the amount of the energy extracted by the air. As the flow rate is increased, the amount of energy absorbed by the working fluid (Air) also increases and as explained in Chapter 6 the heat removal factor is directly related to the mass flow rate therefore the increase of flow leads to more energy extraction by the air. The heat losses from the receiver are also reduced as the air flow increases because of the rapid heat extraction by the air. The peak solar energy that is captured by the PTC is related to its projected area which is 6.8 m^2 as shown in Figure (7.38), but the maximum energy that can be absorbed by the working fluid is the energy available to the working fluid at the parabolic focal point. This energy takes into account the optical losses of the PTC and as shown in Figure (7.38) the peak energy is 5 kW. This is the theoretical limit that the working fluid can absorb and it occurs when the thermal losses are negligible. From this analysis the theoretical limit of solar energy conversion efficiency can be defined as 5 kW/6.8 kW (73%).

Figure (7.39) illustrates the effect of air flow on the temperature profile of the air; the increase in the airflow leads to the decrease of the air exit temperature from the parabolic trough collector. This means that even though less power is harvested at low flow rates, the temperature is higher. To link this result to the thermal energy storage in the packed-bed rock as discussed earlier it is clear that to preserve thermal stratification in the bed using a PTC system the heating of the rocks should be done by varying the airflow rate. At the start of the rocks' charging cycle, the system should be operated at high flow rate because more energy is put into the system and as the system reaches the limit temperature at that flow rate, the flow rate should be reduced to allow the temperature to further rise. This illustration is for a system that does not allow for air recirculation. The effect of recirculating the air and its benefit are discussed in section 7.3.

Figure (7.40) demonstrates the effect of flow rate onto the solar energy conversion efficiency of the collectors. There is a steep increase of the efficiency from flow rates of 5 to 15 l/s, then the graph starts becoming asymptotic to the theoretical efficiency limit of the collectors.

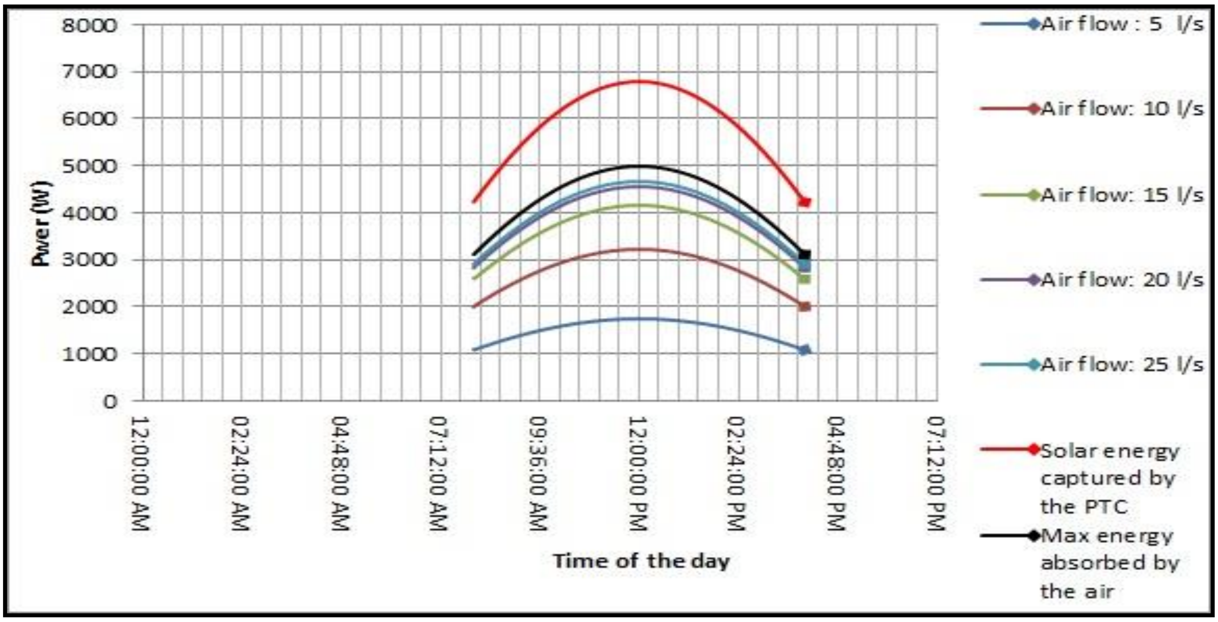

Figure 7.38: PTC solar power graph.

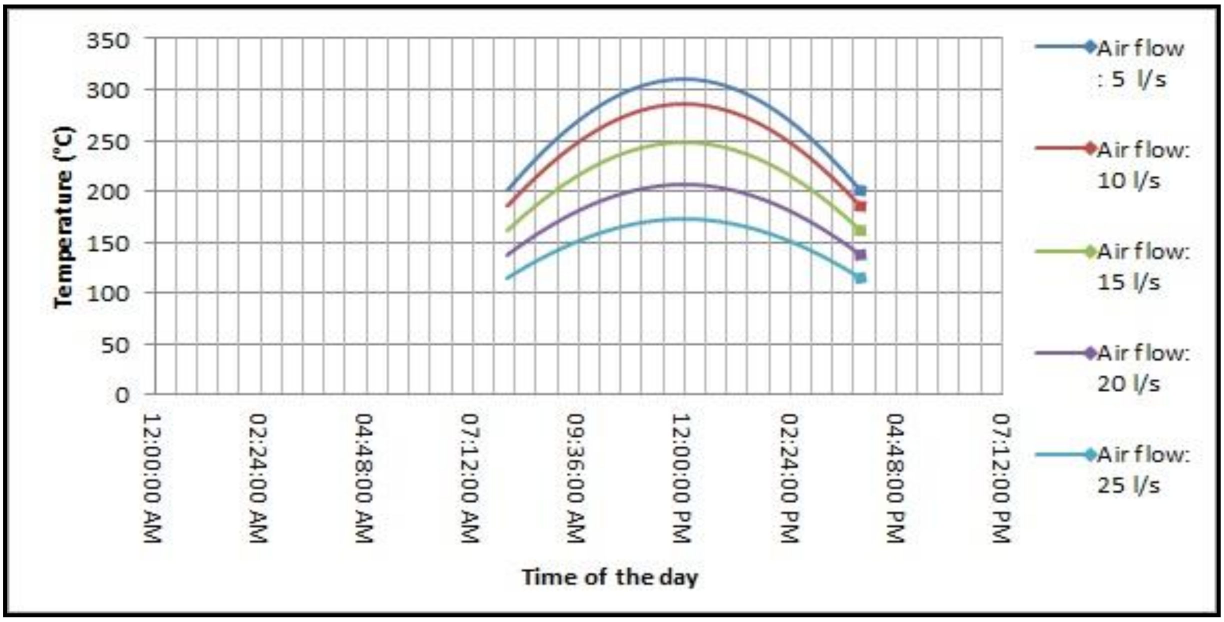

Figure 7.39: Air exit temperature of the PTC at different flow.

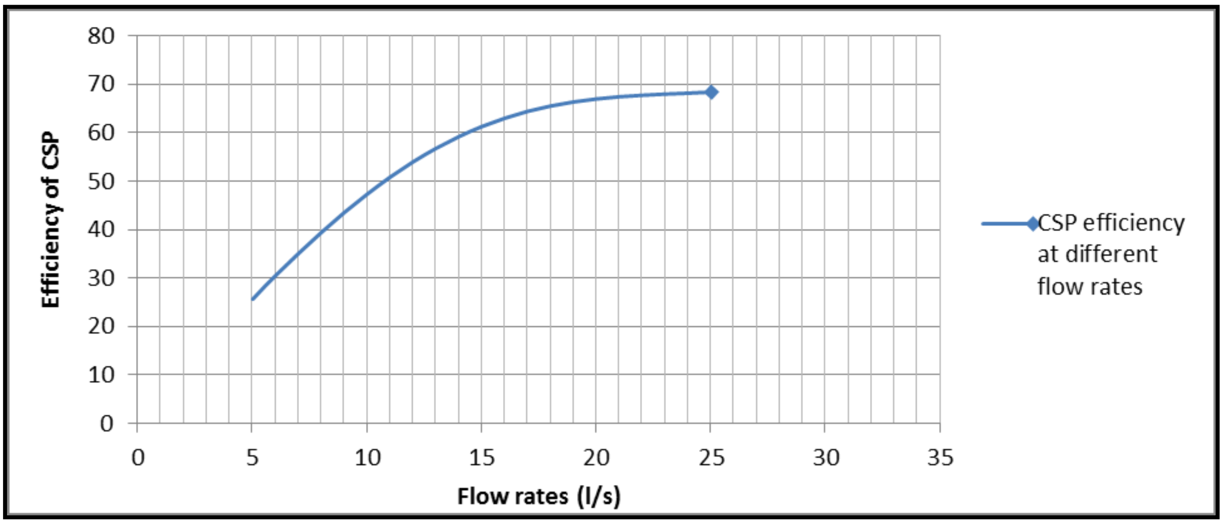

Figure 7.40: Efficiency of solar energy conversion of the CSP at different flow rates

7.3.1 ANALYSIS OF THE EXPERIMENTAL RESULTS:

Two tests were conducted using the manufactured parabolic trough solar collectors at different flow rates through the system by the renewable energy research group in the department of mechanical engineering in Port Elizabeth. The first test was conducted at a flow rate of 5 l/s and the second test at 10 l/s. The tests were conducted from 9:30 am to 15:30 pm in the month of June [40].

The predicted results of the test conducted are shown in Figures (7.41) and (7.42). The prediction results treat the system as if it was one collector and only provide information on the air output results, whereas the actual testing breaks down the information along the whole system. As discussed in Chapter 6, the predictions assumed the two collectors to be designed as one collector having a total length of the two actual collectors.

The agreement between the predicted and the actual results is about 5 % for the test conducted at 5 l/s but the percentage error is about 19% when looking at the results of the test conducted at 10 l/s. This increase in the error comes from the increase in the heat loss in the pipe connecting the two collectors because at high flow rate, the inside convection heat transfer coefficient increases leading to a higher heat loss. Because in the predictions of the results the collectors were treated as a single collector having a total length of two actual manufactured collectors, the piping heat loss connections haven't been taken into consideration.

The summary of the actual and predicted results are shown in Table (7.1).

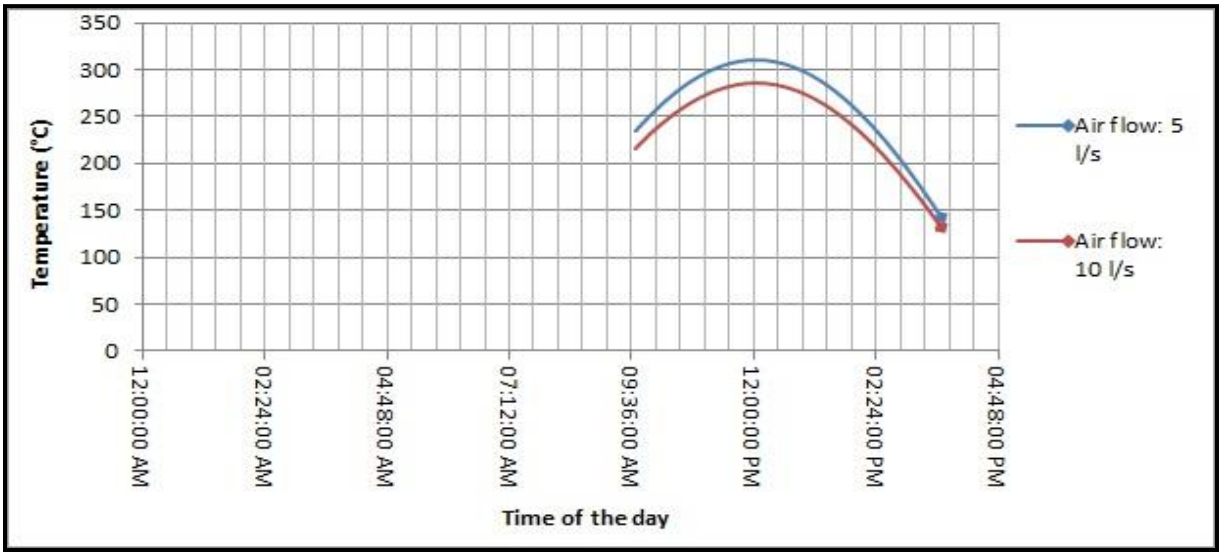

Figure 7.41: Air exit temperature of the PTC at 10 l/s and 5 l/s.

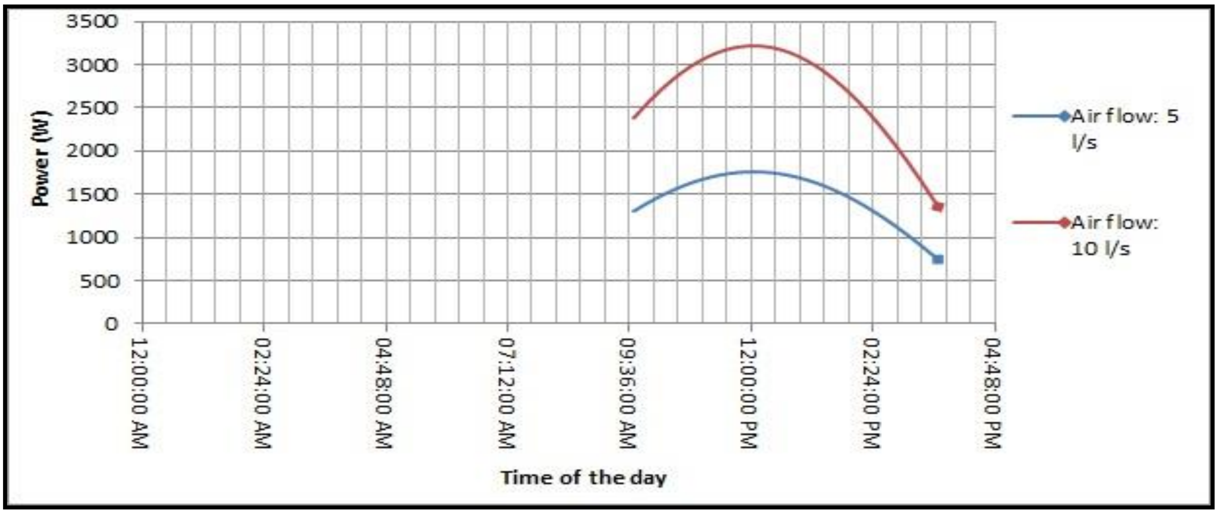

Figure 7.42: PTC solar power graph June test

The loss of data happened for 1 hour when the test was running but the lost data did not affect the results.

- Test 1 (5l/s)

Figures (7.43) and (7.44) graphically represent the data captured during this test at a flow rate of 5 l/s. The resume of the results is shown in Table (7.1). The temperature rose from ambient to 220°C in 20 min (ramp up time) [40].

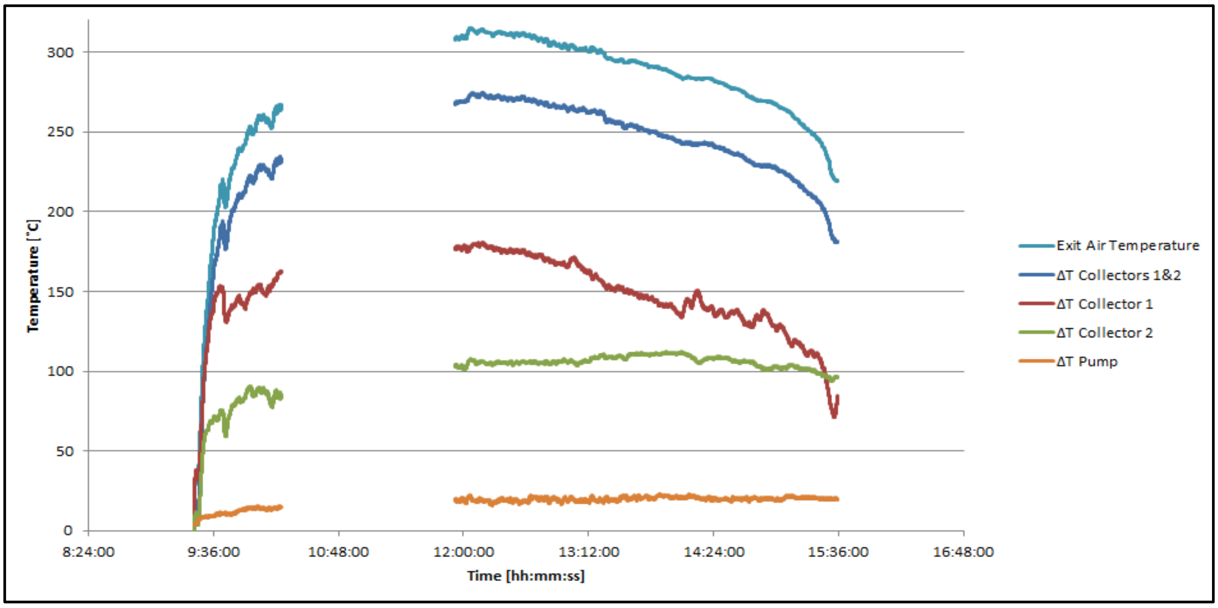

Figure 7.43: Graph of Recorded Temperatures at a flow rate of 5 l/s [40].

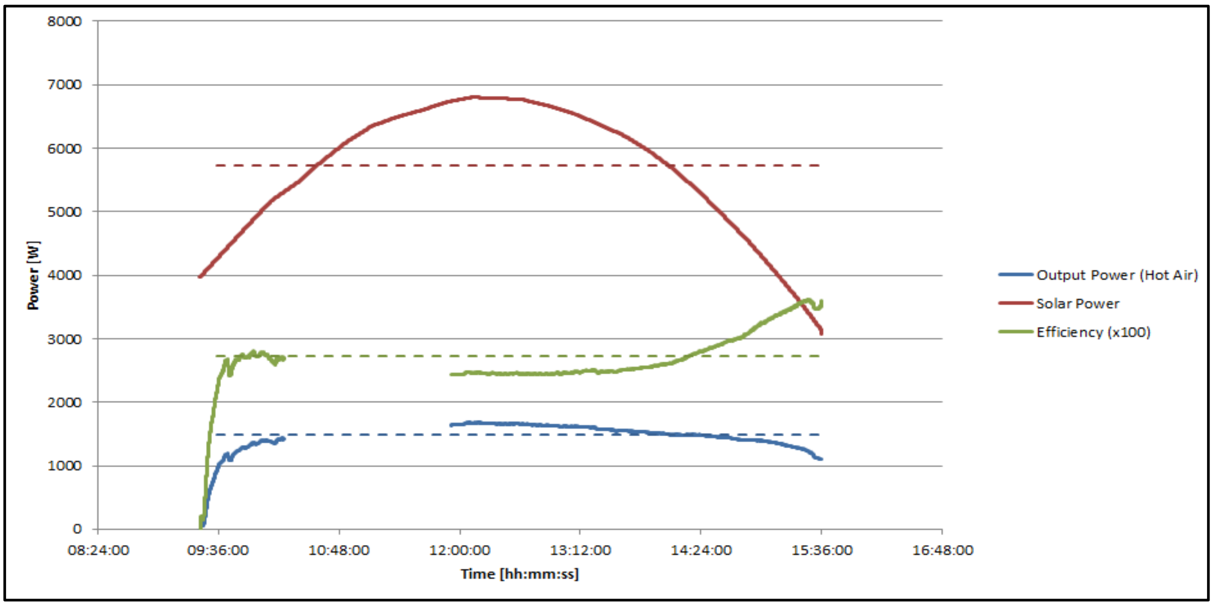

Figure 7.44: Efficiency graphs at a flow rate of at 5 l/s [40].

- Test 2 (10l/s)

Figures (45) and (46) represent the recorded results during this test at a flow rate of 10 l/s. The detailed observation of the results is shown in table (7.1) [40].

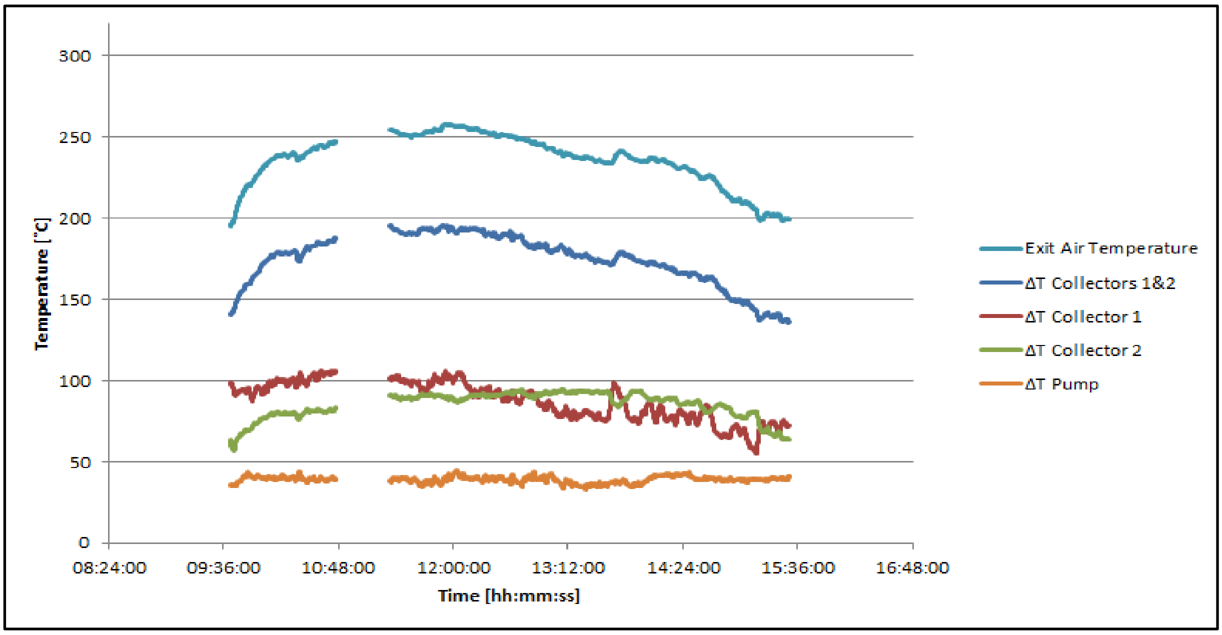

Figure 7.45: Graph of Recorded Temperatures at a flow rate of 10 l/s [40].

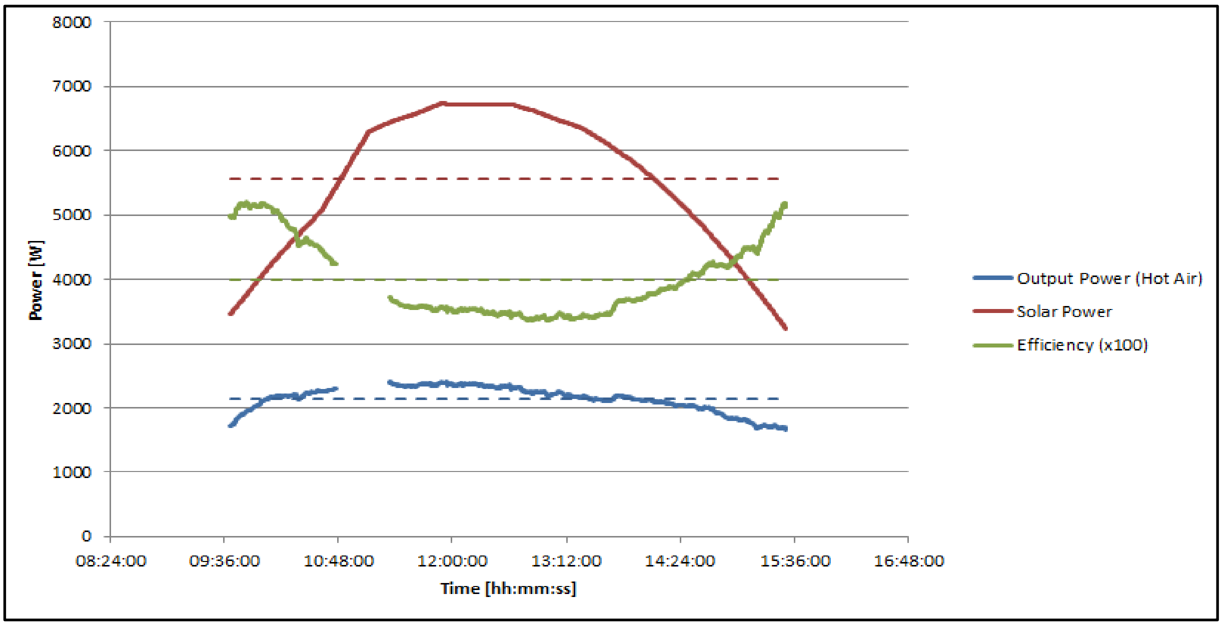

Figure 7.46: Efficiency Graphs at a flow rate of 10 l/s [40].

Table 7.1 : Actual vs predicted results

	Actual	Predicted	Actual	Predicted
	Test 1 (5l/s)	Test 1 (5l/s)	Test 2 (10l/s)	Test 2 (10l/s)
Peak output temperature [˚C]	315	312	258	285
Peak temperature gain (Collector 1&2) [˚C]	275	NA	196	NA
Average power output (Collector 1&2) [W]	1480	1481	2137	2718
Peak power output (Collector 1&2) [W]	1682	1758	2405	3219
Temperature gain through pump [˚C]	23	NA	45	NA
Average efficiency [%]	27	26	40	47
Steady state efficiency (at mid-day) [%]	24.5	NA	35	NA

7.4 INVESTIGATION OF RECIRCULATION OF AIR AND VARYING FLOW RATE USING CSP FOR OPTIMIZATION OF ROCK CHARGING

The spread sheets designed to predict the thermal performance of the packed bed of rocks and the thermal performance of the proposed low cost parabolic trough collectors showed a good agreement between the predictions and the actual recorded results, as discussed earlier in this chapter. To investigate the effect of air recirculation and variation of flow rate using the parabolic trough solar collectors for the optimization of the rock charging, the two spread sheets were combined to a spread sheet where the temperature coming out of the collectors constituted the heat source to charge the rocks. The analysis was broken down into three sections where firstly the investigation of constant flow without recirculation of the air will be conducted, secondly the effect of varying flow rate will be analysed and finally the investigation of air recirculation effect will be analysed

7.4.1 CONSTANT FLOW INVESTIGATION

If the proposed parabolic trough solar collector was used to heat the rocks at constant flow rate for a charging period of 8 hours, Figure (7.47) shows that the maximum energy that can be stored is about 68 MJ at a flow rate of 12 l/s. At higher or lower flow rates, the system is less efficient. As discussed in Chapter 2, to optimize the efficiency of the rock bed storage system, an optimization parameter was defined as the ratio of the energy stored by the rocks to the energy consumed by the blower to propel the air through the rocks (Energy stored / Energy consumed by the blower) and the analysis shows that at a constant flow rate of 12 l/s the system performs to its optimum efficiency.

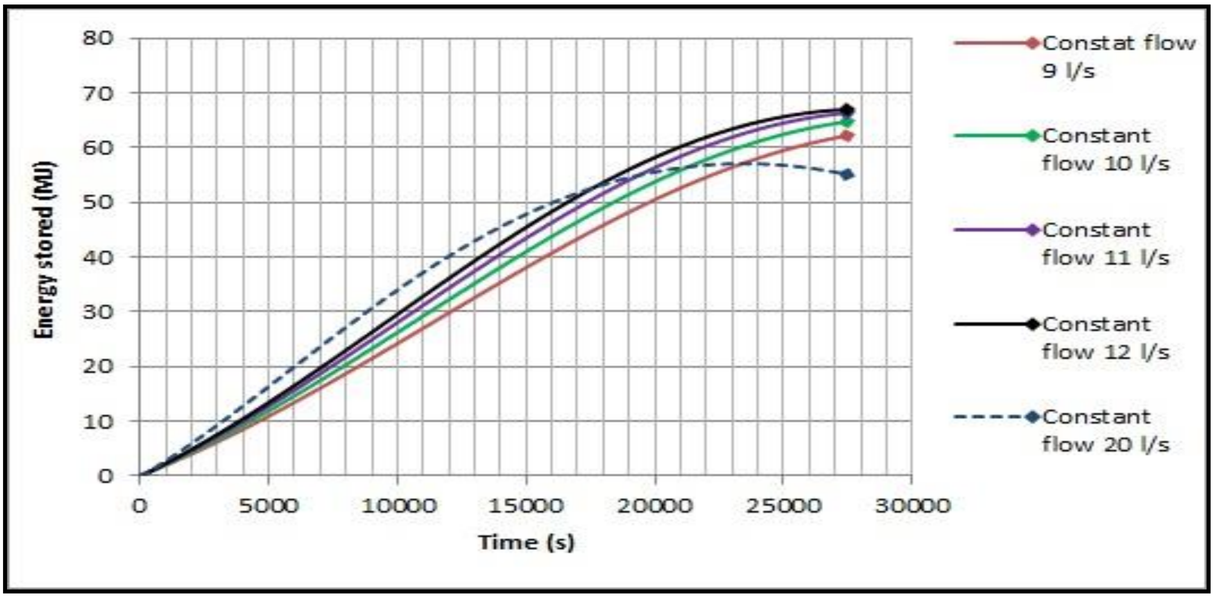

Figure 7.47: Constant flow graphs

7.4.2 VARYING FLOW INVESTIGATION

To understand the effect of flow variation on the thermal energy stored by the rocks, the following approach was pursued. The flow was adjusted whenever the temperature supplied by the parabolic trough collectors was lower than the temperature of rocks in the first layer. The results are presented in Figures (7.48) and (7.49).

Figure (7.48) shows the effect of flow variation from an initial flow of 10 l/s; the flow was reduced by 1 l/s each time the incoming temperature was lower than the first layer rocks temperature and as seen in Figure (7.50), the variation of the flow actually resulted in the reduction of the energy stored by the rocks. This effect is noticed up to a flow rate of 17 l/s but at higher flow rate the variation of flow rate leads to an increase of the energy stored, as shown in Figures (7.49) and (7.51), where the flow was varied from an air flow rate of 20 l/s; however, that increase in energy stored is minimal because as seen in Figure (7.51) the energy stored only increased from 55 MJ to 62 MJ. These results show that running a system at a constant flow of 12 l/s is more effective than running the system at 20 l /s because in Figure (7.47) the energy stored from a constant flow rate at 12 l/s was 68 MJ, whereas only 62 MJ is stored from varying the flow rate from 20 l/s. Also the pressure drop at 20 l/s is more than twice the pressure drop at 12 l/s. So this analysis has shown that variation of flow does not lead to the optimization of the charging of the rocks.

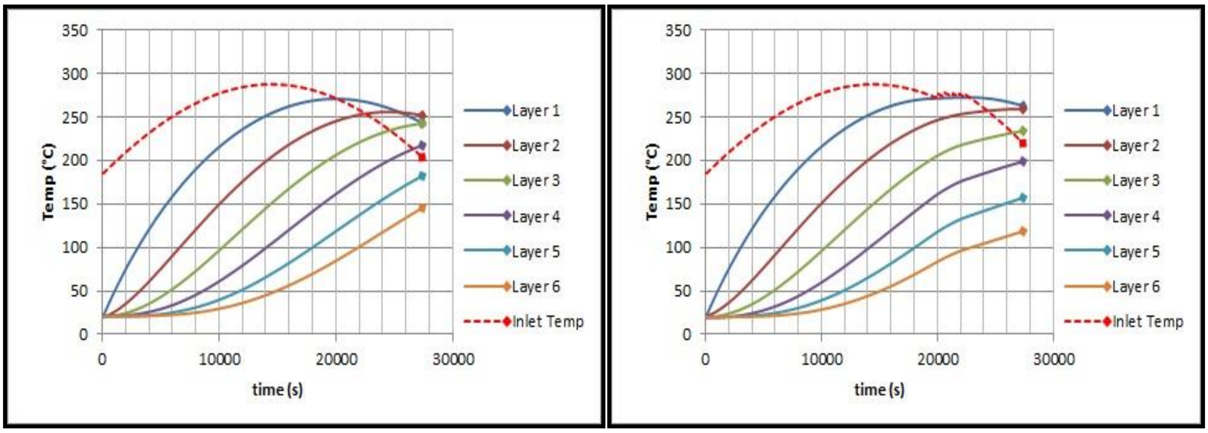

Figure 7.48: Varying flow at 10 l/s

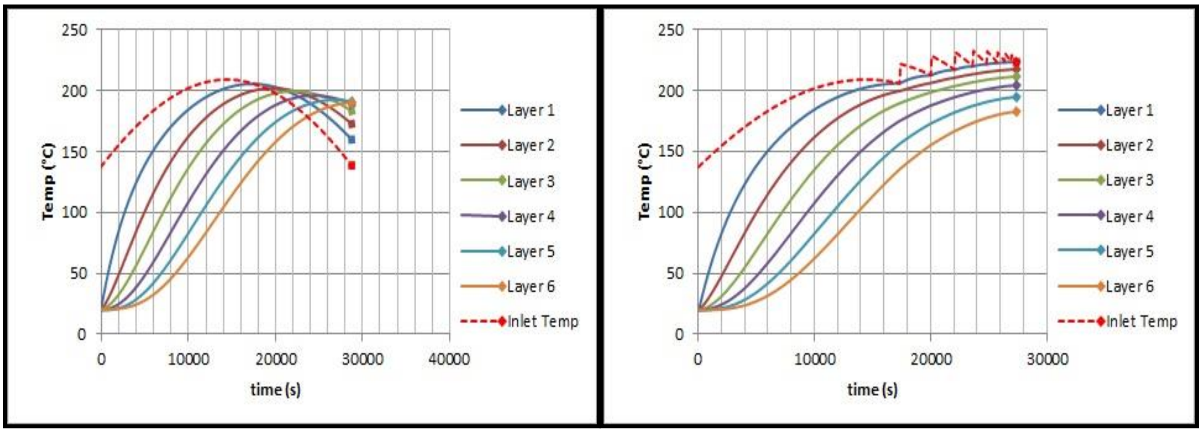

Figure 7.49: Varying flow from 20 l/s

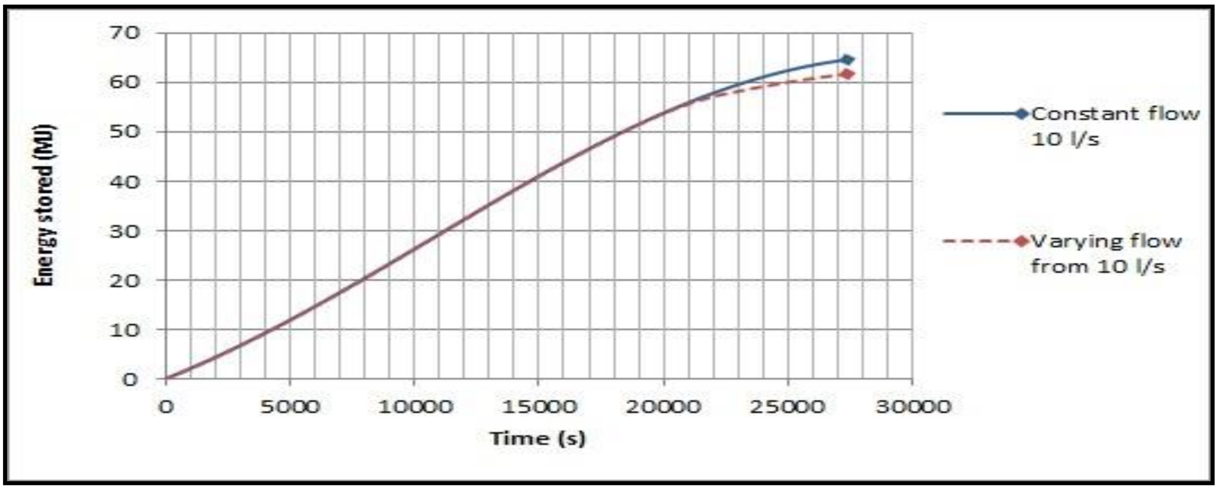

Figure 7.50: Constant vs varying flow at 10 l/s

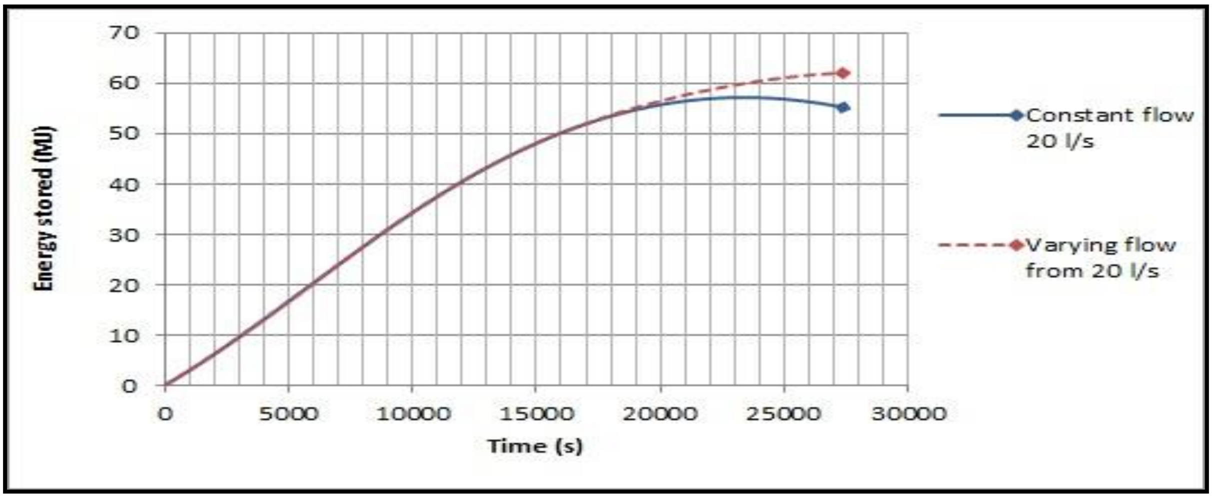

Figure 7.51: Constant vs varying flow at 20 l/s

7.4.3 INVESTIGATION OF RECIRCULATION OF AIR FLOW:

The investigation of air recirculation is performed at a constant flow rate of 12 l/s because in section (7.3.1) it was shown that the charging of the rocks using the proposed solar collectors was optimal at that flow rate and in section (7.3.2) it was also shown that at that flow rate, varying the flow won't improve the charging efficiency of the rocks. Figure (7.52) illustrates the effect of recirculation of the air on the temperature profile of the rocks and it clearly shows a significant improvement of the system. The average temperature of the rocks increased from 232 °C to 304 °C as shown by Figure (7.53) and the energy stored by the rocks went from 68 MJ to 97 MJ as shown by Figure (7.54).

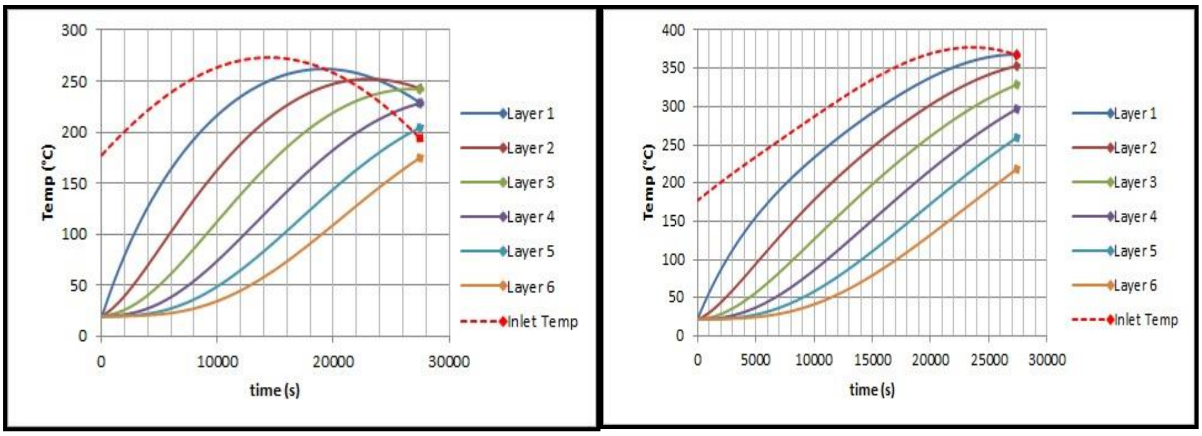

Figure 7.52: The effect of air recirculation at a flow rate of 12 l/s

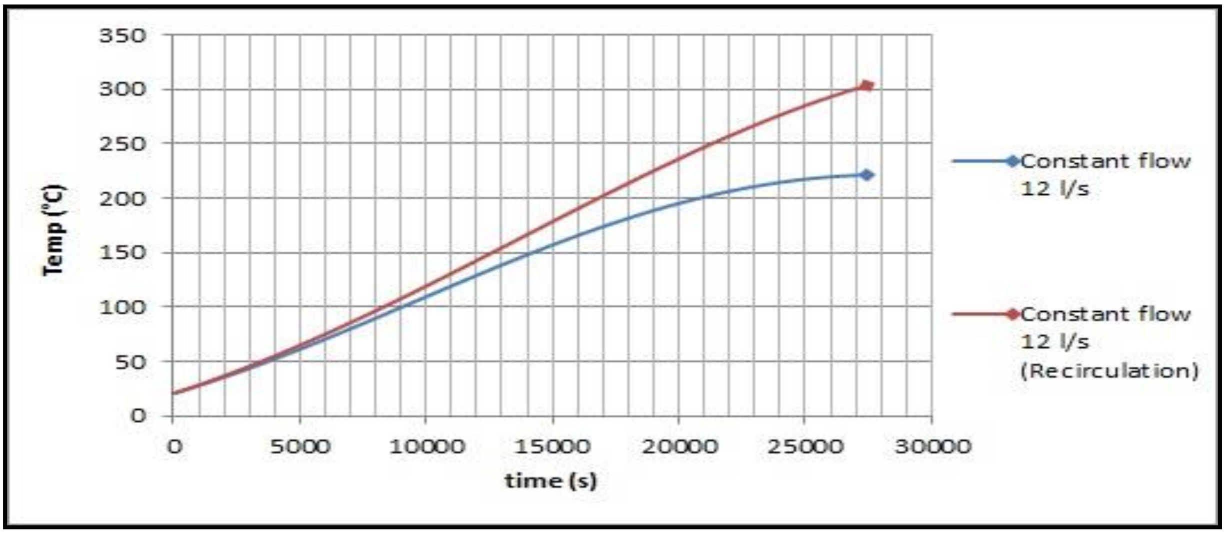

Figure 7.53: Air recirculation effect at 12 l/s on storage temperature.

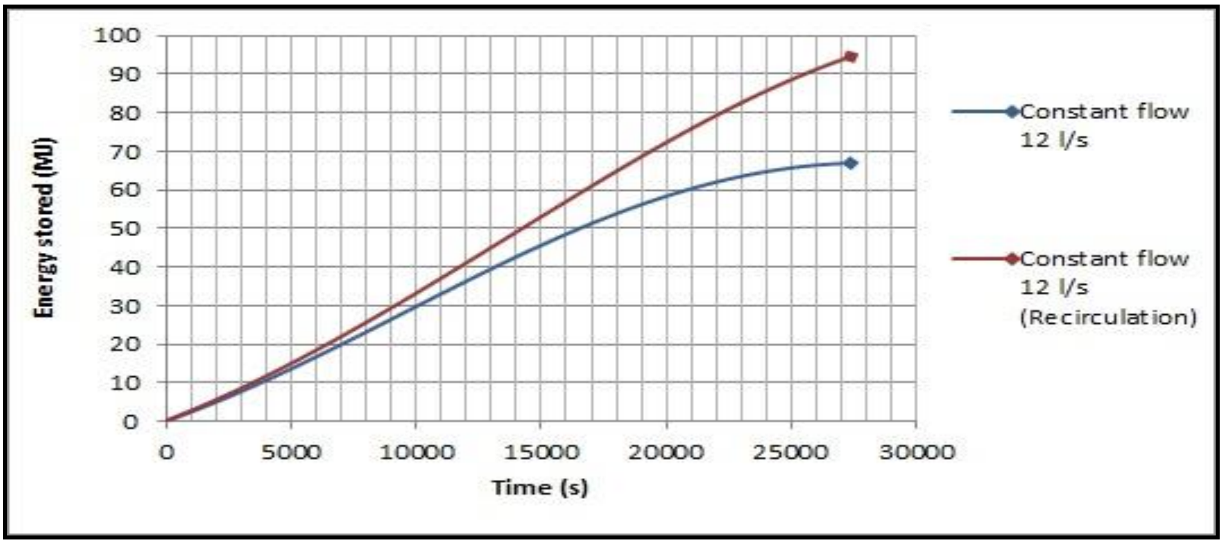

Figure 7.54: Air recirculation effect at 12 l/s on energy stored

7.5 ECONOMIC ANALYSIS OF THE DESIGN

7.5.1 OPERATING COST OF THE ROCK BED SYSTEM

The investigations performed in the previous sections showed that the charging of the rocks for the designed system is optimal at a constant flow rate of 12 l/s with the use of the recirculation of the air. In this section we will investigate the operating cost of the blower at that flow rate.

- The power consumed by the blower to drive the air through the collectors = 186 W
- The measured pressure drop through the storage tank at that flow rate was 580 Pa which corresponds to a power consumed by the blower = 7 W.
- The total power consumed by the blower through the entire system is the sum of the power through the collectors and the storage tank = 186+7 =193W.
- The charging is done in 8 hours so the total energy used by the blower is = 193 x 8 = 1544W = 1.54 kW.h (5.55 MJ).
- The energy stored by the rocks at 12 l/s was recorded to be = 98 MJ = 27.3 kW.h.
- The energy consumed by the blower corresponds to 5.6 % of the energy stored by the system. The power required to pump the air through the collectors was high because the collectors were connected in series and it is estimated the power would be considerably less if the collectors were connected in parallel. An analogy analysis from a similar system shows that the required blower power for that system in parallel will be 104 W instead of 186 W. That implies that the total power consumed by the blower would then be = 111 W (1.1 kW.h) and that corresponds to 4 % of the energy stored by the system.
- The net energy gained through the system would then be = 27.22-1.1 =26.12 kW.h.
- As the price of electricity in South Africa is R1.57 kW.h, the energy stored amounts to a value = 1.57 x 26.12 = R41.

7.5.2 ECONOMIC ANALYSIS OF THE PROPOSED PTC SYSTEM:

The use of a standard solar geyser evacuated tube (@R130 each) as the parabolic trough solar collector receiver tube for the air heating system proved a successful and inexpensive solution to replacing the industry standard solar tubes which cost well over 10 times the price. The economic aspect of the proposed parabolic trough solar collector for air heating application is investigated in this section.

The analysis and the testing done on the proposed CSP showed that the optimum flow rate to run the system is 12 l/s. At that flow rate high temperature is delivered throughout the day and the power consumed by the blower is not significant. The economic analysis conducted here is for the CSP operating at that flow rate.

- The cost of two collectors is R11000 including all the tracking equipment and the blower.
- The replacement of the reflective surface which costs R960 for the two collectors every three years and also cleaning the CSP every week to remove the dust will constitute the maintenance cost of the system.
- The average power delivered by the collectors at the optimum flow rate of 12 l/s for a heating period of 8 hours is 3595 W and the average power consumed by the blower is 111 W, which means a net power of 28 kW.h is produced, which means R43 worth of electricity. If the system is operated for 9 hours, an average of 3510 W will be produced, which means in one day 32 kW.h would be harvested, which corresponds to R51 worth of electricity.

7.6 SUMMARY

An experimental study has been carried out to investigate the effect of heat transfer, heat loss and pressure drop characteristics on the proposed vacuum storage tank for high thermal energy storage.

- Increasing the fluid mass velocity accelerates the charging period, which leads to a fast arrival to steady state. The pressure drop is also increased as the mass flow increases.

- The increase of the rock size leads to a decrease of pressure drop and the amount of energy that can be stored.

- Dolerite has good conduction. This conclusion comes from the fact that at each layer in the tank, two thermocouples were placed. The first measured air temperature, whereas the second was inserted through the dolerite to measure the inside core temperature of the rocks. The results showed that the air and rock thermocouples gave the same reading after just 30 min of heating.

- There is a good correlation between the predicted and the actual results which imply that the baffles incorporated inside the vacuum tank forced the air through the entire tank, thereby resulting in an even lateral temperature distribution across the tank.
- The increase of aluminium foil layers in the evacuated zone leads to a decrease in radiation heat losses and also as the expanded perlite thickness increases the heat losses decrease.
- The investigation of heat loss showed that a Vacuum with expanded perlite is a viable solution to high temperature heat storage for an extended period. A 27 % average daily heat loss efficiency from the test conducted at 70% vacuum was achieved. A full vacuum was not attained due to the limitations of the test equipment. A full vacuum would have resulted in a daily heat loss of only 6% because the effect of a vacuum on thermal conductivity of materials is not linear as seen in Figure (7.27).

The investigation performed on the proposed low cost parabolic trough solar collector for air heating system showed that the use of a standard solar geyser evacuated tube (@R130 each) has cost benefits over the industry standard solar tubes normally used in concentrating solar power systems. The collectors have a solar energy conversion of up to 70 %.

The results showed that if the collectors were used to thermally charge the rocks, running the blower at constant flow rate is more effective than varying the airflow rate. It was also shown that air recirculation increases the charging efficiency of the rocks.

CHAPTER 8: CONCLUSION AND FURTHER WORK REQUIRED

The conclusions of the research findings and the recommendations for further work required are presented in this chapter.

8.1 CONCLUSION ON THE WORK DONE AND RECOMMENDATIONS

The primary objective of this research was the development of affordable solar thermal energy products to increase the use of solar energy in Africa. Packed-bed rock thermal energy storage for high temperature storage using air as a heat transported fluid and crushed dolerite rocks was proposed in this study for an efficient and inexpensive storage device.

The study investigated a vacuum-insulated storage tank for high temperature thermal energy in packed-bed rock for solar air heating system. The parameters affecting the heat transfer and the pressure drop through the bed system have been investigated in order to optimize the efficiency of a packed-bed rock energy system. It was found that the pressure drop and the energy stored by the rocks depended on the air flow rate and the rocks' size. As the air flow rate was raised the pressure drop and the energy stored by the rocks increased and the decrease in rocks' size resulted in higher pressure drop and more energy stored by the rocks.

A numerical model has been developed using excel software for the prediction of the heat transfer and pressure drop through a packed rock storage system. The predicted results correlate well with the measured results. The NTU-method of Hughes predicts the heat transfer through the packed-bed rock system with good accuracy. Allen [18] in his results found the difference between the predicted and the actual results to be around 15% using this method but he mentioned the accuracy of this prediction could be increased if the wall effect through the packed system was reduced. In this research baffles have been incorporated inside the vacuum-insulated storage with the objective of minimising the problem of wall effect through the rocks. The results showed that making use of baffles has resulted in effective heating of the rocks by forcing the air through the entire tank, thereby resulting in an even lateral temperature distribution across the tank. There is a better correlation between the results by making use of baffles because the NTU-method assumes the air is in contact with all the rocks. The difference in the results was about 4%.

The investigation of heat loss showed that vacuum with expanded perlite is a viable solution to high temperature heat storage for an extended period. A 27 % average daily heat loss efficiency from the test conducted at 70% vacuum was achieved. A full vacuum was not attained due to the limitations of the test equipment. A full vacuum would have resulted in a daily heat loss of only 6% because the effect of a vacuum on thermal conductivity of materials is not linear as seen in Figure (7.27). However, the complications involved in maintaining the vacuum and the cost of the vacuum tank, plus the maintenance cost involved, constitute a great handicap of those systems. As the primary aim of this research is the development of an affordable solar energy product to widespread the use of solar energy in Africa, an alternative design is suggested in this section. The mathematical model developed and the investigations done showed that a system using only expanded perlite insulation will produce the same insulation performance as vacuum insulation, resulting in a design that is 6 times cheaper.

In theory vacuum insulation with the use of expanded perlite appeared to be an excellent insulation technique; however, in practice, it results in an unnecessarily complex system.

- Vacuum leaks constitute a major problem here due to the fact that vacuum insulation only starts having an effect when more than 90 % of the air is evacuated; in other words, only at a pressure below 0.1 Bar, as shown in Figure (7.27). It is difficult to achieve those pressures in practice and if those pressures are achieved, leaks make the system lose the vacuum. Even a leak at a microscopic level can cause a considerable loss in vacuum.
- Because of the leaks, the tank must be connected to a vacuum pump to restore the vacuum level whenever the pressure drops, this increases maintenance costs of this system and also the cost of the tank itself with all the pressure level equipment makes this system expensive.

- The predictions have shown that if 180 mm of expanded perlite insulation was used, it will produce the same insulation effect as a combination of vacuum insulation with the use of 60 mm of expanded perlite.

SUGGESTED STORAGE TANK DESIGN

Instead of using vacuum insulation with the use of expanded perlite, a simpler design is suggested that only makes use of expanded perlite insulation. The new design will not be as compact as the original design due to the fact that the required insulation thickness is 180 mm instead of 60 mm, which makes the outside tank bigger. The new design also allows the reduction in conduction heat losses because the stainless steel heat barrier used in the previous design will be replaced by a calcium silicate pipe which has a lower thermal conductivity.

The research also investigated a proposed low cost parabolic trough solar collector for an air heating system. A thorough investigation was performed on the proposed low cost parabolic trough solar collector for an air heating system. The use of a standard solar geyser evacuated tube (@R130 each) has cost benefits over the industry standard solar tubes normally used in concentrating solar power systems. As air is chemically stable and does not have the problem of expansion pressure, the solar geyser evacuated tube is used. The use of air as a working fluid resulted in a simple and inexpensive design having an average solar energy efficiency conversion up to 70 %.

A mathematical model predicting the thermal performance of the parabolic trough solar collector was developed using an excel spreadsheet in this study. It was found that the predictions correlated well with the measured results. This spreadsheet can be used as an operational manual for the collectors. The proposed parabolic trough solar collector can supply heat up to a temperature of 400 °C. The collectors will be used for any applications that require heat. The manufacturing of the collectors cost R11000 with all the equipment.

The economic analysis of the collectors showed that industries will save money by implementing these collectors for their process heat. The average power delivered by the collectors at the optimum flow rate of 12 l/s for a heating period of 8 hours is 3595 W and the average power consumed by the blower is 111 W, which means a net power of 28 kW.h is produced meaning R43 worth of electricity. If the system is operated for 9 hours, an average of 3510 W will be produced which means in one day, 32 kW.h will be harvested, which corresponds to R51 worth of electricity.

These collectors have proven to be a success as many industries have shown interest in the project. However, their concerns are the sustainable aspect of the collectors which is related to the corrosion and maintenance cost of the collectors. Therefore for a sustainable product, the commercialised version should present the following features:

- The frame structure will be made out of fibre glass instead of mild steel and this will reduce the weight of the CSP and the cost of the collectors as well. Because the frame structure is made of fibre glass, there is no concern related to corrosion and therefore there is a great decrease in maintenance cost.
- The total cost will be reduced from R11000 to R9300 and the maintenance cost will only be the replacement of reflective surface each 3 years according to the manufacturer.
- The air flow through the collectors should be channelled in parallel with the aim of minimising the air pressure drop in the piping systems.

The study showed that if the proposed parabolic trough solar collectors were used to thermally charge the rocks in the vacuum insulated storage tank, running the system at constant flow is more effective. An optimization parameter that takes into account the rocks' size and the air flow rate to optimize the charging efficiency of the rocks showed that a constant flow rate of 12 l/s is the optimal flow. Furthermore, it was shown that if the air exiting the storage tank was recirculated in the collectors the energy stored increased from 68 MJ to 96 MJ.

8.2 FURTHER WORK REQUIRED

Further work is required as summarized below:

- The influence of rocks' shape and roughness on the pressure drop and heat transfer should be investigated.
- An experimental investigation should be performed to confirm that connecting the collectors in a parallel network will improve their performance and will result in less piping pressure drop.
- An economic comparison between a packed-bed rock storage system and other storage systems should be investigated to determine its economic feasibility.
- A suggested storage tank making use of only expanded perlite insulation instead of the combination of vacuum and expanded perlites should be experimentally investigated to confirm the predictions performed.
- Further testing should be performed to investigate the effect of adding baffles for air channelling through the bed on the pressure drop.
- Heat extraction out of the bed should be investigated in detail.

REFERENCES

[1]. Duffie JA, Beckman WA. Solar Engineering of Thermal Processes. Third edition. Hoboken, New Jersey: John Wiley & Sons; 2006.

[2]. Chen CJ. Physics of solar energy. Hoboken, New Jersey: John Wiley & Sons; 2011.

[3]. Cengel YA. Heat and mass transfer: A practical approach. Third edition. USA, New York: The McGraw-Hill; 2006.

[4]. Kalogirou SA. Solar energy engineering: processes and systems. San Diego, California: Elsevier; 2009.

[5]. Kreith F, Jan F. Kreider JF. Principles of Solar Engineering. Fourth Volume. Bristol, United States of America: Hemisphere Publishing Corporation; 1992

[6]. Garg HP, Mullick SC, Bhargava AK. Solar thermal Energy Storage. Dordrecht, Holland: D. Reidel; 1985.

[7]. Sorensen B. Energy conversion, transmission and storage. San Diego, California: Elsevier; 2007.

[8]. Goswan YD. Energy: The burning issue. Refocus. 2007; (January-February): 22-25.

[9]. Abu-Zour A, Riffat S. Environmental and economic impact of a new type of solar louver thermal collector. Int.J. Low carbon technol. 2006; 1 (3): 217-22.

[10]. Varun F, Singal SK. Review of augmentation of energy needs using renewable energy resources in India. Renewable and Sustainable Energy Reviews. 2007; 11:1607-15.

[11]. Palo Alto CA. Solar Thermocline Storage Systems: Preliminary Design Study. EPRI. 2010. 1019581.

[12]. Singh R, Saini RP, Saini JS. Models for Predicting Thermal Performance of Packed Bed Energy Storage System for Solar Air Heaters. The Open Fuels & Energy Science Journal, 2009, 2, 47-53
www.benthamscience.com/open/toefj/articles/V002/47TOEFJ.pd

[13 Hänchen M, Brückner S, Steinfeld A. High-temperature thermal storage using a packed bed of rocks: Heat transfer analysis and experimental validation. Applied Thermal Engineering. 2011; 31: 1798-1806.
www.pre.ethz.ch/publications/journals/full/j226.pdf (accessed 2 March 2011)

[14]. Varun F, Singh SK, Tyagi H, Nautiyal. Experimental Investigation of Packed Bed Solar Thermal Energy System with Cylindrical Elements. International Journal of Science and Technology. Volume 1. July 2011.
http://ejournalofsciences.org/archive/vol1no1/vol1no1_8.pdf

[15]. Li PW, Van Lew J, Karaki W, Cho Lik Chan CL, Stephens J, James E, OBrien. Transient Heat Transfer and Energy Transport, 2001; in Packed Bed Thermal Storage Systems, Developments in Heat Transfer, Dos Santos Bernardes (Editor), ISBN: 978-953-307-569-3, InTech, Available from:
http://www.intechopen.com/books/developments-in-heat-transfer/transient-heat-transfer-and-energytransport-in-packed-bed-thermal-storage-systems

[16]. Al Azawi FS, A. K. A. Hassan AKA, Salman AM. Design parameter effects on the thermal performance of special packed bed for heat storage. Energy and Fuel Research Center University of Technology Iraq-Baghdad; 20/6/2007.
http://www.iasj.net/iasj?func=fulltext&aId=38151

[17]. Andreozzi A, Buonomo B, Manca O, Mesolella P, Tamburrino S. Numerical investigation on sensible thermal energy storage with porous media for high temperature solar systems.
www.let.ensma.fr/eurotherm2012/papers/03667-fichier2.pdf (accessed 20-06-2013)

[18]. Allen KG. Performance characteristics of packed bed thermal energy storage for solar thermal power plants. [Master's thesis]. University of Stellenbosch; 2010.
http://www.crses.sun.ac.za/files/research/completed-research/solar/kg_allen.pdf

[19]. Cruickshank CA. Evaluation of a stratified multi-tank thermal storage for solar heating applications. [PhD thesis]. Queen's University Kingston; 2009.

http://qspace.library.queensu.ca/bitstream/1974/1969/1/Cruickshank_Cynthia_A_200906_PhD.pdf

[20 Demharter M. Heat transport in evacuated perlite powder Insulations and its application in Long-Term Hot Water Storages. [Master's thesis]. Technische Universität München; August 2011.
http://www.wmi.badw.de/publications/theses/Demharter_Master_Thesis_2011.pdf

[21]. BeikircherT, Demharter M. Heat Transport in Evacuated Perlite Powders for Super-Insulated Long-Term Storages up to 300 °C. J. Heat Transfer 135(5), 051301 (Apr 11, 2013) (11 pages) doi:10.1115/1.4023351History: Received March 30, 2012; Revised.
http://heattransfer.asmedigitalcollection.asme.org/article.aspx?articleid=1678171

[22]. Torab H, Beasley D E. Optimization of a packed-bed thermal-energy Storage unit, Journal of Solar Energy Engineering (Transactions of the ASME). 1987; 109: 170 – 175.
www.benthamscience.com/open/toefj/articles/V002/31TOEFJ.pdf

[23] Singh R, Saini RP, Saini JS. Nusselt number and friction factor correlation for packed bed solar energy system having large sized elements of different shapes. Solar Energy. 2006; 80:760-71.
ejournalofsciences.org/archive/vol1no1/vol1no1_8.pdf

[24]. Singh H, Saini RP, Saini JS. A review on packed bed solar energy storage system. Renewable and Sustainable Energy Reviews. 2010; 14:1059-1069.

[25]. Chandra P, Willits DH. Pressure drop and heat transfer characteristics of air rock bed thermal storage systems. Sol. Energy. 1981; 27(6):547-53.

[26]. Hughes PJ, Klien S A, Close DJ. Packed bed thermal storage models for solar air heating and cooling systems. J. Heat Transf., (ASME Trans.). 1976; 98: 336-338.

[27]. South African electricity sector jobs to 2030 (Rutovitz, 2011).

[28].Vėjelis S, Gailius A, Vėjelienė J, Vaitkus S. Research on thermal conductivity of vacuum insulating materials. The paper is presented at the 10th international conference on thermal insulation; May 19-21, 2010; Vilnius; Lithuania.
http://dspace.vgtu.lt/bitstream/1/548/1/0313-0317_Vejelis_Gailius_et_al.pdf

[29]. Lahousse SW. Vacuum insulation using Perlite powder sealed in Plastic and Glass. Bachelor thesis. Massachusetts institute of technology; 1993.
http://dspace.mit.edu/bitstream/handle/1721.1/72769/29813396.pdf

[30].Price DM, Jarratt M .Thermal conductivity of PTFE and PTFE composites. The paper is presented at the twenty-eight conference of the North American thermal analysis society., October 4-6, 2000; Orlando, Florida.
http://www.sump4.com/publications/conf015.pdf

[31]. Expanded perlite Genutile M45 data sheet.
http://infigro.co.za/uploads/files/2013%20MSDS%20Genulite%20M45.pdf

[32]. Fasunwon OO, Olowofela JA, Ocan OO, Akinyemi OD. Determination of Conductivity of Rock Samples using Fabricated Equipment. Thermal science; Vol. 12 2008; 2 :119-128
http://www.doiserbia.nb.rs/img/doi/0354-9836/2008/0354-98360802119F.pdf

[33]. Ochs F, Heidemann W, Müller-Steinhagen H. Effective Thermal Conductivity of Moistened Insulation Materials as a Function of Temperature. International Journal of Heat and Mass Transfer. 2008; 51: 539-552

[34]. Barlev D, Vidu R, Stroeve P. Innovation in Concentrated Solar Power, Solar Energy Materials & Solar Cells, Elsevier; 2011.

[35]. Ferna´ ndez-Garcı´a A, E. Zarza E, Valenzuela L, Pe´ rez M. Parabolic-trough solar collectors and their applications, Renewable and Sustainable Energy Reviews, Elsevier; 2010.

[36]. Bauer T, Pfleger N, Breidenbach N, Eck M, Laing D, Kaesche S, Material aspects of Solar Salt for sensible heat storage, Applied Energy, Elsevier, 2013.

[37]. Kenisarin MM. High-temperature phase change materials for thermal energy storage, Renewable and Sustainable Energy Reviews, Elsevier; 2009

[38]. Guillot S, Faik A, Rakhmatullin A, Lambert J, Veron E, Echegut P, Bessada C, Calvet N, Py X. Corrosion effects between molten salts and thermal storage material for concentrated solar power plants, Applied Energy, Elsevier;, 2011.

[39]. Mekaoui S, Dewitte S, Conscience C, Chevalier A, Total solar irradiance absolute level from DIARAD/SOVIM on the International Space Station, Advances in Space Research, Elsevier; 2010.

[40]. Poole S, Phillips R. Development of a low cost CSP for heating of air. 2013.

[41]. http://www.timeanddate.com/worldclock/astronomy.html?n=111

[42]. Kreith F, Kreider JF. Principles of Solar Engineering. Fourth Volume. Bristol, United States of America: Hemisphere Publishing Corporation; 1992

[43]. http://en.wikipedia.org/wiki/Multi-layer_insulation. (May 13, 2011)

[44]. Xiao G. A closed parabolic trough solar collector; 2007, http://wims.unice.fr/xiao/solar/collector.pdf

[45]. Fricke, J. Physical aspects of heat transfer and the development of thermal insulations, in Proc. of the International Conference and Workshop EMPA Duebendorf. 2001; 13–22.